ΠΟΛΥΤΕΧΝΕΙΟ ΚΡΗΤΗΣ
ΓΕΝΙΚΟ ΤΜΗΜΑ
ΠΡΟΓΡΑΜΜΑ ΜΕΤΑΠΤΥΧΙΑΚΩΝ ΣΠΟΥΔΩΝ:
ΕΦΑΡΜΟΣΜΕΝΕΣ ΕΠΙΣΤΗΜΕΣ ΚΑΙ ΤΕΧΝΟΛΟΓΙΑ

Nanocomposite coatings for enhanced barrier properties

Νανοσύνθετα υμένια με χαμηλή διαπερατότητα σε αέρια

Μαρία Σ. Στρατηγάκη

Επιβλέπων: Αλέξανδρος Δ. Γκότσης

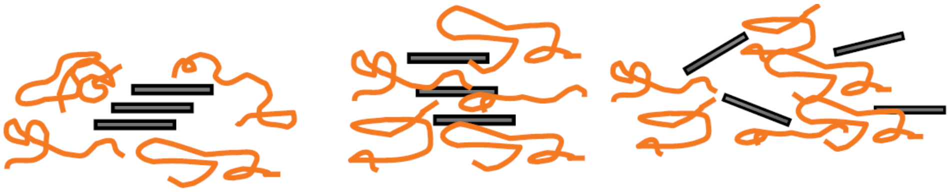

ΔΙΠΛΩΜΑΤΙΚΗ ΔΙΑΤΡΙΒΗ ΜΕΤΑΠΤΥΧΙΑΚΟΥ ΔΙΠΛΩΜΑΤΟΣ ΕΙΔΙΚΕΥΣΗΣ
«ΜΗΧΑΝΙΚΗ ΚΑΙ ΤΕΧΝΟΛΟΓΙΑ ΥΛΙΚΩΝ ΚΑΙ ΚΑΤΑΣΚΕΥΩΝ»

ΠΟΛΥΤΕΧΝΕΙΟ ΚΡΗΤΗΣ
ΓΕΝΙΚΟ ΤΜΗΜΑ

NANOCOMPOSITE COATINGS FOR ENHANCED BARRIER PROPERTIES

Νανοσύνθετα υμένια με χαμηλή διαπερατότητα σε αέρια

Μαρία Σ. Στρατηγάκη

Διπλωματική διατριβή υποβληθήσα στα πλαίσια των απαιτήσεων για
την απόκτηση του Μεταπτυχιακού Διπλώματος Ειδίκευσης
στη κατεύθυνση
«ΜΗΧΑΝΙΚΗ ΚΑΙ ΤΕΧΝΟΛΟΓΙΑ ΥΛΙΚΩΝ ΚΑΙ ΚΑΤΑΣΚΕΥΩΝ»
του Γενικού Τμήματος του Πολυτεχνείου Κρήτης

3 Δεκεμβρίου, 2012

ΔΙΠΛΩΜΑΤΙΚΗ ΔΙΑΤΡΙΒΗ ΜΕΤΑΠΤΥΧΙΑΚΟΥ ΔΙΠΛΩΜΑΤΟΣ ΕΙΔΙΚΕΥΣΗΣ

Μαρία Σ. Στρατηγάκη,
αρ. μητρώου: 2010040273
e-mail: mstratigaki@isc.tuc.gr

Η εργασία εγκρίθηκε από την ακόλουθη τριμελή συμβουλευτική επιτροπή:

1. Αλέξανδρος Δ. Γκότσης, αναπλ. καθηγητής Πολυτεχνείου Κρήτης, Επιβλέπων

2. Μαρία Σταυρουλάκη, λέκτωρ Πολυτεχνείου Κρήτης

3. Παγώνα Μαραβελλάκη, επικ. καθηγήτρια Πολυτεχνείου Κρήτης

την 30η Νοεμβρίου, 2012

Εικόνα εξωφύλλου:
Stacked, intercalated and exfoliated nano-platelets in a polymeric matrix
[Paul and Robeson, 2008]

ΔΙΕΥΘΥΝΣΗ ΕΡΓΑΣΤΗΡΙΟΥ:

ΠΟΛΥΤΕΧΝΕΙΟ ΚΡΗΤΗΣ, ΓΕΝΙΚΟ ΤΜΗΜΑ
ΕΡΓΑΣΤΗΡΙΟ ΜΗΧΑΝΙΚΗΣ ΤΩΝ ΥΛΙΚΩΝ

Κτήριο Επιστημών, Πανεπιστημιούπολη, Κουνουπιδιανά, 73100 Χανιά

τηλ. 2821037259
fax. 2821037672
e-mail: gotsis@science.tuc.gr

Contents

DECLARATION

I hereby declare that the work presented here has been my independent work and has been performed during the course of my M.Sc. studies at the Department of Applied Sciences, Technical University of Crete, Chania.
All contributions drawn from external sources have been acknowledged with due reference to the literature.

ΔΗΛΩΣΗ

Δηλώνω υπεύθυνα ότι η παρούσα διατριβή είναι προϊόν ανεξάρτητης εργασίας μου που διεξήχθη κατά τις μεταπτυχιακές μου σπουδές στο Γενικό τμήμα του Πολυτεχνείου Κρήτης, στα Χανιά.
Για ό,τι δεδομένα ή πληροφορίες χρησιμοποίησα που προέρχονται από εξωτερικές πηγές έχουν δοθεί οι αρμόζουσες αναγνωρίσεις και αναφορές.

Μαρία Σ. Στρατηγάκη

Acknowledgements

First and foremost I would like to thank my thesis supervisor, Prof. A. D. Gotsis, for giving me the opportunity to carry out the present M.Sc. Thesis study. His supervision, motivation and guidance led to the successful completion of the present work.

I would also like to thank Prof. M. E. Stavroulaki and Prof. P. Maravelaki for their participation and contribution as members of the advisory committee.

Special thanks are further due to Prof. Dr. Reinhard Krause-Rehberg and the group members for their hospitality and friendly atmosphere in the Positron Annihilation Laboratory, Department of Physics in Martin - Luther University, Halle – Wittenberg, since part of the work was done while visiting Halle an der Saale / Germany.

I wish to thank the members and staff of the Technical University of Crete in Chania, the University of Crete in Heraklion, as well as the Institute of Electronic Structure and Laser in Heraklion, IESL FORTH, for allowing me to conduct the required experiments throughout the study.

Last, but not least, it gives me great pleasure in acknowledging the support of my family and friends throughout my studies.

Abstract

It all began in 1985, when a research group at Toyota Central Research and Development Laboratories Co. Inc. (TCRD) prepared a Nylon-6/MMT nanocomposite, in which very small amounts of layered silicate loadings resulted in pronounced improvements in thermal and mechanical properties. This invention gave birth to a new concept, that of polymer/clay nanocomposites, and led to new applications due to the improvements in properties such as high moduli, increased strength and heat resistance, decreased gas permeability and flammability, etc. Since the Nylon-6/MMT nanocomposites, the research in these materials has been extended to a varying range of polymer systems and different types of nanoclays.

The aim of the present study is to reveal the interactions between the inorganic clay particles and the organic matrix. This is achieved utilizing various experimental characterisation techniques. The present work employed water- or solvent-based acrylic and polyurethane resins, hydrophilic nano-particles of montmorillonite, MMT, and/or organically modified nano-particles of MMT available under the trade name of Cloisite®.

The characterization of the obtained nano-structures was based on X-ray diffraction measurements by detecting the characteristic diffraction peak that indicates the intercalation/exfoliation state of the nanoparticles into the organic matrix. Techniques such as Differential Scanning Calorimetry (DSC) and Thermogravimetric analysis (TGA) have been carried out to study the thermal behavior of the samples. The glass transition temperature, T_g, was defined by DSC measurements, whereas the mass fraction of the organo-clay was confirmed through TGA experiments. The change in free volume of the nanocomposites, as functions of temperature and added mass fraction of MMT, was obtained by conducting Positron Annihilation Lifetime Spectroscopy (PALS). The T_g was also established through PALS measurements and then compared with the one obtained from DSC. The gas permeation properties of the nano-films were studied for CO_2 molecules by utilizing an experimental permeability/diffusion measuring setup.

Nomenclature

A	surface area (m^2) εμβαδόν (δι)επιφάνειας
C	constant used to evaluate the free volume (eq. 4.4), $\approx$ 0.0018 σταθερά στην εξίσωση eq. 4.4
D	diffusion coefficient (m^2/s) συντελεστής διάχυσης
$E_{coh,i}$	cohesive energy of group i, (J/mol) συνεκτική ενέργεια της ομάδας i
H	gallery height (nm) διάκενο γαλαριών
I_1	para-positronium annihilation intensity ένταση εξαϋλωσης παρα-ποζιτρονίων
I_2	positron direct annihilation intensity ένταση κατ’ ευθείαν εξαϋλωσης ποζιτρονίων
I_3	ortho-positronium annihilation intensity ένταση εξαϋλωσης ορθο-ποζιτρονίων
I_i	intensity of positron annihilation in mode i ένταση της εξαϋλωσης ποζιτρονίων σύμφωνα με τον τρόπο i
J	mass flux (kg m^{-2} s^{-1}) ροή μάζας
K	permeability (mol Pa^{-1} m^{-1} s^{-1}) διαπερατότητα
L/W	aspect ratio, length over thickness λόγος διαστάσεων, μήκος προς πάχος
$N(t)$	positron lifetime spectrum φάσμα χρόνου ζωής ποζιτρονίων

P	pressure (Pa) πίεση
P_w	vapour pressure (Pa) πίεση ατμών
R	free volume hole radius (Å) ακτίνα οπής ελεύθερου όγκου
R'	gas constant (J mol^{-1} K^{-2}) σταθερά των αερίων
S	sorption coefficient (mol m^{-3} Pa^{-1}) συντελεστής προσρόφησης
T_b^o	normal boiling point (K) κανονικό σημείο βρασμού
T_g	glass transition temperature (K) θερμοκρασία υαλώδους μετάπτωσης
T_m	melting point / temperature (K) θερμοκρασία/σημείο τήξης
V_f	free volume (Å^3) ελεύθερος όγκος
V_h	volume of a free volume hole (Å^3) όγκος οπής ελεύθερου όγκου
$V_{m,i}$	molar volume of group i, (m^3/mol) γραμμομοριακός όγκος της ομάδας i
ΔH_v	latent heat of evaporation (J/mol) ενθαλπία εξάτμισης
β^+	positron ποζιτρόνιο
δ, δ_0	solubility parameter (MPa$^{1/2}$) παράμετρος διαλυτότητας
δ_H	hydrogen bridges contribution to the solubility parameter (MPa$^{1/2}$) συνεισφορά των γεφυρών υδρογόνου στην παράμετρο διαλυτότητας
δ_d	dispersion contribution to the solubility parameter (MPa$^{1/2}$) συνεισφορά της διασποράς στην παράμετρο διαλυτότητας
δ_p	polar contribution to the solubility parameter (MPa$^{1/2}$) συνεισφορά της πολικότητας στην παράμετρο διαλυτότητας

γ	gamma photon γάμμα φωτόνιο
γ_s	surface tension (N/m) επιφανειακή τάση
λ	X-ray wavelength (nm) μήκος κύματος ακτίνων X
ν_e	electron neutrino ηλεκτρονιακό νετρίνο
ϕ	volume fraction of the particles κλάσμα όγκου σωματιδίων
τ	tortuosity δαιδαλώδες
τ_1	para-positronium lifetime (s) μέσος χρόνος ζωής παρα-ποζιτρονίων
τ_2	positron lifetime (s) μέσος χρόνος ζωής ποζιτρονίων
τ_3	ortho-positronium lifetime (s) μέσος χρόνος ζωής ορθο-ποζιτρονίου
τ_i	lifetime for positron annihilation in mode i (s) μέσος χρόνος ζωής για την εξαΰλωση ποζιτρονίων σύμφωνα με τον τρόπο i
θ	diffraction angle (°) γωνία περίθλασης
c	concentration συγκέντρωση
d	membrane thickness (μm) πάχος μεμβράνης
d_{001}	distance between (001) planes (Å) απόσταση ανάμεσα στα (001) επίπεδα
e^+	positron ποζιτρόνιο
e^-	electron ηλεκτρόνιο
m	mass (kg) μάζα

n	diffraction peak order τάξη κορυφής περίθλασης
t_0	time required to obtain a steady permeation flow through the membrane (s) χρόνος για σταθερή ροή μάζας μέσα από τη μεμβράνη
w	weight fraction κλάσμα βάρους
2C	solvent-based polyurethane resin ρητίνη πολυουρεθάνης σε διαλύτη
2M2HT	dimethyl, dihydrogenated tallow, quaternary ammonium
2MBHT	dimethyl, benzyl, hydrogenated tallow, quaternary ammonium
AR 0.96	water-based acrylic resin ακρυλική ρητίνη σε υδατική διασπορά
BEOA	montmorillonite organically modified with octadecylamine μοντμοριλλονίτης (MMT) τροποποιημένος με οκταδεσυλαμίνη
C10A	natural MMT modified with 2MBHT φυσικός MMT τροποποιημένος με 2MBHT
C20A	natural MMT modified with 2M2HT φυσικός MMT τροποποιημένος με 2M2HT
C30B	natural MMT modified with MT2EtOH φυσικός MMT τροποποιημένος με MT2EtOH
C93A	natural MMT modified with M2HT φυσικός MMT τροποποιημένος με M2HT
CEC	cation exchange capacity δυνατότητα ανταλλαγής κατιόντων
DSC	differential scanning calorimetry διαφορική θερμιδομετρία σάρωσης
DTA	differential thermal analysis διαφορική θερμική ανάλυση
FWHM	full width at half maximum πλάτος στο μισό ύψος της κορυφής
HT	hydrogenated tallow υδρογονωμένο tallow
M2HT	methyl, dihydrogenated tallow ammonium

MFFT	minimum film formation temperature ελάχιστη θερμοκρασία για τη δημιουργία του υμενίου
MMT	montmorillonite μοντμοριλλονίτης
MT2EtOH	methyl, tallow, bis-2-hydroxyethyl, quaternary ammonium
o-Ps	ortho-positronium όρθο-ποζιτρόνιο
p-Ps	para-positronium παρα-ποζιτρόνιο
PALS	positron annihilation lifetime spectroscopy φασματοσκοπία χρόνου ζωής εξαΰλωσης ποζιτρονίων
PCN	polymer/clay nanocomposite νανο-σύνθετο υλικό πολυμερούς/πηλού
PU 0.98	water-based polyurethane resin ρητίνη πολυουρεθάνης σε υδατική διασπορά
TGA	thermogravimetric analysis θερμοσταθμική ανάλυση
XRD	X-ray diffraction analysis ανάλυση με περίθλαση ακτίνων X

Σύνοψη

Σκοπός της παρούσας μεταπτυχιακής διατριβής είναι η παρασκευή νανο-σύνθετων υλικών πολυμερικής μήτρας ενισχυμένης με ανόργανα σωματίδια καθώς και ο προσδιορισμός των αλληλεπιδράσεων, και η μελέτη και ο χαρακτηρισμός των ιδιοτήτων τους. Κύριος στόχος είναι η μελέτη και κατανόηση της φύσης των συστατικών και των αντιδραστηρίων που χρησιμοποιούνται για την σύνθεση των νανοϋλικών, ώστε να προκύψει βελτιστοποίηση των ιδιοτήτων που αφορούν στην μείωση της διαπερατότητας αερίων από τις υπό μελέτη μεμβράνες/επιχρίσματα.

Τα νανοσύνθετα υλικά αποτελούνται από πολυμερική μήτρα ενισχυμένη με ανόργανα σωματίδια τα οποία έχουν τουλάχιστον μία διάσταση σε νανο-κλίμακα (nm). Οι ιδιότητες των σύνθετων υλικών που προκύπτουν είναι ιδιαίτερα βελτιωμένες σε σύγκριση με τα συμβατικά σύνθετα υλικά ή την αρχική, μη ενισχυμένη, μήτρα πολυμερούς. Εχουν παρατηρηθεί δραματικές βελτιώσεις σε ιδιότητες όπως το μέτρο ελαστικότητας, η αντοχή σε εφελκυσμό, η μέγιστη θερμοκρασία χρήσης (HDT), καθώς επίσης και μειωμένη διαπερατότητα σε διάφορα αέρια όπως διοξείδιο του άνθρακα, CO_2, οξυγόνο, O_2, κ.ά. Βασικό πλεονέκτημα είναι το γεγονός ότι η απαιτούμενη κατά βάρος συγκέντρωση της ανόργανης ουσίας είναι χαμηλή (συνήθως λιγότερο από 5 wt%). Συνεπώς, τα υλικά είναι ελαφρύτερα από τα περισσότερα συμβατικά σύνθετα υλικά. Επιπλέον, το μικρό αυτό απαιτούμενο ποσοστό ενίσχυσης του πολυμερούς καθιστά τα νανο-σωματίδια μια ιδιαίτερα οικονομική κατηγορία υλικών πλήρωσης για τα οργανικά πολυμερή. Ο λόγος που τα νανοτεμαχίδια οδηγούν στις βελτιώσεις αυτές οφείλεται κυρίως στις μορφολογικές παραμέτρους που τα χαρακτηρίζουν: το μέγεθος και το λόγο διαστάσεων. Το μέγεθος των τεμαχιδίων είναι σημαντικό, γιατί τα μικρά τεμαχίδια έχουν μεγαλύτερη ειδική επιφάνεια και έτσι δημιουργείται μεγαλύτερη διεπιφάνεια με το πολυμερές συγκριτικά με μεγαλύτερα τεμαχίδια. Οσο ο λόγος διαστάσεών τους αυξάνει, τόσο αυξάνει και η συνολική επιφάνεια τους για μια συγκεκριμένη μάζα. Π.χ., φύλλα αργίλου με μεγάλη διάμετρο σε σχέση με το πάχος τους, έχουν μεγαλύτερη ειδική επιφάνεια και είναι πιο αποτελεσματικά στην ενίσχυση του πολυμερούς από πιο χοντρά στρώματα.

Οι βελτιωμένες ιδιότητες προκύπτουν μόνο εφόσον το πυριτικό φυλλόμορφο ορυκτό είναι διεσπαρμένο πλήρως στα πρωτογενή του τεμαχίδια. Ετσι προκύπτει ένα πολυμερές πληρωμένο με λεπτά πλακίδια πυριτικού ορυκτού, με διαστάσεις της τάξης των 1×100×100 nm και με μία διεπιφάνεια της τάξεως των 700 m^2/g. Σημαντικός παράγοντας που επηρεάζει τα σύνθετα υλικά (nanocomposites) είναι ο μεγάλος λόγος διαστάσεων (L/D) των νανοπλακιδίων που χρησιμοποιούνται, συγκριτικά με τα συμβατικά (conventional composites), όπως σχηματικά αναπαρίσταται στο σχήμα 1.

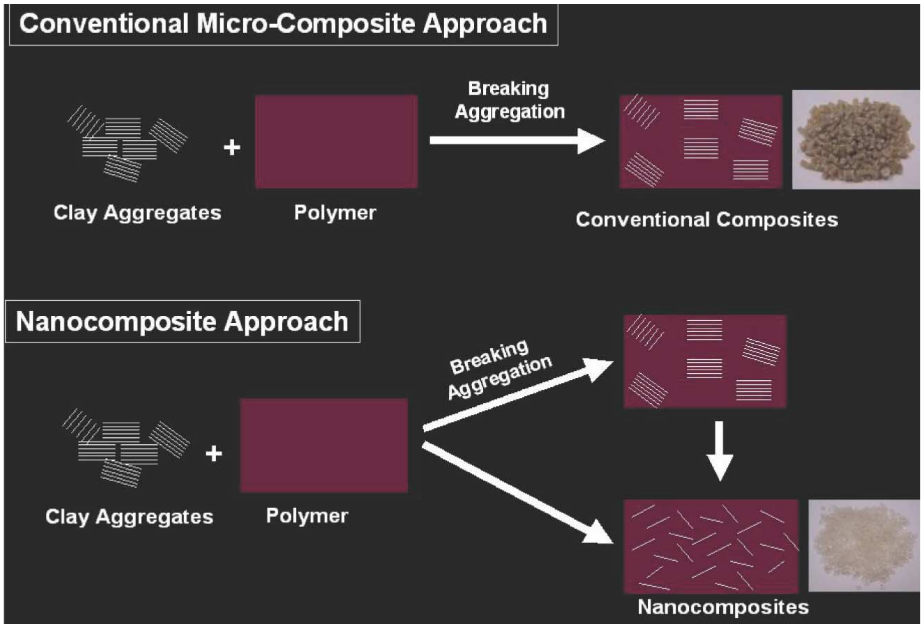

[Gao, 2004]

Σχήμα 1: Συμβατικά σύνθετα υλικά (conventional composites) και νανοσύνθετα υλικά (nanocomposites).

Τα νανοσύνθετα πολυμερών/φυλλόμορφων αργιλοπυριτικών ορυκτών έγιναν ευρύτερα γνωστά την δεκαετία του 1990 από ερευνητική ομάδα της Toyota Central Research & Development Co. Inc. (TCRD), με την σύνθεση του πολυαμιδίου/μοντμοριλλονίτη (Nylon-6/MMT), το οποίο αποτέλεσε το πρώτο εμπορικό νανοσύνθετο υλικό με άργιλο. Η ενίσχυση του πολυμερούς προέκυψε με ένα μικρό ποσοστό ανόργανου υλικού και οδήγησε σε σημαντικές βελτιώσεις των θερμικών και μηχανικών ιδιοτήτων του πολυαμιδίου. Συγκεκριμένα, παρατηρήθηκε πως με την προσθήκη μόλις 4.2 wt% ανόργανων σωματιδίων, το νανοσύνθετο εμφάνισε σημαντική βελτίωση σε ιδιότητες όπως αντοχή σε εφελκυσμό, αντοχή κάμψης και θερμική σταθερότητα. Σημαντικό είναι επίσης ότι το βάρος του νανοσύνθετου παρέμεινε χαμηλό , λόγω της πυκνότητας των σωματιδίων και της χαμηλής τους περιεκτικότητας (κλάσμα βάρους).

Σωματίδια

Ο κυριότερος τύπος φυλλοπυριτικών αργιλικών ορυκτών που χρησιμοποιείται για την σύνθεση των νανοσύνθετων πολυμερικών υλικών είναι ο πηλός αργίλου «2:1», οποίος περιλαμβάνει τον εκτορίτη (hectorite), τον μοντμοριλλονίτη (montmorillonite), τον σαπωνίτη (saponite) κ.ά. Τα ορυκτά αυτά ανήκουν στην οικογένεια του σμεκτίτη, ενώ η κρυσταλλική τους δομή απαρτίζεται από δύο εξωτερικά φύλλα αποτελούμενα από τετράεδρα πυριτίας (SiO_2), μεταξύ των οποίων κείτεται ένα κεντρικό φύλλο δομημένο από οκτάεδρα αλούμινας (Al_2O_3) ή μαγνησίας (MgO). Η διαμόρφωση αυτή επιτρέπει στα ιόντα οξυγόνου των οκταεδρικών φύλλων να ανήκουν και στα τετραεδρικά φύλλα. Το πάχος του δημιουργούμενου στρώματος είναι περίπου 1 nm.

Οι δομές αυτές αποτελούνται από τις συστοιχίες των ανωτέρω στρωμάτων. Οι πλευρικές τους διαστάσεις ποικίλουν και ξεκινούν από τα 300 Å ενώ είναι δυνατό να φτάσουν μέχρι μερικά μm. Το στοίβαγμα των στρωμάτων δημιουργεί έναν διαστρωματικό χώρο ή γαλαρία (gallery). Οι δυνάμεις που χαρακτηρίζουν την δομή είναι τύπου van der Waals. Σημαντικά χαρακτηριστικά των συγκεκριμένων ορυκτών, αναφορικά με την χρήση τους ως πληρωτικό μέσον σε νανοσύνθετα υλικά, είναι η αφθονία τους στην φύση, το χαμηλό τους κόστος και κυρίως ο μεγάλος λόγος διαστάσεων (aspect ratio), πλάτους προς ύψος, των ξεχωριστών φύλλων (L/D). Επιπλέον, το σχετικά χαμηλό ιοντικό φορτίο τους επιτρέπει στα μόρια του νερού να εισέλθουν ανάμεσα στα κρυσταλλικά επίπεδά. Αυτό οδηγεί σε διόγκωση της αργίλου. Κατά τη διάρκεια της διαδικασίας της διόγκωσης η απόσταση μεταξύ των πλακιδίων της αργίλου αυξάνεται, ενώ η ισχύς του ιοντικού δεσμού μειώνεται. Η δυνατότητά τους να υποστούν παρεμβολή (intercalation) είναι επίσης καθοριστικός παράγοντας στο βαθμό που μπορούν να τροποποιηθούν χημικά ώστε να γίνουν συμβατά με τα οργανικά πολυμερή.

Οργανική τροποποίηση του πηλού

Τα φυλλόμορφα αργιλοπυριτικά ορυκτά, όπως προκύπτουν στην φύση, είναι υδρόφιλα, γεγονός το οποίο τα καθιστά μη συμβατά με την υδρόφοβη φύση των περισσότερων πολυμερών. Εξαίρεση αποτελούν υδρόφιλα πολυμερή όπως το πολυαιθυλενοξείδιο (PEO) και η πολυβινυλική αλκοόλη (PVA). Προκειμένου τα ανόργανα σωμα-

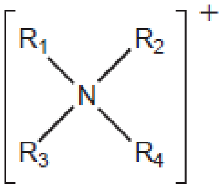

Σχήμα 2: Τετραπλό κατιόν αμμωνίου. Τα R_i είναι υδρόφοβες αλκυλικές αλυσίδες.

τίδια να καταστούν συμβατά με την οργανική φύση των πολυμερών, είναι αναγκαίο να υποστούν οργανική τροποποίηση των επιφανειών τους μέσω αντιδράσεων ιοντικής εναλλαγής, ώστε η εξασφάλιση της συμβατότητας να οδηγήσει σε ικανοποιητική διασπορά και αύξηση των αλληλεπιδράσεων με την πολυμερική μήτρα.

Η διαδικασία της ιοντικής εναλλαγής περιλαμβάνει την παρεμβολή των οργανικών μορίων μεταξύ των φύλλων της αργίλου: τα αρχικά κατιόντα των ενδιάμεσων στρωμάτων αντικαθίστανται με οργανικά κατιονικά επιφανειοδραστικά μέσα ή οργανικά μόρια που φέρουν χημικές ομάδες, οι οποίες μπορούν να δημιουργήσουν σύμπλοκα με τα κατιόντα. Τα κατιονικά επιφανειοδραστικά μέσα είναι ενεργές ενώσεις με τουλάχιστον μια υδρόφοβη αλκυλική αλυσίδα και μια ή περισσότερες υδρόφιλες ομάδες που φέρουν ένα θετικό φορτίο. Τα οργανικά κατιόντα ελαττώνουν την επιφανειακή ενέργεια του ορυκτού και βελτιώνουν την διαβροχή με την πολυμερική μήτρα. Για τις αντιδράσεις αυτές χρησιμοποιούνται, συνήθως, ενώσεις τετραπλού ιόντος αμμωνίου (Σχήμα 2).

Η διαδικασία της παρεμβολής οδηγεί σε διογκωμένους αργίλους. Το ποσό των κατιόντων που μπορεί να ανταλλαχθεί εκφράζεται από την 'ικανότητα ανταλλαγής κατιόντων' (cation exchange capacity, CEC) του αργίλου. Η ικανότητα ανταλλαγής κατιόντων ενός τυπικού μοντμοριλλονίτη νατρίου είναι της τάξης των 80 έως 140 meq (milli-equivalent) ανά 100 g του αργίλου.

Συνεπώς, τα στρώματα αργίλου είναι διαχωρισμένα λόγω της παρουσίας των οργανικών μορίων ανάμεσά τους. Το γεγονός αυτό χαμηλώνει την ιοντική αλληλεπίδραση μεταξύ των φύλλων της αργίλου και παρέχει ένα περιβάλλον που είναι συμβατό με τα πολυμερή. Με την εισαγωγή πολυμερών (ή μονομερών) στα διογκωμένα διαστήματα ανάμεσα στα στρώματα, μπορούν να προκύψουν πλήρως αποφυλλωμένα στρώματα και να δημιουργηθεί ένα νανο-σύνθετο υλικό.

Δομές νανοσύνθετων υλικών

Οι πιθανές θερμοδυναμικές διαμορφώσεις που μπορούν να προκύψουν, αναφορικά με τις αλληλεπιδράσεις ανάμεσα στα συστατικά που απαρτίζουν το υλικό, μπορούν να ταυτοποιηθούν με περίθλαση ακτίνων X (XRD) και είναι ως ακολούθως (Σχήμα 3):

- Διαχωρισμός φάσεων – immiscible nanocomposite

Τα ανόργανα εγκλείσματα διατηρούν την αρχική τους μορφή χωρίς να αλληλεπιδρούν με το πολυμερές. Το πολυμερές αδυνατεί να εισχωρήσει μεταξύ των στρωμάτων και έτσι προκύπτει υλικό που αποτελείται από χωριστές φάσεις. Χαρακτηριστικό της κατάστασης αυτής είναι η κορυφή που εμφανίζεται σε μια συγκεκριμένη γωνία ανάκλασης στα γραφήματα XRD. Η γωνία αυτή αντιπροσωπεύει τις αποστάσεις ανάμεσα στα κύρια κρυσταλλικά επίπεδα των ανόργανων συσσωματωμένων τεμαχιδίων.

- Δομή παρεμβολής – intercalated nanocomposite

  Οι αλυσίδες του πολυμερούς παρεμβάλλονται ανάμεσα στα φύλλα διαμορφώνοντας μία πολυστρωματική δομή εναλλασσόμενων πολυμερικών και ανόργανων στρωμάτων. Συνήθως παρατηρείται μία κορυφή στα γραφήματα XRD, η οποία όμως είναι μετατοπισμένη σε μικρότερες τιμές της γωνίας 2θ. Η μετατόπιση αυτή συνεπάγεται μια μικρής τάξεως αύξηση της απόστασης ανάμεσα στα φύλλα.

- Δομή αποφύλλωσης – exfoliated nanocomposite

  Τα μεμονωμένα στρώματα είναι πλήρως διαχωρισμένα και τυχαία διασκορπισμένα στην μήτρα του πολυμερούς. Η διαμόρφωση αυτή χαρακτηρίζεται από την απώλεια οποιασδήποτε κορυφής σε γράφημα XRD, γεγονός το οποίο επιβεβαιώνει την πλήρη αποφύλλωση των στρωμάτων της αργίλου. Οι αλληλεπιδράσεις ανάμεσα στο πολυμερές και τα σωματίδια μεγιστοποιούνται ενώ η διασπορά των σωματιδίων στο πολυμερές καθιστά την επιφάνεια των στρωμάτων διαθέσιμη.

Σύνθεση των υλικών

Η μέθοδος παραγωγής νανοσύνθετων πολυμερικών υλικών που χρησιμοποιήθηκε στην παρούσα μεταπτυχιακή διατριβή αποκαλείται παρεμβολή πολυμερούς από διάλυμα (intercalation of polymer from solution). Πρόκειται για διεργασία δύο σταδίων: αρχικά επιτυγχάνεται η διασπορά των σωματιδίων σε ένα μέσο διασποράς και έπειτα διασπορά στην μήτρα του πολυμερούς με απομάκρυνση του μέσου διασποράς.

Η σύνθεση των νανοϋλικών υπό μορφή επιχρισμάτων (membrane/film), περιλαμβάνει τα ακόλουθα στάδια:

Αρχικά τα ανόργανα σωματίδια υφίστανται αποφύλλωση σε ξεχωριστά στρώματα χρησιμοποιώντας κάποιο μέσο διασποράς: Απιονισμένο νερό στην περίπτωση των ανόργανων σωματιδίων ή κάποιος οργανικός διαλύτης για τα οργανικά τροποποιημένα σωματίδια. Το αιώρημα υπόκειται σε διαδικασία ανάμιξης με χρήση υψηλής διατμητικής ροής και υπερήχων. Επειτα, αφού επιτευχθεί η διόγκωση, το διάλυμα εισάγεται στο υδατικό αιώρημα της ρητίνης (πολυμερικής μήτρας), ενώ προστίθεται επίσης μικρή ποσότητα κατάλληλου διασταυρωτή. Ο τελευταίος είναι μια ουσία που προκαλεί τη διαδικτύωση των πολυμερικών αλυσίδων της ρητίνης (cross-linker) και τη σκλήρυνση του υλικού. Για την ανάκτηση μιας πλήρης διασποράς πραγματοποιείται και δεύτερο στάδιο ανάμιξης με χρήση διατμητικής ροής και υπερήχων. Η

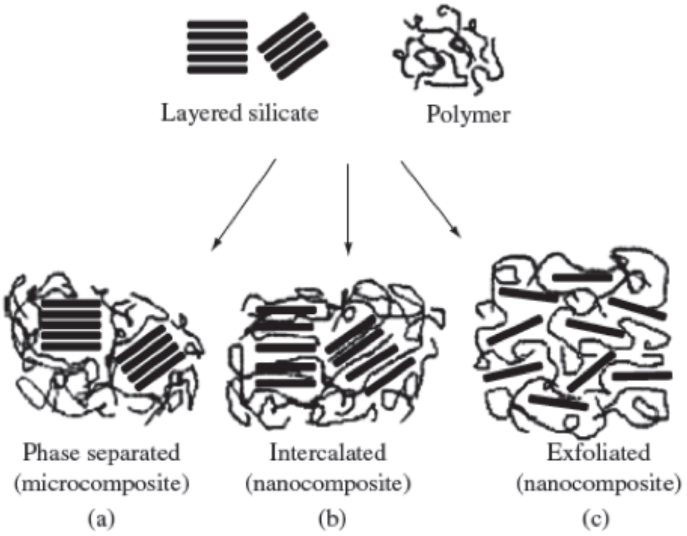

[Camargo et al, 2009]

Σχήμα 3: Καταστάσεις αποδόμησης των συσσωματωμάτων των πλακιδίων της αργίλου στα νανο-σύνθετα υλικά: a) διαχωρισμός φάσεων (συμβατικό σύνθετο υλικό), b) δομή παρεμβολής (νανο-σύνθετο υλικό), και c) δομή αποφύλλωσης (νανο-σύνθετο υλικό).

διασπορά που προκύπτει χρησιμοποιείται για να καλύψει πλήρως κατάλληλα φίλτρα (υπόστρωμα) ώστε να προκύψουν μεμβράνες/φιλμ. Τέλος, τα φιλμ υπόκεινται σε θερμική διαδικασία που εξυπηρετεί την τελική σκλήρυνση της ρητίνης μέσω της απομάκρυνσης του νερού και της εξάτμισης των διαλυτών.

Είναι σημαντικό να σημειωθεί πως η συγκεκριμένη μέθοδος σύνθεσης απαιτεί την αλληλεπίδραση και συμβατότητα ανάμεσα στα συστατικά που απαρτίζουν το σύνθετο υλικό: τα ανόργανα σωματίδια, την μήτρα του πολυμερούς και τους διαλύτες που χρησιμοποιούνται ως μέσα διασποράς. Είναι, συνεπώς, αναγκαίο να κατανοηθεί πλήρως η φύση των συστατικών που συμμετέχουν στην σύνθεση των νανοϋλικών καθώς επίσης και να γίνει μελέτη όλων των αλληλεπιδράσεων που προκύπτουν ανάμεσα στα συστατικά, ώστε το υλικό που προκύπτει να είναι πλήρως λειτουργικό και να καλύπτει τις απαιτήσεις.

Συστατικά

Τα νανοσύνθετα υλικά, στην παρούσα μεταπτυχιακή διατριβή, αποτελούνται από πολυμερικές ρητίνες ενισχυμένες με νανοσωματίδια μοντμοριλλονίτη, ο οποίος είναι μια τυπική φυλλόμορφη άργιλος, με κρυσταλλική δομή 2:1, και αποτελεί το κύριο συστατικό του ορυκτού μπεντονίτη.

Παρασκευάστηκαν δείγματα δύο τύπων ανάλογα με την φύση των σωματιδίων. Συγκεκριμένα, χρησιμοποιήθηκαν ανόργανα σωματίδια υδρόφιλου, μη τροποποιημένου MMT, ο οποίος μπορεί να διογκωθεί εύκολα στο νερό, καθώς και μια σειρά οργανικά τροποποιημένων και υδρόφοβων τύπων MMT οι οποίοι είχαν την εμπορική ονομασία Cloisite®.

Τα πολυμερή που χρησιμοποιήθηκαν ως μήτρα είχαν σαν βάση ακρυλικές ρητίνες και ρητίνες πολυουρεθάνης. Χρησιμοποιήθηκαν κολλοειδείς διασπορές σταγόνων ρητίνης πολυμερούς μέσα σε νερό (water borne) για δυο διαφορετικούς τύπους ρητίνης: μία ρητίνη πολυουρεθάνης και μία ακρυλική ρητίνη. Χρησιμοποιήθηκε και μία ρητίνη πολυουρεθάνης δύο συστατικών που περιείχε οργανικούς διαλύτες (solvent-based). Οι συγκεκριμένες ρητίνες ανήκουν στην κατηγορία των θερμοσκληρυνόμενων πολυμερών (thermosetting polymers) στα οποία η σκλήρυνση και δικτύωση των αλυσίδων επέρχεται όταν αυξηθεί η θερμοκρασία στο μίγμα πολυμερούς και σκληρυντή, π.χ. σε ένα φούρνο. Η θερμική αυτή διαδικασία εξυπηρετεί επίσης την εξάτμιση του νερού από το δείγμα καθώς και την απομάκρυνση κάθε πιθανού υπολείμματος διαλύτη.

Ως μέσο διασποράς των σωματιδίων χρησιμοποιήθηκαν κατάλληλοι οργανικοί διαλύτες (ακετόνη, αιθανόλη, ξυλένιο) ή/και απιονισμένο νερό.

Χαρακτηρισμός των υλικών

Για τον χαρακτηρισμό της δομής των νανο-σύνθετων υλικών έγινε χρήση φασματοσκοπίας περίθλασης ακτίνων X (X-ray Diffraction Analysis, XRD). Η τεχνική αυτή αποτελεί ερευνητικό εργαλείο για την μελέτη της κρυσταλλικής δομής των υλικών. Στην παρούσα έρευνα χρησιμοποιήθηκε για την μελέτη των αρχικών νανοσωματιδίων (υπό μορφή σκόνης) ώστε να καταγραφεί η γωνία περίθλασης για όλους τους τύπους MMT.

Μέσω της εξίσωσης Bragg και της τιμής 2θ για κάθε πηλό, υπολογίστηκε και η απόσταση ανάμεσα στα στρώματα της αργίλου (inter-layer spacing). Η τεχνική XRD δίνει επίσης μια σαφή εικόνα για την δομή των νανο-σύνθετων δομών, εφόσον γνωρίζουμε πως απώλεια κορυφής συνεπάγεται πλήρη αποφύλλωση των δομών στο πολυμερές.

Για την μελέτη της θερμικής συμπεριφοράς των υλικών έγινε χρήση των τεχνικών της θερμοσταθμικής ανάλυσης (Thermogravimetric Analysis, TGA) και διαφορικής θερμιδομετρίας σάρωσης (Differential Scanning Calorimetry, DSC). Η τεχνική TG/DTA αφορά στην συνεχή καταγραφή της μάζας ενός δείγματος σε μια ελεγχόμενη ατμόσφαιρα, ως συνάρτηση της θερμοκρασίας ή του χρόνου, καθώς η θερμοκρασία του δείγματος αυξάνει με τον χρόνο. Με την τεχνική DSC παρακολουθείται η διαφορά ροής θερμότητας προς μία ουσία-δείγμα και προς μία ουσία-αναφορά, ως συνάρτηση της θερμοκρασίας του δείγματος, εφόσον οι δύο ουσίες υπόκεινται σε ένα ελεγχόμενο πρόγραμμα θερμοκρασίας. Στα υπό μελέτη δείγματα, η θερμοκρασία υαλώδους μετάπτωσης (T_g) προσδιορίστηκε με DSC, ενώ η κατά βάρος περιεκτικότητα των δειγμάτων σε ανόργανη ουσία επιβεβαιώθηκε με μετρήσεις TGA.

Η μελέτη της συμπεριφοράς των νανοϋλικών και συγκεκριμένα του ελεύθερου όγκου, συναρτήσει της θερμοκρασίας, καθώς επίσης και συναρτήσει της κατά βάρος σύστασης σε νανο-σωματίδια, διεξήχθη με τη χρήση της τεχνικής φασματοσκοπίας χρόνου ζωής εκμηδένισης/εξαΰλωσης ποζιτρονίων (Positron Annihilation Lifetime Spectroscopy, PALS). Πρόκειται για τεχνική που καταγράφει τον χρόνο ζωής των ποζιτρονίων (e^+) στην ύλη μέχρι την εξαΰλωση τους με σύγκρουση με ηλεκτρόνια. Τα ποζιτρονια εκπέμπονται από μια ραδιενεργό πηγή και εισέρχονται στο δείγμα. Οταν συναντήσουν ένα ηλεκτρόνιο (e^-) επέρχεται η εκμηδένιση του ζεύγους e^+e^- (annihilation). Μεγάλος χρόνος ζωής συνεπάγεται ότι υπάρχουν περιοχές του πολυμερούς που είναι χαμηλής πυκνότητας σε e^- και άρα πρόκειται για περιοχές ελεύθερου όγκου. Μετρήσεις PALS πραγματοποιήθηκαν σαν συνάρτηση της θερμοκρασίας και αντλήθηκαν πληροφορίες για την συμπεριφορά του πολυμερούς, και συγκεκριμένα τον ελεύθερο όγκο, καθώς αυξάνεται η θερμοκρασία. Επιπλέον, μέσω της τεχνικής PALS προσδιορίστηκε και η θερμοκρασία T_g ορισμένων δειγμάτων και η τιμή συγκρίθηκε με τα αποτελέσματα που προέκυψαν από τις μετρήσεις DSC.

Τέλος οι ιδιότητες φραγής αερίων και συγκεκριμένα για το CO_2, μελετήθηκαν για έναν αριθμό δειγμάτων με διαφορετικές τιμές συγκέντρωσης ανόργανης ουσία. Η διεξαγωγή των μετρήσεων διαπερατότητας έγιναν υπό σταθερή πίεση, σε ένα κελί στο οποίο εσωκλείονταν η υπό μελέτη νανοσύνθετη μεμβράνη/επίχρισμα. Πραγματοποιήθηκαν μετρήσεις τόσο για τις αρχικές, μη ενισχυμένες μεμβράνες ρητίνης πολυμερούς, όσο και για νανο-σύνθετα φιλμ με αυξανόμενη κατά βάρος ενίσχυση από νανοσωματίδια. Από τις μετρήσεις αυτές είναι δυνατό να προσδιοριστεί ο συντελεστής διάχυσης των μορίων CO_2 από τον χρόνο που χρειάζονται τα μόρια να διαπεράσουν την μεμβράνη. Κύριος στόχος της έρευνας ήταν να προκύψουν επιχρίσματα/φιλμ τα οποία έχουν βελτιωμένες ιδιότητες φραγής. Οι τιμές του συντελεστή διάχυσης για τα νανοφίλμ θα πρέπει να είναι μικρότερες συγκριτικά με τις τιμές που αφορούν στην μη ενισχυμένη, καθαρή ρητίνη πολυμερούς.

Αναφέρουμε πως η διάχυση των αερίων μειώνεται καθώς αυξάνεται το μήκος της πορείας των μορίων μέσα στο υλικό. Πρέπει επομένως τα πλακίδια της αργίλου να διαχωριστούν πλήρως και να διασπαρούν τυχαία στην πολυμερική μήτρα ώστε να δημιουργούν φυσικά εμπόδια και συνεπώς να επιβραδύνουν τη διάχυση αερίων στο σύνθετο υλικό, καθώς τα μόρια του αερίου πρέπει να διαχυθούν μέσα από ένα πολύπλοκο δρόμο. Οι ιδιότητες φραγής επηρεάζονται από την ύπαρξη των σωματιδίων στο πολυμερές και συγκεκριμένα από τον λόγο των διαστάσεων των σωματιδίων, το κλάσμα όγκου των σωματιδίων καθώς και τον προσανατολισμό τους σε σχέση με την κατεύθυνση της διάχυσης.

Αποτελέσματα

Η διερεύνηση της δομής των νανοφίλμ προσδιορίστηκε με την χρήση διαφόρων τεχνικών οι οποίες παρέχουν πληροφορίες για τις αλληλεπιδράσεις μεταξύ των συστατικών που χρησιμοποιήθηκαν για την σύνθεση των υλικών αυτών. Τα αποτελέσματα παρουσιάζονται αναφορικά με την κάθε τεχνική που χρησιμοποιήθηκε:

- Οι μετρήσεις DSC πραγματοποιήθηκαν για τις τρεις ρητίνες πολυμερούς καθώς και για ένα δείγμα νανοσύνθετου υλικού ακρυλικής ρητίνης ενισχυμένης με 5 wt% ανόργανης ουσίας MMT (ARBE50). Τα δείγματα αρχικά θερμάνθηκαν σε θερμοκρασία 75 °C και παρέμειναν σε αυτήν για 1 min. Επειτα η θερμοκρασία αυξήθηκε από τους 75 °C στους 200 °C με ρυθμό θέρμανσης 10 °C/min. Η θερμοκρασία διατηρήθηκε στους 200 °C για 2 min και έπειτα τα δείγματα ψύχθηκαν έως τους 75 °C, με τον ίδιο ρυθμό των 10 °C/min. Η διαδικασία αυτή αποτέλεσε τον πρώτο κύκλο μετρήσεων (σχήμα 5.1) και επαναλήφθηκε σε δεύτερο στάδιο ώστε να επιβεβαιωθεί η πειραματική ακρίβεια των αποτελεσμάτων. Η μελέτη της θερμικής συμπεριφοράς των δειγμάτων αποσκοπούσε κυρίως στον προσδιορισμό της θερμοκρασίας υαλώδους μετάπτωσης, T_g. Τα αποτελέσματα των πειραμάτων αναπαραστάθηκαν γραφικά με την χρήση κατάλληλου προγράμματος. Η θερμοκρασία T_g προσδιορίστηκε με γραμμική προσέγγιση των πειραματικών σημείων για όλα τα δείγματα (σχήμα 5.2). Αναφορικά με τις δύο ρητίνες που είχαν βάση το νερό, προέκυψε θερμοκρασία υαλώδους μετάπτωσης στο εύρος θερμοκρασιών 120 – 130 °C ενώ για την ρητίνη με βάση το ξυλένιο στο εύρος 130 – 140 °C. Το νανο-σύνθετο δείγμα με ενίσχυση 5 wt% ανόργανης ουσίας παρουσίασε T_g περίπου ίσο με 125 °C, συνεπώς μπορούμε να αναφέρουμε πως η πρόσθεση νανοσωματιδίων, σε χαμηλό επίπεδο συγκέντρωσης, δεν επηρεάζει την θερμοκρασία T_g.

- Η τεχνική TGA χρησιμοποιήθηκε ως μέσο προσδιορισμού του ποσοστού ενίσχυσης των υλικών με ανόργανη ουσία MMT. Τα δείγματα θερμάνθηκαν από τους 100 °C έως τους 950 °C με ρυθμό θέρμανσης 50 °C/min, ενώ ο ρυθμός καταγραφής ορίστηκε ως 0.5 σημεία/s. Τα υπό ανάλυση δείγματα αρχικά ζυγίστηκαν σε ζυγό ακριβείας, ώστε να επιβεβαιωθεί η ακρίβεια της πειραματικής διάταξης του TG/DTA οργάνου. Αρχικά μετρήθηκαν δείγματα καθαρού πολυμερούς, των οποίων οι γραφικές αναπαραστάσεις του ποσοστού βάρους συναρτήσει της θερμοκρασίας επέστρεψαν μηδενικές τιμές (σχήμα 5.3). Επειτα μετρήθηκαν τα δείγματα ARBE10 και ARBE50, ενισχυμένα με 1.0 και 5.0 wt% MMT αντίστοιχα, των οποίων οι γραφικές αναπαραστάσεις επιβεβαίωσαν το ποσοστό του MMT που είχε υπολογιστεί θεωρητικά (σχήμα 5.4).

- Μέσω της τεχνικής XRD χαρακτηρίστηκε η δομή των νανοφίλμ που παρασκευάστηκαν εργαστηριακά. Επιπροσθέτως, μελετήθηκε η δομή των διαφόρων τύπων μοντμοριλλονίτη (ανόργανου, μη τροποποιημένου καθώς και οργανικά τροποποιημένου), υπό μορφή σκόνης (σχήμα 5.5). Η δομή των νανοσωματιδίων είναι επαναλαμβανόμενη και είναι χαρακτηριστική για κάθε τύπο MMT. Συνεπώς, μέσω της εξίσωσης Bragg και της τιμής της γωνίας περίθλασης, 2θ, για κάθε τύπο, υπολογίστηκε και η απόσταση ανάμεσα στα στρώματα της αργίλου (πίνακας 5.1). Τα αποτελέσματα, αναφορικά με τα αρχικά νανο-σωματίδια MMT, επιβεβαιώνουν πως καθώς αυξάνεται η υδροφοβικότητα του οργανικού τροποποιητή αυξάνεται και η απόσταση ανάμεσα στα φύλλα της αργίλου. Συγκεκριμένα, ο υδρόφιλος, μη τροποποιημένος τύπος μοντμοριλλονίτη παρουσίασε κορυφή σε γωνία 2θ = 6.36° που αντιστοιχεί σε διαστρωματικό πάχος, d_{001}, ίσο με 13.9 nm. Η υδροφοβικότητα της επιφανείας του τροποποιητή αυξάνεται ως εξής: C30B, C10A, C93A, C20A. Ετσι, σε αντιστοιχία προκύπτουν και τα εξής: ο τύπος C30B παρουσίασε κορυφή σε γωνία 2θ = 4.77° που αντιστοιχεί σε διαστρωματικό πάχος, d_{001}, ίσο με 18.5 nm, ο τύπος C10A κορυφή σε 2θ = 4.59° με d_{001} = 19.2 nm, ο τύπος C93A κορυφή σε 2θ = 3.74° με d_{001} = 23.6 nm ενώ ο τύπος C20A κορυφή σε 2θ = 3.65° με d_{001} = 24.2 nm. Τα αποτελέσματα αυτά είναι αναμενόμενα καθώς η τροποποίηση του MMT έχει σαν στόχο την συμβατότητα με την υδρόφοβη φύση των πολυμερών και συνεπώς καθιστά πιο εύκολη την είσοδο των αλυσίδων του πολυμερούς ανάμεσα στα φύλλα του μοντμοριλλονίτη. Η γραφική αναπαράσταση των XRD αντιστοιχεί στην πρώτη περίθλαση, όπου n = 1. Το εύρος μέτρησης γωνιών ξεκινούσε από 2° έως και 15°, ο ρυθμός καταγραφής ήταν ανά 0.02° για χρονικό βήμα ίσο με 0.2 s, ενώ το μήκος κύματος των ακτίνων X αντιστοιχεί σε λ = 1.5405 Å.

  Η τεχνική XRD χρησιμοποιήθηκε επίσης για την μελέτη των νανο-σύνθετων δομών. Η διερεύνηση της δομής με ακτίνες X κατέδειξε την επιτυχή ή μη διασπορά των νανοσωματιδίων, εφόσον απώλεια κορυφής συνεπάγεται πλήρη αποφύλλωση των στρωμάτων στο πολυμερές. Επιχρίσματα με βάση ρητίνη πολυουρεθάνης παρασκευάστηκαν με ενίσχυση υδρόφιλου MMT και διασπορά του σε απιονισμένο νερό, σε ποσοστά 0.50, 0.75, 1.00, 1.25 και 1.50 wt%. Τα αποτελέσματα της περίθλασης (σχήμα 5.6) δείχνουν πως πλήρη διασπορά έχει επιτευχθεί μόνο για το κλάσμα βάρους 0.50 %. Καθώς αυξάνεται το ποσοστό του μοντμοριλλονίτη, η κορυφή περίθλασης γίνεται πιο ευκρινής στα γραφήματα έντασης συναρτήσει της γωνίας περίθλασης και αντιστοιχεί σε τιμές 2θ = 6.4°. Αντίστοιχη διασπορά δοκιμάστηκε με υδρόφιλο MMT σε ακρυλική ρητίνη πολυμερούς σε ποσοστά 0.5, 1.0, 2.0 και 5.0 wt% (σχήμα 5.7). Παρατηρήθηκε παρόμοια συμπεριφορά με την PU ρητίνη, εφόσον δομές αποφύλλωσης επιτεύχθηκαν μόνο όταν η ποσότητα ενίσχυσης διατηρήθηκε σε χαμηλό επίπεδο (0.5 και 1.0 wt%).

  Αναφορικά με τους τροποποιημένους τύπους C10A και C93A (σχήμα 5.8 και 5.9): η διασπορά τους δοκιμάστηκε σε δύο τύπους διαλυτών, ακετόνη και αιθανόλη, σε ποσοστά 0.6, 1.2 και 1.8 wt% καθαρού MMT. Προκύπτει πως η ακετόνη, ως μέσο διασποράς, εισέρχεται επιτυχώς ανάμεσα στα φύλλα της αργίλου, ενώ για την αιθανόλη προκύπτουν δομές με διαχωρισμό φάσεων. Είναι ενδιαφέρον να αναφερθεί πως στην περίπτωση της αιθανόλης, η γωνία περίθλασης του συνθέτου αντιστοιχεί σε τιμή 2θ περίπου ίση με 6.4°, όπως και του υδρόφιλου MMT. Στην περίπτωση του τύπου C30B (σχήμα 5.10), παρατηρείται ομοίως κορυφή γύρω στις 6° για διασπορά σε αιθανόλη, ενώ για διασπορά σε ακετόνη προκύπτει αποφύλλωση σε ποσοστό 0.5 wt% καθαρού MMT. Σε ποσοστό ενίσχυσης 1.0 wt% έχουμε κορυφή γύρω στις 5°, όπως δηλαδή και η κορυφή του C30B, υπό μορφή σκόνης. Επιπροσθέτως, δοκιμάστηκε η διασπορά του πηλού BEOA, με οκταδεσυλαμίνη ως τροποποιητή, στους διαλύτες αιθανόλη, ακετόνη και ξυλένιο, χωρίς όμως επιτυχές αποτέλεσμα (σχήμα 5.11). Παρόλο που η κορυφή περίθλασης του BEOA είναι περίπου 4°, παρουσιάζεται και πάλι κορυφή γύρω στις 6° στο σύνθετο. Φαίνεται πως η ανόργανη φάση των τροποποιημένων σωματιδίων συμβάλλει ενεργά στις ρητίνες που έχουν βάση το νερό, εφόσον η χαρακτηριστική κορυφή περίθλασης στις μη αποφυλλωμένες δομές τείνει να εμφανίζεται στις 6.4°, ανεξάρτητα από τον τύπο τροποποιημένου MMT που έχει χρησιμοποιηθεί.

Για την διασπορά οργανικά τροποποιημένων σωματιδίων στην ρητίνη πολυουρεθάνης που ήταν διαλυμένη σε ξυλένιο χρησιμοποιήθηκε ως μέσο διασποράς ένα δυαδικό σύστημα διαλυτών ξυλένιου και αιθανόλης σε αναλογία 70:30 wt/wt %. Η ενίσχυση με νανο-σωματίδια αποπειράθηκε σε χαμηλό ποσοστό της τάξεως του 1.0 wt%. Η διασπορά του C10A φαίνεται πως ήταν επιτυχής (σχήμα 5.12) εφόσον τα δεδομένα XRD δεν παρουσιάζουν ουδεμία χαρακτηριστική κορυφή περίθλασης. Η διασπορά του C30B οδήγησε σε δομή παρεμβολής (σχήμα 5.13) και μετατόπιση της κορυφής σε χαμηλότερες τιμές γωνιών. Συγκεκριμένα προέκυψε αύξηση της απόστασης ανάμεσα στα φύλλα της τάξεως του 12 %, από 18.5 Å στα 20.7 Å, εφόσον η κορυφή των νανοσωματιδίων υπό μορφή σκόνης εμφανίζεται σε 2θ = 4.77° , ενώ η κορυφή στο νανο-σύνθετο σε 2θ = 4.27°. Η παρουσία μιας δεύτερης κορυφής σε 2θ = 6.4° μπορεί να αποδοθεί στο γεγονός ότι η δομή είναι εν μέρει αποφυλλωμένη και ενδεχομένως η ανόργανη φύση του τύπου C30B να επηρεάζει την τελική δομή. Στην περίπτωση της διασποράς του C20A προκύπτει δομή με μείωση της διαστρωματικής απόστασης (σχήμα 5.14) περίπου ίση με 5 Å, ενώ η διασπορά του BEOA (σχήμα 5.15) οδηγεί σε δομή παρεμβολής με 60 % αύξηση της απόστασης, από 21.5 Å στα 34.5 Å. Η επιτυχής διασπορά νανοσωματιδίων στην ακετόνη, σε αντίθεση με τον διαχωρισμό φάσεων που προέκυπτε από την διασπορά στην αιθανόλη, μπορεί να αποδοθεί σε θερμοδυναμικές παραμέτρους. Συγκεκριμένα, χρησιμοποιώντας τη θεωρία συνεισφοράς των ομάδων (group contribution theory) υπολογίστηκαν οι παράμετροι διαλυτότητας (solubility parameters) των τροποποιητών για τους τύπους C10A, C20A, C93A, C30B νανοσωματιδίων (πίνακας 6.2). Οι παράμετροι διαλυτότητας των οργανικών διαλυτών (ακετόνη, αιθανόλη και ξυλένιο) μπορούν να βρεθούν σε βιβλιογραφικές αναφορές και αναφέρονται επίσης (πίνακας 6.3). Βεβαιώθηκε έτσι πως οι τιμές που προκύπτουν για τις ομάδες τροποποίησης του MMT συμπίπτουν περισσότερο με τις τιμές της ακετόνης. Επομένως, η μη επιτυχής διασπορά στην αιθανόλη οφείλεται στην μεγάλη διαφορά ανάμεσα στις παραμέτρους διαλυτότητας.

- Μέσω της τεχνικής PALS προσδιορίστηκε ο ελεύθερος όγκος στην πολυμερική μήτρα σε κάθε νανοϋλικό. Οι μετρήσεις που πραγματοποιήθηκαν ήταν δύο τύπων:(α) έλεγχος ελεύθερου όγκου, υπό σταθερή θερμοκρασία δωματίου ίση με 300 K ως συνάρτηση του κατά βάρους ποσοστού ενίσχυσης MMT, και (β) έλεγχος του ελεύθερου όγκου συναρτήσει της θερμοκρασίας, από 300 K έως 473 K. Η τεχνική PALS χρησιμοποιεί ραδιενεργά ισότοπα ως πηγή παραγωγής ποζιτρονίων, τα οποία εισέρχονται στο δείγμα και αναζητούν περιοχές πλούσιες σε ηλεκτρόνια. Ο χρόνος που απαιτείται για να επέλθει η εξαΰλωση του ζεύγους ηλεκτρονίου / ποζιτρονίου καταγράφεται συνεχώς, παράλληλα με την ένταση της μέτρησης, και αποτελεί ένδειξη για την ηλεκτρονιακή πυκνότητα του υπό μελέτη δείγματος. Οσο αυξάνεται ο απαιτούμενος χρόνος για την εξαΰλωση του ζεύγους, τόσο πιο μεγάλες είναι οι περιοχές του ελεύθερου όγκου. Ο χρόνος ζωής των ποζιτρονίων μεταφράζεται σε ακτίνα οπών ελεύθερου όγκου, R, ενώ η ένταση μεταφράζεται σε συγκέντρωση οπών ελεύθερου όγκου V_f (%). Το ραδιενεργό ισότοπο για την διεξαγωγή των πειραμάτων ήταν ^{22}Na ενώ οι μετρήσεις που καταγράφηκαν για κάθε δείγμα υπερβαίνουν τις 10^6.

Τα δείγματα ακρυλικής ρητίνης με ενίσχυση υδρόφιλου MMT σε ποσοστά 0.5, 1.0 και 5.0 wt% (σχήμα 5.19) φανερώνουν πως ο χρόνος ζωής παραμένει σταθερός γύρω στα 2.2 ns. Επομένως πρόκειται για οπές ελεύθερου όγκου με ακτίνα γύρω στα 3 Å. Η ένταση της εκμηδένισης, από την άλλη μεριά, παρουσιάζει μείωση, ακόμη και για το δείγμα με συγκέντρωση 5% στο οποίο δεν έχει επιτευχθεί πλήρης αποφύλλωση. Το κλάσμα ελεύθερου όγκου μειώνεται, καθώς η συγκέντρωση MMT αυξάνεται. Τέλος, μελετήθηκαν τα δείγματα πολυουρεθάνης με βάση το ξυλένιο (σχήμα 5.21). Στην μη ενισχυμένη ρητίνη πολυμερούς απαιτείται χρόνος γύρω στα 2.4 ns, επομένως η ακτίνα των οπών είναι περίπου 3.2 Å. Η τιμή της έντασης στο δείγμα αυτό οδηγεί σε κλάσμα ελεύθερου όγκου ίσο με 5.6%. Παράλληλα, μελετήθηκαν δείγματα συγκέντρωσης 1 wt% με ενίσχυση σωματιδίων τύπου BEOA και C20A. Τα αποτελέσματα είναι σύμφωνα με εκείνα που προέκυψαν από την τεχνική XRD. Συγκεκριμένα, στο δείγμα με διασπορά πηλού C20A παρατηρείται αύξηση τόσο του χρόνου όσο και της έντασης. Συνεπώς, το κλάσμα ελεύθερου όγκου αυξάνεται από 5.6 % στο 6.2 %. Αντιθέτως, στο δείγμα με διασπορά τύπου BEOA, έχουμε μείωση του χρόνου και άρα μικρή μείωση της ακτίνας από τα 3.2 στα 3.1 Å.

Ενα γενικότερο συμπέρασμα που προκύπτει από την τεχνική PALS είναι το γεγονός πως η ακρυλική ρητίνη με βάση το νερό παρουσιάζει το χαμηλότερο κλάσμα ελεύθερου όγκου, 4.71 %, συγκριτικά με την ρητίνη πολυουρεθάνης με βάση το νερό, 5.11 %, και την ρητίνη πολυουρεθάνης με βάση το ξυλένιο, 5.64 %. Επιπροσθέτως, διεξήχθησαν μετρήσεις δύο δειγμάτων (μη ενισχυμένης ακρυλικής ρητίνης και ρητίνης ενισχυμένης με 1.0 wt% υδρόφιλου MMT) συναρτήσει της θερμοκρασίας. Τα αποτελέσματα αποδεικνύουν πως καθώς αυξάνεται η θερμοκρασία, αυξάνεται ο ελεύθερος όγκος των δειγμάτων (σχήμα 5.26). Με γραμμικές προσεγγίσεις των πειραματικών σημείων του δείγματος ARBE10 προκύπτει θερμοκρασία υαλώδους μετάπτωσης στο εύρος 100 - 110 °C. Με μετρήσεις DSC δείξαμε πως το T_g είναι περίπου 120 με 130 °C. Η διαφορά αυτή οφείλεται στον ρυθμό θέρμανσης της κάθε τεχνικής. Οι μετρήσεις PALS είχαν μεγαλύτερη διάρκεια συγκριτικά με εκείνες του DSC, εφόσον οι πρώτες διήρκεσαν αρκετές ώρες ενώ οι δεύτερες μόνο μερικά λεπτά της ώρας. Επιπλέον παρατηρήθηκε πως οι ρητίνες με βάση το νερό δεν παρουσιάζουν ιδιαίτερες διακυμάνσεις μεταξύ τους, αναφορικά στον ελεύθερο όγκο που προέκυψε από μετρήσεις PALS. Αντιθέτως, η ρητίνη με βάση το ξυλένιο διαφοροποιείται εφόσον δείχνει μεγαλύτερη ακτίνα οπών ελεύθερου όγκου καθώς και μεγαλύτερο κλάσμα συνολικού ελεύθερου όγκου.

- Μετρήσεις διαπερατότητας/φραγής αερίων διεξήχθησαν για έναν αριθμό δειγμάτων στα οποία μεταβαλλόταν η κατά βάρος συγκέντρωση ανόργανης ουσίας. Η πειραματική διάταξη περιλάμβανε ένα κελί κατάλληλα σχεδιασμένο ώστε να εσωκλείει το νανοφίλμ υπό μορφή μεμβράνης. Τα μόρια του αερίου, CO_2 στην παρούσα έρευνα, εισέρχονται υπό σταθερή πίεση στον όγκο του αριστερού τμήματος, διαπερνούν την μεμβράνη και παράλληλα καταγράφεται η ροή της συγκέντρωσης στο άλλο τμήμα του κελιού. Εάν παραστήσουμε γραφικά την μεταβολή της συγκέντρωσης του αερίου συναρτήσει του χρόνου, παρατηρούμε πως, έπειτα από κάποιο συγκεκριμένο χρόνο, η καμπύλη γίνεται ευθεία γραμμή. Ο χρόνος αυτός χρησιμοποιείται για τον υπολογισμό του συντελεστή διάχυσης. Σκοπός των πειραμάτων ήταν να προκύψουν μεμβράνες/επιχρίσματα με βελτιωμένες ιδιότητες φραγής. Αυτό απαιτεί τις τιμές του συντελεστή διάχυσης για τα νανοφίλμ να είναι μικρότερες συγκριτικά με τις τιμές στην μη ενισχυμένη, καθαρή ρητίνη.

  Δείγματα καθαρής ρητίνης πολυουρεθάνης και ακρυλικής ρητίνης μετρήθηκαν και προέκυψαν τα ακόλουθα αποτελέσματα: η ρητίνη PU με βάση το νερό έχει συντελεστή διάχυσης D = 7.4 cm^2/s, η ακρυλική ρητίνη με βάση το νερό έχει D = 2.3 cm^2/s, ενώ η ρητίνη PU με βάση το ξυλένιο έχει D = 4.6 cm^2/s (σχήμα 5.31). Η ενίσχυση της ρητίνης PU με 1.2 και 1.8 wt% πηλού C93A οδηγεί σε συντελεστή ίσο με 4.9 cm^2/s και 2.1 cm^2/s, αντίστοιχα. Συνεπώς, πρόκειται για μείωση του συντελεστή διάχυσης της τάξεως του 34% και 72 %, αντίστοιχα (σχήμα 5.35). Παρομοίως, η ενίσχυση της PU ρητίνης με 1.2 και 1.8 wt% πηλού C10A οδηγεί σε συντελεστή ίσο με 4.7 cm^2/s και 2.4 cm^2/s, άρα μείωση του συντελεστή διάχυσης της τάξεως του 36% και 68 %, αντίστοιχα (σχήμα 5.34). Στην περίπτωση της ενίσχυσης με υδρόφιλο MMT (σχήμα 5.32), έχουμε μείωση 72 % σε δείγμα με ποσοστό μόλις 0.5 wt% στην ρητίνη πολυουρεθάνης, ενώ μείωση εμφανίζεται επίσης σε δείγμα με ποσοστό 0.5 wt% στην ακρυλική ρητίνη, οπού ο συντελεστής μειώθηκε από 2.3 cm^2/s στα 1.8 cm^2/s άρα μείωση 22%.

Συμπεράσματα

Στην παρούσα μεταπτυχιακή διατριβή παρασκευάστηκαν μεμβράνες που βασίζονται στην ιδέα των νανο-σύνθετων υλικών. Πρόκειται για επιχρίσματα πολυμερικής μήτρας ενισχυμένα με σωματίδια μοντμοριλλονίτη, ενός φυλλόμορφου αργιλοπυριτικού ορυκτού.

Η διερεύνηση της τελικής δομής των φιλμ φανερώνει πως σε ορισμένες περιπτώσεις η δομή ήταν εκείνη της παρεμβολής, όπου παρατηρήθηκε μετατόπιση της χαρακτηριστικής κορυφής προς μικρότερες γωνίες. Αυτό συνεπάγεται την εν μέρει διεύρυνση των διαστρωματικών αποστάσεων και συνεπώς την διείσδυση των πολυμερικών αλυσίδων ανάμεσα στα φύλλα της αργίλου. Δομές αποφύλλωσης παρατηρήθηκαν κυρίως όταν η ποσότητα ενίσχυσης του MMT διατηρήθηκε σε χαμηλό επίπεδο. Πλήρης διασπορά των νανοσωματιδίων επιτεύχθηκε και στους τρεις τύπους ρητίνης. Στις ρητίνες με βάση το νερό η διασπορά πραγματοποιήθηκε σε απιονισμένο νερό καθώς και στην ακετόνη. Αναφορικά με την ρητίνη με βάση το ξυλένιο, η διασπορά ήταν επιτυχής για ένα μίγμα διαλυτών με κύριο διαλύτη το ξυλένιο. Η επιτυχής διασπορά στην ακετόνη, σε αντίθεση με τον διαχωρισμό φάσεων που προέκυψε από τη διασπορά στην αιθανόλη, μπορεί να αποδοθεί σε θερμοδυναμικές παραμέτρους.

Τα αποτελέσματα της παρούσας έρευνας προτείνουν πως η διαφορά των παραμέτρων διαλυτότητας του οργανικού τροποποιητή των νανοσωματιδίων και του διαλύτη πρέπει να είναι όσο το δυνατό μικρότερη. Οι μετρήσεις διαπερατότητας επιβεβαιώνουν πως η ενίσχυση πολυμερών με χαμηλά ποσοστά MMT μπορεί να οδηγήσει στην σύνθεση νανοϋλικών με βελτιωμένες ιδιότητες φραγής αερίων. Χαρακτηριστικά αναφέρουμε πως η μείωση στην διάχυση μορίων CO_2, στην παρούσα έρευνα, επιτεύχθηκε έως και ποσοστό της τάξεως 72 % για μόλις 0.5 wt% ενίσχυση. Συμπερασματικά, σημειώνουμε πως η διασπορά των σωματιδίων του μοντμοριλλονίτη είναι εφικτή εφόσον έχουν μελετηθεί οι παράμετροι που επηρεάζουν τις αλληλεπιδράσεις ανάμεσα στα συστατικά που μετέχουν στην σύνθεση των νανοϋλικών.

Κύριος παράγοντας που καθιστά τον MMT κατάλληλη επιλογή σωματιδίων είναι τα μορφολογικά χαρακτηριστικά που διέπουν την φύση του συγκεκριμένου αργιλοπυριτικού ορυκτού, εφόσον πρόκειται για σωματίδια με μεγάλο λόγο διαστάσεων. Επιπροσθέτως, το ότι τα σωματίδια του MMT μπορούν να υποστούν οργανική τροποποίηση συνεπάγεται πως είναι δυνατή η διασπορά και η αποφύλλωσή του στα περισσότερα πολυμερή, εφόσον με την τροποποίησή τους εξασφαλίζεται η συμβατότητα με την μήτρα του υδρόφοβου πολυμερούς.

Η παρούσα εργασία δείχνει ότι η χρήση κολλοειδών αιωρημάτων της πολυμερικής ρητίνης σε νερό είναι μια κατάλληλη μέθοδος για την παρασκευή νανο-σύνθετων επιχρισμάτων και υλικών.

Προτάσεις για βελτιώσεις

Η φραγή των αερίων επιτυγχάνεται με την τυχαία διασπορά των νανοσωματιδίων και την πλήρη αποφύλλωση των στρωμάτων τους στην μήτρα του πολυμερούς. Εφόσον προκύψει ο διαχωρισμός των πλακιδίων της αργίλου, αυξάνεται και το μήκος της πορείας των μορίων μέσα στην μεμβράνη καθώς τα πλακίδια συμπεριφέρονται ως φυσικά εμπόδια και επιβραδύνουν τη διάχυση των αερίων. Τα μόρια του αερίου πρέπει να ακολουθήσουν έναν πιο πολύπλοκο και χρονοβόρο δρόμο, συγκριτικά με την μη ενισχυμένη μεμβράνη του καθαρού πολυμερούς. Βασική παράμετρος που πρέπει να ληφθεί υπόψιν είναι πως οι ιδιότητες της διαπερατότητας επηρεάζονται από τις μορφολογικές παραμέτρους των σωματιδίων και συγκεκριμένα από τον λόγο των διαστάσεων, το κλάσμα όγκου καθώς και τον προσανατολισμό τους σε σχέση με την κατεύθυνση της διάχυσης. Τα περισσότερα μοντέλα μελέτης της διάχυσης των μορίων, αναφορικά στις ιδιότητες φραγής σε νανο-σύνθετα υλικά, βασίζονται στην εικασία πως ο προσανατολισμός των σωματιδίων είναι κατάλληλος ως προς την κατεύθυνση της διάχυσης των μορίων. Στα περισσότερα εργαστηριακά όμως δείγματα η υπόθεση αυτή δεν είναι σίγουρο πως ισχύει. Θα ήταν, επομένως, επιθυμητό να αναπτυχθεί ένας μηχανισμός για τον έλεγχο του προσανατολισμού, ώστε να προκύψουν φιλμ με τις βέλτιστες ιδιότητες φραγής. Η έρευνα της νανο-σύνθετων υλικών θα μπορούσε επιπλέον να επεκταθεί στην μελέτη της διάχυσης άλλων αέριων μορίων ώστε να προκύψουν υλικά που καλύπτουν μεγαλύτερο φάσμα εφαρμογών.

Chapter 1

INTRODUCTION

Nano-structured composites of montmorillonite-type silicates embedded within various polymer matrices have been intensively studied in recent years.

The major finding that stimulated the incorporation of nano-particles in polymer matrices was reported, for the first time, from Toyota Central Research & Development Co. Inc. (TCRD); they successfully prepared exfoliated Nylon 6/MMT nanocomposites. In the resulting composite with a loading of only 4.2 wt% clay the modulus had doubled in value, the strength had been enhanced by 50%, and an increase in heat distortion temperature (HDT) of 80 °C was seen compared to the neat Nylon 6, as shown in Table 1.1.

Since the development of montmorillonite/nylon nanocomposites by Toyota researchers, there has been a tremendous activity in the reinforcement of polymers by incorporating surface treated layered alumino-silicates. These nanocomposites, either intercalated or exfoliated, are found to be very effective in improving the physical, mechanical and thermal properties of polymers at very low filler loadings in comparison to conventional composites.

The investigation has been extended to a varying range of polymer systems including different types of clay, yet alternative methods that facilitate the dispersion of the inorganic clay into the organic matrix have to be established.

Table 1.1: Mechanical and thermal properties of Nylon 6/MMT nanocomposite

Properties	Nanocomposite	Nylon-6
Clay content (wt %)	4.2	0
Density (g/cm^3)	1.15	1.14
Tensile strength (MPa)	107	69
Tensile modulus (GPa)	2.1	1.1
Impact strength (kJ/m^2)	2.8	2.3
HDT (°C at 1.8 MPa)	147	65

[Okamoto, 2003]

1.1 The scope of the Thesis

Polymers are large molecules, consisting of many repeated structural units derived from monomers. Their chemistry is extremely diverse, and their concept is far from being simple. Yet, they are materials with a wide variety of properties and possess several advantages; they are light-weight, usually low-cost and can be easily processed and manufactured. Yet, the incorporation of nanoclay into polymers can dramatically enhance their properties. This makes the nanocomposites a promising area of study and a real challenge in the field of research. Further, apart from their improved properties relative to conventional composites or polymers, the fact that only very low clay addition is required for an improved performance, in the order of less than 5 wt/wt %, renders these nanocomposites an economically interesting field of research.

In the present work our attention is mainly drawn towards the gas barrier properties of polymer/clay nanocomposite systems. Many studies can be found in literature regarding their enhanced permeation properties; it has been reported that a reduction in gas permeability in the order of 50% to 500% can be attained by incorporating low silicate filler content, usually in the order of 5 wt % (or less) of nanoclay dispersion. [Yano et al., 1993] reported that in the presence of exfoliated organoclay the permeability of polyimide films to water vapour, helium, and oxygen is greatly reduced. Only 2 wt% addition of montmorillonite could result in permeability coefficients of various gases to values less than half of those of ordinary polyimide. This result is explained by an increase in the tortuosity factor. Similar reductions in permeability of nanocomposite films are also reported [Lan et al., 1994], [Messersmith and Giannelis, 1995], [Strawhecker and Manias, 2000], [Gain et al., 2005].

Wang et al [2005] investigated nanocomposites that involved the dispersion of rectorite in a matrix of styrene-butadiene rubber. The rectorite/SBR permeability was 68.8% lower than that of the pure SBR matrix. Such reduction in permeability can be attributed to the tortuous diffusional path that the gas molecules need to travel, due to the clay existence. Moreover, [Ogasawara et al, 2006] reported that the increase of montmorillonite loading in an epoxy matrix resulted in the decrease of the gas diffusivity of Helium.

This enhancement in permeation properties is accomplished due to the sheets of layered minerals that act as impermeable barriers to diffusing molecular species and, therefore, force the gas molecules to find alternative pathways in order to pass through the nanocomposite. It should be noted, though, that the gas barrier properties are only enhanced when the nano-layers are uniformly dispersed and not aggregated, so that they attain the highest amount of interfacial zone.

The concept is rather simple; the addition of organoclays in polymers increases the barrier properties by creating a maze or tortuous path [Ray and Okamoto, 2003]. The presence of filler (crystalline reinforcing particles), introduces a tortuous path for the diffusing gas penetrants; the reduction of permeability is due to the longer diffusive path that the penetrants need to travel in the presence of filler, since the particles are considered totally impermeable by the gas molecules.

This ‘zig – zag’ diffusion path of gas molecules in layered silicates is provided in figure 1.1. For comparison reasons, the diffusion path in conventional composites is also depicted in this figure.

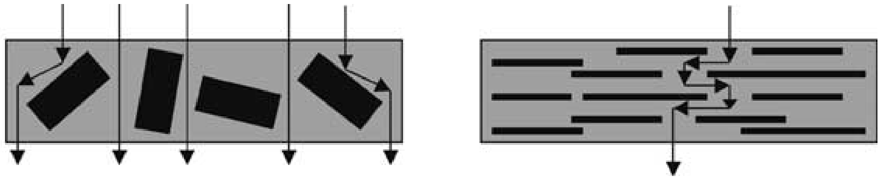

Ray and Okamoto [2003]

Figure 1.1: Diffusion path of gas molecules in conventional composite materials (left) and layered silicate nanocomposites (right).

Chapter 2

NANOCOMPOSITE MATERIALS

Polymer/clay nanocomposites present a relatively new generation of materials. The unique and functional properties of the nanocomposite films are the main driving force stimulating a huge development of such materials.

Polymer/clay nanocomposites are ternary systems; they are composed of clay particles (untreated and hydrophilic or organically modified and hydrophobic), organic solvents (and/or water) and a polymer matrix. The crucial stage is the selection and thus interaction of the three components involved. The compatibility between the clay particles and the polymer matrix is essential; if these components are not compatible with each other an increase in free volume in the matrix at the interfaces is probable to appear. It should be stated that the size as well as concentration of free volume holes in the nanocomposite can affect and control the rate of gas diffusion and permeation properties. On the other hand, it is also important to maintain good interaction between the clay and the solvents used as a dispersion medium, in addition to the interactions between the solvents and the polymer matrix. It is therefore evident that much effort needs to be devoted to the design of polymer / clay nanocomposites to ensure that they meet all needs and expectations.

Nanocomposites are particle-filled polymers. At least one dimension of the dispersed particles is in the nanometer range. This particular family of materials exhibits a significant enhancement in the properties of the polymer matrix at very low filler content, usually less than 5 wt%. Such enhancements might include an increase in thermal stability, higher modulus or increased strength. Furthermore, polymer/clay nanocomposites are ideal as barrier systems since their permeability and diffusion coefficient decreases with the addition of clay particles. The degree of these enhancements strongly depends on the final structure of the nanocomposite materials.

2.1 Structure and properties of inorganic particles

The fabrication of polymer/clay nanocomposites is usually based on a group of inorganic particles that belongs to the structural family known as 2:1 phyllosilicates. Their crystal structure consists of layers made up of two tetrahedrally co-ordinated silicon

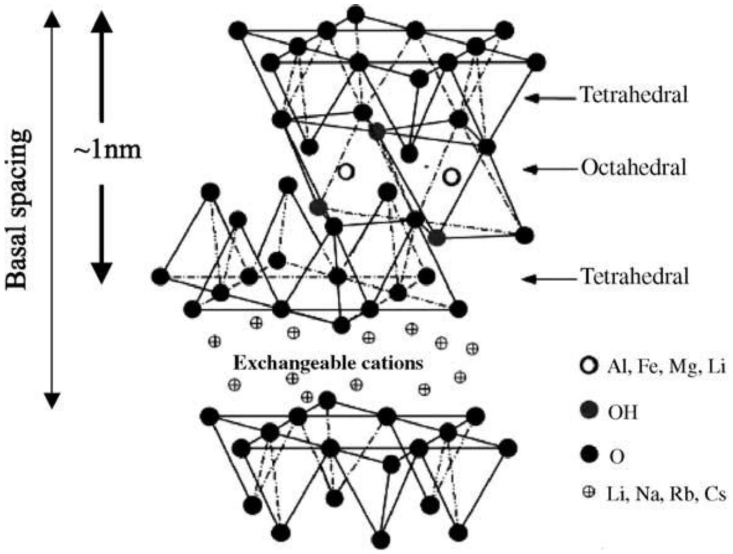

[Ray and Okamoto, 2003]

Figure 2.1: Crystal structure of 2:1 phyllosilicates.

atoms fused to an edge-shared octahedral sheet of either aluminium or magnesium hydroxide. The thickness of one such layer may be in the order of 1 nm, whereas the lateral dimensions range from 300 Å to several microns, depending on the particular silicate. This results in very high aspect ratios and large interfacial area. Their structure is illustrated in Fig. 2.1.

The aspect ratio (L/W) of mineral clays is a structural parameter that strongly affects the nano-scale arrangement; it takes into account both the length and the thickness of the dispersed particles. In the case of polymer layered silicate nanocomposites, high values of aspect ratio represent a well-exfoliated structure; whereas, low values of aspect ratio indicate a structure not completely exfoliated because the silicate aggregates increased the effective thickness of dispersed particles, as illustrated in figure 2.2.

The layers in clay minerals are held together by van der Waals forces and are organised to form stacks; the gaps between the layers are called galleries or simply interlayer spacing. A representation of such layers is provided in figure 2.3.

There are many types of phyllosilicates. The most frequently used are the montmorillonites, hectorites and saponites.

Montmorillonite (MMT) is a 2:1 phyllosilicate mineral and is the main constituent of bentonite. It has been employed in many nanocomposite systems due to the high aspect ratio (length over thickness) of its primary particles, which can lead to a decrease in the diffusion coefficient. In addition, this particular type of the smectite clay

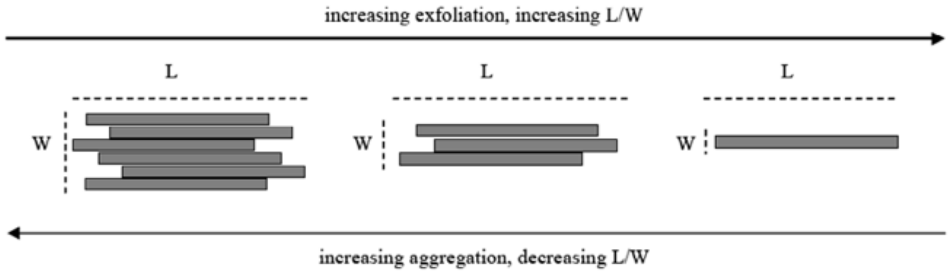

Figure 2.2: Effect of the incomplete silicate exfoliation on average value of aspect ratio of dispersed particles (L/W).

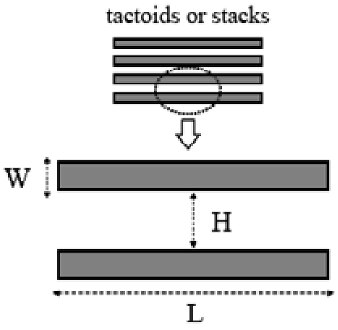

Mittal [2010]

Figure 2.3: Schematic representation of a layered silicate stack and its geometrical parameters: length and thickness of individual layers (L, W) and gallery height between two adjacent layers (H).

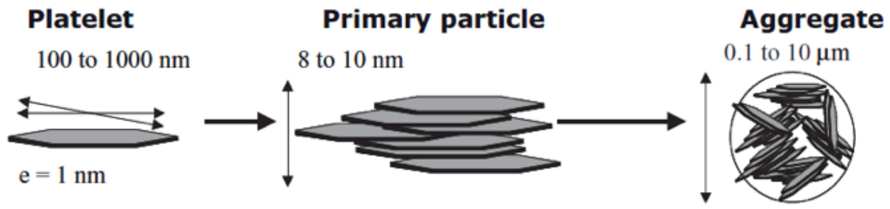

[Pascault and Williams, 2010]

Figure 2.4: Montmorillonite's multi-scale structure

family can be found in abundance, since it is naturally occurring, and, therefore, it is environmentally friendly and available in large quantities. Smectites are a valuable mineral class for industrial applications due to their high cation exchange capacity, surface area and surface reactivity.

Montmorillonite elementary particles (thickness $\sim$1 nm) are of platelet morphology; the primary particles include 5 to 10 platelets (size 8 to 10 nm) whereas the MMT aggregates consist of several MMT primary particles stacked together without any preferential orientation (size 0.1 to 10 µm), as shown in Figure 2.4. The chemical composition of MMT is $(Al_2Mg_3)(Si_4O_{10})(OH)_2 \cdot nH_2O$. Its structure is provided in figure 2.5.

The layers in MMT are held together by weak bonds. Hence water molecules and various ions can be attracted and enter the galleries between these layers. This can cause expansion of the clays enabling the delamination and the complete dispersion in water giving platelets with thickness of nano-dimensions.

The degree of the expansion of MMT strongly depends on the type of the exchangeable cations. Common clay minerals, such as montmorillonite, are hydrophilic in their pristine state, which renders them incompatible with the hydrophobic nature of most polymers. Due to this incompatibility the clay surface has to be chemically modified, in order to achieve complete dispersion and exfoliation of the clay nanoparticles into the polymer matrix. The surface modification can be realised through cation-exchange reactions, usually with salts (alkyl-ammonium or alkyl-phosphonium (onium) cations) that contain appropriate substituents to lower the surface energy and "hydrophobise" the clay mineral. The insertion of the cations into the galleries causes an increase in the inter-layer spacing which promotes the intercalation or exfoliation of the polymer chains into the galleries during the nanocomposite preparation. The modification of the nanoclay with the addition of cations through ion-exchange reactions is provided in figure 2.6.

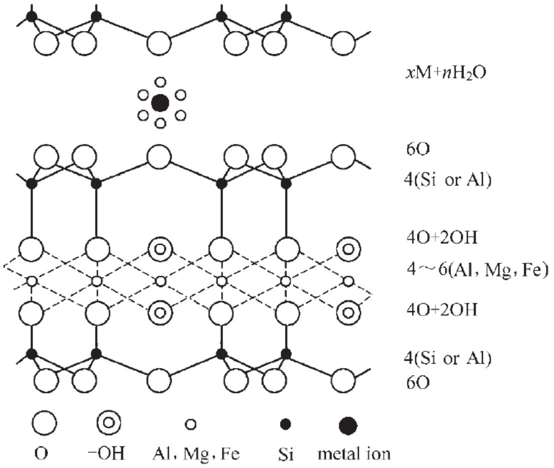

[Ke and Stroeve, 2005]

Figure 2.5: Diagrammatic sketch of montmorillonite

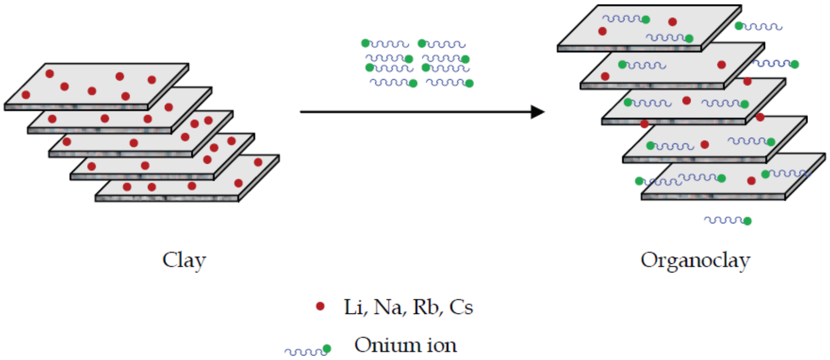

[Olad, 2000]

Figure 2.6: Schematic representation of the modification of clay layers with cations by ion-exchange reactions

2.2 Morphology of nanocomposites

Depending on the interaction between the inorganic clay particles and the organic matrix, and the level of intercalation and exfoliation of the polymer chains into the galleries, three types of morphologies can be achieved thermodynamically. The terms used to describe the nanocomposite morphologies are: immiscible, intercalated and exfoliated and are necessary to realise the performance benefits. These types are illustrated in figure 2.7 and explained below:

Immiscible nanocomposite There is poor physical interaction between the inorganic particles and the organic matrix. The clay platelets are incapable of dispersion or separation into primary particles in the polymer. The clay is, thus, dispersed as aggregates or particles with layers stacked together within the polymer matrix. As a consequence, an X-ray diffraction graph of this state is reminiscent of the graph for the pure clay powder; the nanocomposite diffraction peak is located at values equal to the ones of the pure organoclay.

Intercalated nanocomposite The polymer chains manage to penetrate into the galleries between the clay layers. The expansion of the original silicate layers results in the appearance of a new basal reflection at lower 2θ values, which corresponds to a larger gallery height. The peak is reminiscent of the pure clay peak, but shifted to lower 2θ. The resulting structure is a well ordered multilayer morphology with alternating polymeric and inorganic layers.

Exfoliated nanocomposite The silicate layers are completely separated and randomly dispersed throughout the polymer matrix. This state of exfoliation results in the absence of any clay peaks in the XRD spectra. The silicate layers are delaminated in the matrix and, thus, no coherent X-ray diffraction peak is visible in the graph.

2.3 Properties and applications of PCNs

The addition of clay minerals into a polymer matrix aims at the improvement of polymer properties, as well as the production of nanocomposites with appropriate characteristics for desired applications.

Polymer/clay nanocomposites are a new class of materials which differs from the conventional composites in terms of the interactions between the organic and inorganic phases. PCNs have several advantages and can be utilised to yield improvement in more than one property. Due to their low cost, availability and high aspect ratio, the nanoparticles can provide dramatic enhancements at very low filler loadings. As a consequence, the minerals are added into a series of new products for applications as engineering materials, functional materials, coatings, etc. These nanocomposites can be applied to fields where pure polymers or conventional composites have been utilised so far.

While the reinforcement aspects are a major part of the nanocomposite investigations reported in the literature, many other variants and property enhancements are under active study and, in some cases, commercialisation. The advantages that the

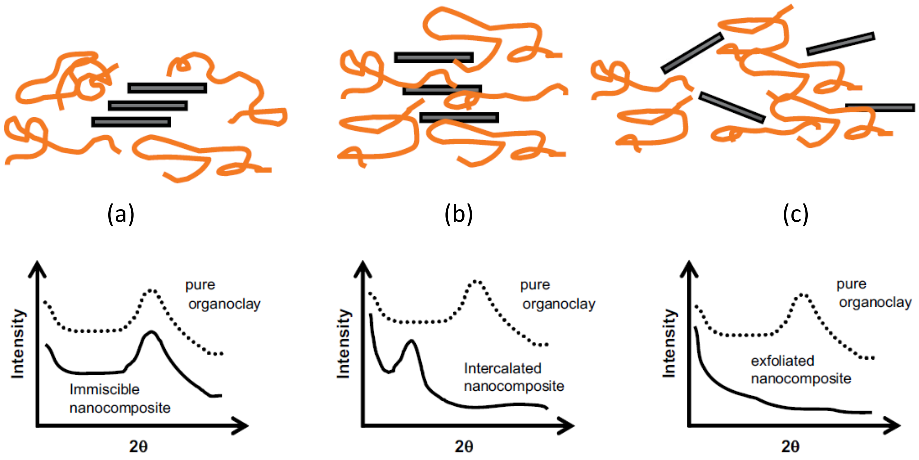

Paul and Robeson [2008]

Figure 2.7: Illustration of different states of dispersion of organoclays in a polymer matrix for a) immiscible, b) intercalated, c) exfoliated (top) and typical XRD patterns confirming such types (bottom).

incorporation of nano-particles yields can lead to a myriad of application possibilities. These include areas where mechanical and thermal properties are relevant, where barrier and anti-corrosive properties are needed, membrane separation, UV screens, flammability resistance, electrical conductivity, impact modification, and biomedical applications [Alexandre and Dubois, 2000]. It should be noted, though, that in order to take advantage of the potential offered by nanoparticles in such areas high levels of fully dispersed and delaminated nanoparticles must be achieved.

The nanocomposite materials used for packaging applications are designed to provide high barrier properties to gas molecules such as oxygen, O_2, and carbon dioxide, CO_2. The gas barrier properties are enhanced by the incorporation of high aspect ratio nano-platelets which create a complex network in the polymer matrix. The various penetrating gas molecules introduced into the nanocomposite diffuse slowly through the polymer chains of the amorphous part of the organic matrix around this network. The decreased diffusivity of oxygen and/or other gases mainly points to the use of the nanocomposites for food (e.g. to keep oxygen out) and liquid packaging (e.g. to keep carbon dioxide in). Moreover, they can be used as a plastic package or lightweight gas containers, to reduce the thickness of the commercial packaging materials, where a thick substrate is required in order to provide enhanced barrier properties to gases. This can lead to a significant amount of savings in the material costs and can make the polymer materials lighter.

Other application areas include the use of polymer/clay nanocomposites as fire retardant materials, engineering plastics or even impregnated clothes with good insulating properties. Their use in films and coatings has also been under investigation. The nanoparticles introduced into coatings create many positive effects in their properties and highly improve their quality. They provide new functions such as absorption of light or insulating sounds. The introduction of nanoparticles into traditional coatings can also improve their properties regarding adhesive strength, functionality, resistance to ageing and environmental protection. Further, the coating quality or grade is enhanced to a higher level.

Biomedical applications, electrical and electronic applications can also be added to the list. Polymer nanotechnology and nanocomposites are applicable to the emerging biomedical and biotechnological applications. Reports can be found in literature regarding tissue engineering applications, as well as the utilisation of electrically conducting nanofibres based on conjugated polymers for regeneration of nerve growth in a biological living system. Polymer matrix nanocomposites have also been proposed for drug delivery and release applications. The addition of nanoparticles can provide an impediment to drug release allowing slower and more controlled release. For instance, iron oxide nanoparticles have been investigated for various applications including drug delivery and cellular therapy.

The utility of polymer-based nanocomposites in areas of advanced devices for electronic and optoelectronic applications is quite diverse. One specific nanocomposite type receiving considerable interest involves conjugated polymers and carbon nanotubes. Potential applications include photovoltaic cells and photodiodes, sensors and light emitting diodes (LEDs). Other applications involve the dispersion of graphene sheets in polymers for applications in photovoltaic and field emission devices.

Chapter 3

COATINGS

3.1 Basics

Coatings are everywhere: they can be found in the house, on the walls and the furniture, on wires, computer systems, inside and outside of beverage cans and food packaging. Coatings are widely used for many purposes; they are applied to protect materials from a variety of detrimental effects of the environment. Adhesive coatings are used for the preparation of composite materials. Other coatings may serve as barriers for gases and liquids. They are used to improve the surface properties of an object (referred to as substrate), i.e. their appearance, adhesion properties, wettability, corrosion resistance, wear resistance, scratch resistance, etc.

Coatings are applied in the form of liquid, gas or solid. The coating materials that are applied in liquid form are either solutions of a resin and the rest of the components or suspensions in the form of colloidal droplets or particles in a suspension medium. This medium is often water. Apart from water-borne resins, solvent-based coatings are also used, although there is a strong trend nowadays towards the water-based varieties, due to the increasing attention to their environmental impact. The use of water instead of solvents leads to emission reduction. In addition, water presents no toxic hazard, is odour free, and its use does not require expensive recycling of the solvent. Economic reasons, thus, lead the industry towards water-borne coatings. However, water presents several problems in the application of the coatings; the evaporation of water is strongly affected by the relative humidity, RH %. When the RH increases, water evaporates slower, whereas when RH reaches 100 %, the evaporation of water stops. If there is water residue in the lower layers of a film, bubbles might be created, leading to a not properly cured film. On the other hand, in solvent-based systems, there is also the chance that years after the films have been formed, there will still be residual solvent left in them. This possible retention of solvents and/or water in coating films is a factor to be considered, since it can be a major problem in systems designed to cure rapidly.

3.2 Materials

Each coating usually contains several components, which fall into four general categories: the resin, the solvent(s), pigments and additives. These components are described below:

The resin In general, the resin is the most important component of the coating since it holds the system as a unit and creates a uniform consistency. Resins are also called binders; they bind together all the other substances in the coating. They are responsible for the formation of a continuous film that adheres to the substrate (the surface being coated), and present an adequate outer surface.

The resins are either one-component systems (just the liquid resin, or the resin in the solvent) or two-component systems (two parts, A and B, which need to be blended together to cause a chemical reaction). Either way, it is of significant importance to know the amount of resin that will be in the system after the solidification reaction.

Solvents or dispersion medium These are volatile components that control the viscosity during the application and the film formation and, therefore, allow the application of a coating in the liquid state. Most resins are solids or highly viscous materials. Thus, they have to be diluted with a liquid to lower their viscosity. This diluting agent can either be an organic solvent for the resin or just a suspension medium, such as water, in systems where the resin is in colloidal form.

It is of primary importance that the solvent dissolves the resin completely in order to obtain a solution that can be used to disperse other ingredients during the coating and film formation processes. After the application process, the solvents or the suspension media are supposed to evaporate to give a dry cured film with smooth and uniform surface.

Pigments and other particles These are mostly solid particles, coloured or non-coloured, which can be dispersed in a medium, such as the resin, without being dissolved. These components are the ones that give the colour to the produced film. Apart from their use for decorative and artistic purposes, pigments can also be used in coatings to enhance their UV resistance properties, their durability (when exposed to atmospheric weathering), their barrier properties (water resistance, protection when subjected to extreme weather conditions), or their mechanical properties (tough but also flexible films that resist abrasion).

It is worth mentioning that the nano-particles used in the present study fall into this category.

Additives These are ingredients that are included in small quantities (usually less than 5%) to modify some coating properties. Even though the major components of a film (by mass) are the resin, solvent and pigments, as mentioned above, in some cases these additives can play the role of specialised agents added to achieve the required performance. Examples are catalysts for the polymerisation reactions, stabilisers, and rheology modifiers.

3.3 Film formation

The predominant step in any coating process is arguably the formation of the film. This is the conversion of the coating from a liquid into a dry, solid and continuous film after its application on the substrate. The final cured film has to be uniform and all materials involved need to adhere strongly to the substrate. The process of film formation is critical to the ultimate appearance and performance of the coating. During the film formation of water-borne dispersions six processes occur that can be grouped into three stages and will be further discussed. It is worth mentioning though, that during this solidification process, where the liquid becomes solid, the resin goes through its glass transition, which is the most characteristic transition of the polymers. Basic information regarding the glass transition temperature is given below.

3.3.1 The glass transition in polymers

Polymers can be distinguished in two groups with respect to their structure: crystalline or amorphous. Materials that are completely crystalline undergo only one transition, the melting point, T_m, whereas completely amorphous polymers undergo a transition at T_g which marks the glass transition temperature. As for partially crystalline (semi-crystalline) polymers, they exhibit both transition temperatures. T_m and T_g are significant transitions that mark dramatic changes in the polymer properties. Their values strongly affect the mechanical properties and determine the temperature range in which the polymers can be processed or used. The differences between the two types are reflected in the changes of the specific volume with changing temperature. Thus, monitoring these changes of the free volume is the clearest way to understand the glass transition, as demonstrated in figure 3.1:

Crystalline material The specific volume increases slowly as the temperature increases. This behaviour is due to the vibrations of the atoms and molecules which increase with temperature. At the melting temperature the molecules suddenly attain the ability to move freely and the substance melts. Consequently, the material occupies more volume compared to that of the crystal, at the same temperature. Above this melting point, the specific volume still increases with increasing the temperature.

Amorphous material Similarly, at the beginning at least, there is an increase in the specific volume of the material as the temperature increases. Since a melting point does not exist now, there is no temperature at which an abrupt change in volume is observed. Yet, when reaching the glass transition temperature, there is a change in the rate of increase of the specific volume as a function of the temperature.

Semicrystalline material There is no 100% crystalline polymer. When crystallinity is present, then only a portion of the material is crystalline and the rest is amorphous. The material, thus, is a mixture and its behaviour is intermediate between those of the crystalline and the amorphous parts. The changes in the free volume around the glass transition take place only in the amorphous part.

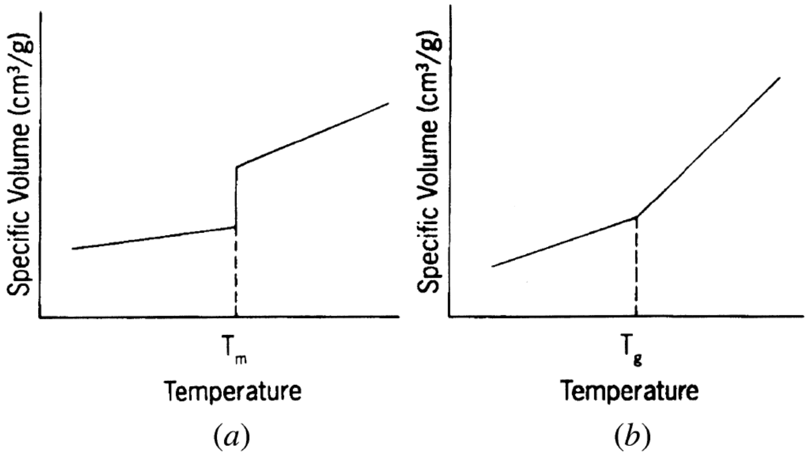

[Wicks et al., 2007]

Figure 3.1: Specific volume as a function of temperature for (a) crystalline material and (b) amorphous material.

> The crystalline part shows the melting/crystallisation transition. The changes in the mechanical properties around T_g, therefore, are not so strong and depend on the degree of crystallinity.

The polymers used in coating technology and applications are, with few exceptions, completely amorphous. As a consequence, it is the glass transition that needs to be fully understood for the present study. The glass transition can be defined in various ways, but in a broad sense, it signals the onset of small-scale motions in a polymer. The glass transition temperature marks an important change in all properties of a polymer. It is related to the mobility of the chain segments and to the amount of the thermal energy the polymer needs to change conformation in space. The T_g is heavily influenced by the chemical structure, in particular, by the structural groups of the polymer. By selection of the proper monomers, the glass transition temperature of the polymer and, therefore, the likely application area can be varied.

Around T_g the polymer changes from a hard and often brittle material into one with soft, rubber-like properties. The glass transition temperature is useful as a guideline and should be used to choose the appropriate application area. For instance, polymers that exhibit a T_g between 35 and 50 °C are suggested for general industrial coatings, whereas the ones that exhibit a T_g between 80 and 100 °C are suggested for heat resistant coatings.

For temperatures below T_g the segmental motions of the chain of an amorphous polymer are frozen, changes in free volume are restricted and the material exhibits properties associated with the solid state. Very slow relaxations can still occur, and these can have a significant impact on the properties of polymers. As the temperature rises above T_g, the specific volume increases faster due to the molecular motions that

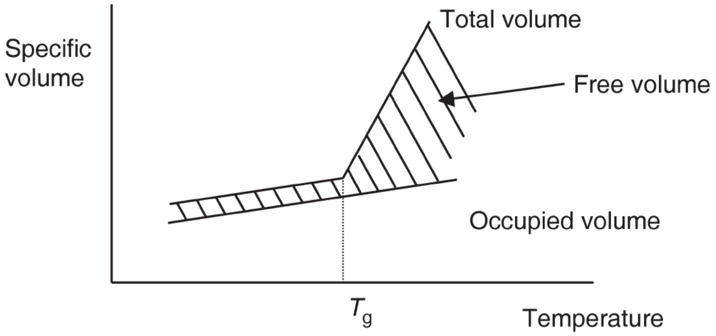

[Marrion, 2004]

Figure 3.2: Free volume - the 'empty space' in polymers - showing an increase at temperatures above the glass transition temperature, T_g.

are now possible and intensify as the restrictions on segment mobility decrease. The slope of the free volume vs. temperature curve (figure 3.2), thus, increases.

The value of the glass transition temperature can be estimated by making use of various techniques such as dilatometry, differential scanning calorimetry (DSC), dynamic mechanical analysis (DMA) and positron annihilation lifetime spectroscopy (PALS) a.o. It should be emphasised though, that the results obtained from different experimental techniques may vary; the measured T_g depends on the method and the conditions under which the experiments are conducted. The heating rate, for instance, is a significant factor that might affect the obtained value of T_g. When the heating rate is slow, there is more time for the molecular motions and for thermal expansion to take place. This means that the measurement returns a low value of T_g. On the other hand, if the heating rate is fast, the T_g values could be higher than the real (equilibrium) value. This pattern in T_g variations is also observed in the present work (DSC and PALS measurements) and will be discussed further in the experimental results section.

3.3.2 Stages of film formation

During film formation of a water-borne coating, a stable colloidal dispersion, comprising polymer particles in water, transforms into a continuous and homogeneous polymer film. The entire process of film formation in such dispersions includes six processes that can be divided into the following three stages:

1. Drying and particle ordering
2. Particle deformation
3. Polymer chain diffusion and coalescence

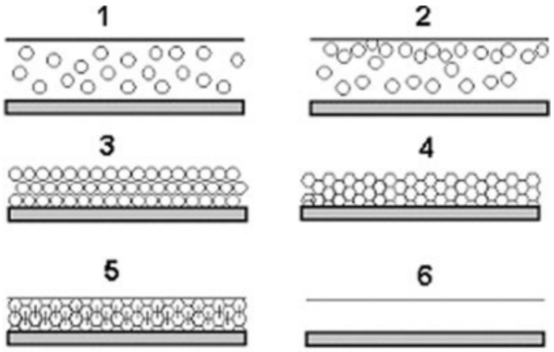

[Nobel et al., 2007a]

Figure 3.3: Stages of the film formation process regarding waterborne dispersions: 1 and 2 water evaporation/flocculation; 3 and 4 consolidation/coalescence; 5 and 6 coalescence/autohesion

Figure 3.3 schematically depicts the three stages during the process of film formation.

Stage I In most water-borne dispersions, the first step of drying refers to the process of water and solvent evaporation accompanied by the particle ordering. The particles initially move with Brownian motion, which leads to the creation of close-packed layers. External factors like air speed, relative humidity, and temperature of the environment influence the process of drying, during which the dispersion becomes less stable. This first step is the longest of the three and lasts until the polymer has reached approximately a volume fraction of 60-70 % [Steward et al, 2000]. It should be noted that the mechanism of water loss from water-borne dispersions is rather complex and strongly affects the structure of the final film:

Initially, the water evaporates at a constant rate close to that of pure water. This is observed when the dispersion is still dilute and water can escape freely through the water-air interface. Then, the rate of water loss starts to decrease rapidly. This is attributed to the increased region of coalesced film that reduces the total available area of the air-water interface. Finally, the deceleration of the water loss decreases. The remaining water escapes now from the film by diffusion through the polymer. More details regarding water/solvent evaporation are provided in section 3.4.2.

Stage II The second stage begins as soon as the particles come into contact. The polymer particles are deformed by strong forces to render a structure without voids. Casting at high temperatures gives the particles sufficient energy to overcome their mutual repulsion and pack into an ordered structure, leading, thus, to the formation of a continuous layer. The deformed particles during this step finally coalesce. The term coalescence is used to describe the fusion of two particles with the elimination of the boundary between them.

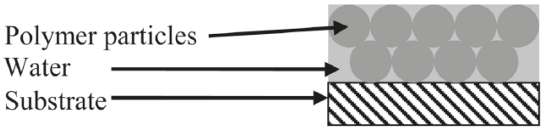

[Patel et al, 2010]

Figure 3.4: Condition of dispersion before stage II of particle deformation

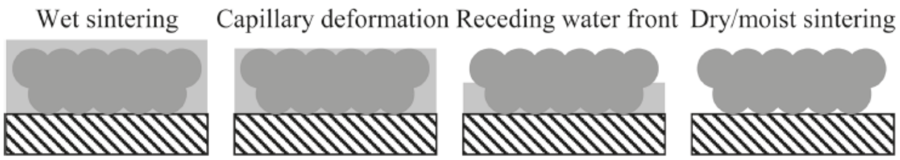

[Patel et al, 2010]

Figure 3.5: Possible mechanisms of driving forces regarding the particle deformation

The initial condition of the dispersion before the stage of particle deformation is illustrated in figure 3.4. The driving force of particle deformation can be the water-air, polymer-water or polymer-air interfacial tension. Dry sintering is driven by the polymer-air interfacial tension and refers to cases where the particles are sufficiently hard, so that the dispersion dries before the particles lose their shape on deformation. Wet sintering is driven by the polymer-water interfacial tension and refers to cases where the particles are sufficiently soft and they deform before the water evaporation. An alternative mechanism is capillary deformation (water-air interfacial tension) which suggests that the evaporation of water and particle deformation are concurrent phenomena. The water creates a capillary pressure in the film. These possible mechanisms are depicted in figure 3.5.

Stage III The third and last stage starts with the initial formation of a continuous film. The remaining water leaves the film by diffusion through any remaining holes. The particles lose their identity and the polymer chains become entangled. The polymer particles and molecules inter-diffuse across the particle-particle interface. Any thermosetting reactions take place at this stage and the film obtains its final mechanical properties, strength and form.

3.3.3 Film Formation Temperature

The formation of a continuous and transparent film is dependent on the temperature of the deposition process relative to the minimum film formation temperature, MFFT, of the polymer colloids [Wang and Keddie, 2009]. The MFFT, in turn, is dependent on the viscoelastic resistance of the polymer to deformation. A major factor also controlling MFFT is the T_g of the polymer in the particles [Wicks et al., 2007].

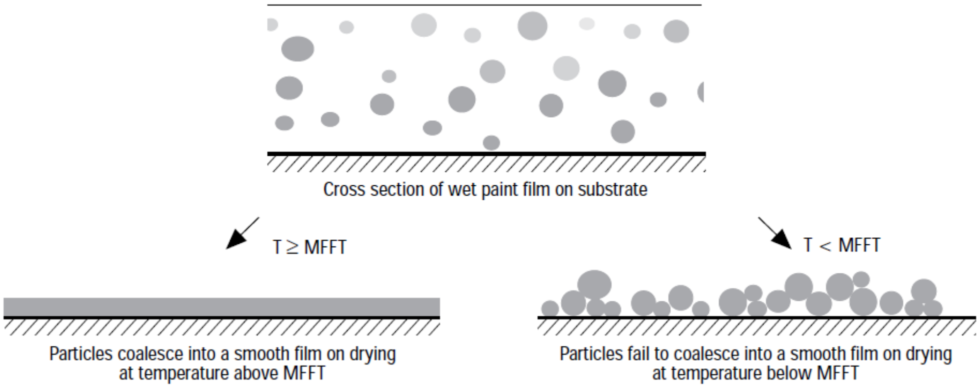

[Sewell, 1998]

Figure 3.6: The effect of temperature on the film formation process

The term MFFT has been described, [Sewell, 1998], as the minimum temperature at which a waterborne synthetic latex or emulsion will coalesce when laid on a substrate as a thin film. If the film is cast above its MFFT, and no pigments are present, then deformation and cohesion of the latex particles can occur leading to a smooth, clear and transparent film. However, if casting takes place below the MFFT, then a discontinuous, powdery film may form, which is typically opaque due to the presence of voids capable of scattering light. The two possible results of film formation regarding the effect of temperature are provided in figure 3.6.

In the case of thermosetting resins, the film formation temperature plays an important role since the dispersions that were applied on the filter substrate need to be conditioned in an oven in order to form a solid and continuous film.

3.4 Solvents

Various organic compounds and mixtures can be used as solvents and dispersion media for the initial form of the coating. Solvents can be classified in three broad categories: weak hydrogen-bonding, hydrogen-bond acceptor, and hydrogen-bond donor–acceptor solvents. The weak hydrogen-bonding solvents are non-polar aliphatic and aromatic hydrocarbons, such as xylene; the hydrogen-bond acceptor solvents are esters and ketones, such as acetone; the hydrogen-bond donor-acceptor solvents are alcohols, such as ethyl alcohol.

A solvent's character can be expressed in terms of solubility. The solubility parameter, δ is a significant factor that can be used for the rational selection of solvents.

The solubility of a solvent can be expressed by the three-dimensional system of Hansen; Hansen reasoned that since there are three types of interactive forces between molecules, there should be three types of solubility parameters. Thus, we obtain Hansen's solubility parameters for which the total solubility parameter is equal to the square root of the sum of the squares of the partial solubility parameters:

$$\delta_0^2 = \delta_d^2 + \delta_p^2 + \delta_H^2 \ , \tag{3.1}$$

where δ_0 is the total solubility parameter, δ_d is the component due to dispersion forces, δ_p is due to polar forces and δ_H is due to hydrogen bonding forces.

The dispersion (van der Waals) forces have low strength and are the only ones that hold non-polar symmetrical molecules together, e.g., the molecules of ethane. Non-symmetrical molecules, those having a dipole moment, interact with polar forces of varying strength. Classic hydrogen-bonding forces occur in substances where hydrogen (proton)-donor and proton-acceptor groups are present. Proton donors are groups where hydrogen atoms are directly attached to oxygen, nitrogen or fluorine atoms.

The three-dimensional solubility parameters can be determined or calculated by a variety of methods. Table 6.3 lists the solubility parameters for the solvents used in the present work.

3.4.1 Solvent selection

The proper selection of solvents for polymer/clay nanocomposites is a great challenge and may have a detrimental effect on the structure and final properties of nanocomposites, since the preparation method involves the dispersion of the nanoclay into a solvent prior to its dispersion in the polymer matrix.

Numerous studies have been carried out concerning the solvents used in nanocomposites and their effect on the interactions in polymer/clay systems [Ho and Glinka, 2003; Burgentzle et al, 2004]. The dispersion and degree of exfoliation of inorganic particles into the organic matrix depends on the solvents, and particularly on the balance between their hydrophilic and hydrophobic character. In addition, solvents with relative low polarity and poor-hydrogen bonding force would preferentially interact with the hydrophobic organically modified clay surface [Tran et al, 2006]. It is also reported that solvents that combine high polarity with high organophilic characteristics might be the most effective for the dispersion of inorganic clay nanoparticles. Examples of such solvents are benzonitrile and nitrobenzene [Jordan, 1949]. On the contrary, toluene which is highly organic but not sufficiently polar and acetonitrile which is polar but deficient in organic character do not meet the expectations. For comparison reasons, the chemical formula of these solvents is illustrated in figure 3.7

3.4.2 Solvent evaporation rates

During application and film formation, the volatile materials involved in the coating tend to evaporate out of it. The rate at which evaporation occurs affects not only the time required to convert a coating to a dry film, but also the thermosetting reaction, and the appearance and physical properties of the final film.

In the case of single solvents the rate of evaporation is affected by four variables: the temperature (at and near the surface), the vapour pressure, the surface/volume ratio (available surface through which mass transfer takes place), and the rate of air

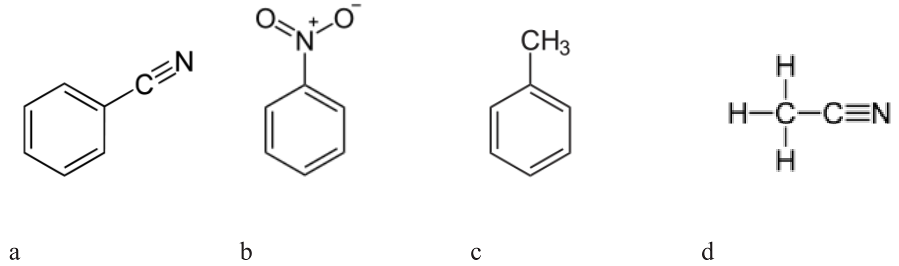

Figure 3.7: The chemical structure of (a) benzonitrile, (b) nitrobenzene, (c) toluene, (d) acetonitrile solvents

flow over the surface. The rate of evaporation of water is also affected by relative humidity.

The evaporation of solvents from water-borne coating films is a more complex process. Stefanis and Panayiotou [2008] described two stages for the drying phenomena encountered in film formation by solvent evaporation.

In the first stage, the initial rates of evaporation are almost the same as the rates of evaporation of the solvents alone under the same conditions: temperature, vapour pressure, air flow over the surface and surface to volume ratio. Similar to what is described in section 3.3.2 for the water, however, as solvent loss continues, a stage is reached at which the rate of evaporation slows sharply. As the viscosity of the coating increases, the availability of free volume decreases. During the second stage, the diffusion rate of solvent molecules is controlled by free volume availability. The rate of solvent evaporation becomes dependent on the rate of diffusion of solvent molecules through the film; the solvent molecules move through the film by jumping from free volume hole to free volume hole.

Although the boiling point is an important property of the solvents for the curing process of film formation, yet it is a poor indicator for the evaporation process, as [Wicks et al., 2007] reported. Before diffusion starts to control the process, the vapour pressure is a better indicator of a liquid's evaporation rate, since it relates to the tendency of the particles to escape from the liquid at the given temperature. The vapour pressure at some temperature, T (K), below the normal boiling point, T_b^o, is found by the Clasius-Clapeyron equation:

$$\ln P_w = \frac{-\Delta H_v}{R'}\left(\frac{1}{T} - \frac{1}{T_b^o}\right) . \tag{3.2}$$

For comparison reasons, the boiling points and vapour pressure of the solvents used in the present work are provided in Appendix A (Table A.3). For instance, acetone has a boiling point of 56 °C and o-xylene has a boiling point of 144 °C, but at 20 °C, their respective vapour pressures are 240 and 6.0 hPa. Consequently, acetone evaporates more rapidly than o-xylene, at 20 °C, under the same conditions.

3.5 Applications of coatings

Hundreds of different types of coatings are used to protect a variety of materials from corrosion, wear, and erosion, or even to provide thermal insulation [Marrion, 2004]. For instance, thermal barrier coatings must operate in the most demanding high-temperature environment of aircraft and industrial gas-turbine engines. They are comprised of metal and ceramic multilayers to insulate engine components and improve the durability and energy efficiency of these engines.

Coatings are widely used in structures and buildings that include concrete, brick, wood, steel and plastic substrates to protect them in case they are exposed to weather conditions. Wood, for example, is a porous material and inclined to expand and contract with variations in humidity. Applications can also be found in steel structures such as bridges and pipelines to enhance their corrosion resistance, as aircraft exterior coatings, or food and beverage cans that need to be lined with a continuous film of a highly resistant material.

The functionality of coatings is also addressed in printing processes such as on paper and fabric, self adhesive properties in addition to water resistant or waterproof coatings.

In the present work our interest lies on the application of coatings as barrier layers on packaging that prevents the diffusion/permeation of small molecules, such as gases. These coatings can prevent, e.g., harmful gases to enter the packaged product (e.g. oxygen into food) or desired gases to leave the product (e.g. carbon dioxide from carbonated beverages). They can be used to impregnate clothes for personal protection against harmful gases in cases of chemical accidents, to protect objects against pollution gases, etc.

Chapter 4

EXPERIMENTAL

4.1 Materials

4.1.1 Resins

Three types of resins were used in this study: a two-component solvent-based polyurethane resin (referred to as “2C”), a water-borne polyurethane resin system (“PU 0.98”) and a water-borne acrylic resin system (“AR 0.96”).

Polyurethanes are polymers composed of a chain of organic units joined by carbamate linkages. The acrylic resin stands for a group of organic substances derived from acrylic acid, methacrylic acid or other related compounds. For comparison reasons, the chemical structure of carbamate, as well as acrylic acid, are provided in figure 4.1

In the case of the waterborne polyurethane resin, a methylated melamine-formaldehyde resin was used as the crosslinking agent under the brand name Cymel 328 by Akzo-Nobel Paints. This crosslinker has good compatibility with the polyurethane resin, is designed for low temperature curing and for fast reaction speed, and is suitable for fast cure in waterborne coating formulations and systems. The same cross-linking agent was used for the water-borne acrylic resin. In the case of the solvent-based resin, the resin and the hardener are dissolved in a one-to-one ratio (1:1 v/v %) in the solvent.

The resins used are thermosetting polymers (a term applied to polymers that cross-link when heated or that can cross-link at ambient temperature). Therefore they need to be conditioned in an oven at specific temperature ranges in order to form a solid

Figure 4.1: Chemical structures of carbamate (left) and acrylic acid (right)

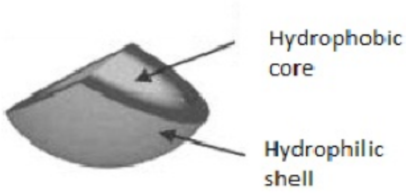

Figure 4.2: Core-shell structure of water-based resins

film.

The water-borne polyurethane and acrylic resins used in the present study are colloidal dispersions in a liquid continuous phase, demineralised water in our case. The colloidal droplets are approximately 60 - 70 nm in diameter and have a core-shell structure (figure 4.2) consisting of a hydrophobic core and a hydrophilic shell. The suspension contains 40 wt% polymer droplets.

The density of the cured resins are approximately 1.0, 1.1 and 0.9 g/cm^3 for "PU 0.98", "AR 0.96" and "2C", respectively. The relationship between the weight percentage of solid resin in the dispersion and the volume fraction of solid resin in the dispersion can be calculated using the following equation:

$$V_{f,resin} = \frac{\frac{w_{resin}}{\rho_{resin}}}{\frac{w_{resin}}{\rho_{resin}} + \frac{1 - w_{resin}}{\rho_{water}}} \tag{4.1}$$

For instance, 40 wt% of the polyurethane dispersion contains a volume fraction of 39.7% of solid resin, whereas 40 wt% of the acrylic dispersion contains 37.7 v/v %.

4.1.2 Clays

The montmorillonite clays occur naturally as sheets or platelets stacked together in minerals such as bentonite. They are supplied as agglomerated stacks of platelets and under the influence of a polar activator, such as alcohols or water, and mechanical dispersion, the platelets become fully dispersed. The pure MMT nanoclay (Na-montmorillonite, referred to as 'BE'), with the chemical formula $H_2Al_2O_6Si$ and molecular weight of 180.1 g/mol, was supplied from Sigma-Aldrich, in the form of granules, and used as received. It is hydrophilic and has a density of 2.7 g/cm^3.

The organically surface modified clay (BEOA), modified with 25 to 30% octadecylamine ($CH_3(CH_2)_{16}CH_2NH_2$) was also supplied from Aldrich.

Other clays used in the study were natural montmorillonites modified with organic modifiers, under the trade name of Cloisite®, namely C10A, C20A, C30B, C93A. The chemical formulas of these clays are shown in Table 4.1.

An important property of the organoclays is their cation exchange capacity (CEC), which represents the surface charge of the clay and is expressed as meq/100g clay. This and other properties of the Cloisite clays are provided in table 4.1.

4.1.3 Solvents

Demineralised water as a suspension medium and three organic solvents (xylene, acetone, and ethyl alcohol) were mainly used in this study. Their chemical structure, relative polarity and solubility parameters are useful factors that need to be taken into consideration when it comes to choosing the type of clay. Some typical properties of these solvents are provided in tables 4.2 and 4.3.

As far as the solvents miscibility is concerned, it can be found in the literature that acetone as well as ethyl alcohol is miscible in water in all proportions (100% w/w). O-xylene is immiscible in water but miscible in ethyl alcohol. The solvents miscibility table is included in appendix A.

4.2 Sample Preparation

The MMT clay in dry form exists in clusters or aggregates of platelets with low aspect ratio. Little surface area of the montmorillonite is, then, exposed. The challenge is to create conditions favourable for the exposure of all this potential surface area to the polymer, i.e., exfoliation. The exfoliation can be verified when the individual montmorillonite platelets no longer exhibit an XRD reflection peak. When this condition is achieved, the promised surface area is exposed and high aspect ratios are gained. In conclusion, the aggregates of MMT must be exfoliated into primary platelets, and these platelets must be distributed throughout the polymer matrix homogeneously.

In this study, the preparation method involved the dispersion of the nano-layers into a solvent prior to dispersion in the polymer matrix. A clay suspension was prepared first by introducing the layered clay particles into the solvent (or mixture of solvents). To achieve the intercalation of the solvent into the stacked layers, the mixture was subjected to both high-shear mixing and ultrasound. The solutions were stirred upon application of high shear with the use of a batch homogeniser, Polytron PT 45/80 (Kinematica, inc.). The suspensions were then exposed to sonication for several minutes, with an Ultrasonic Processor UP 400s, of 400 W, frequency of 24 kHz, adjustable amplitude of 20 to 100% and adjustable pulse from 0 to 100%. The required amount of clay suspension was then added into the organic matrix solution/suspension. A proper proportion of crosslinker was added and the final mixture was once again stirred and sonicated for several minutes. The nanocomposite dispersions were smeared on substrates made from glass microfibre filters (Whatman, GF/B) until the filter was completely covered by the solution. The films were, finally, conditioned in a drying oven (DOD series, Raypa Trade), at a varying range of temperatures to complete the crosslinking reactions of the thermosetting organic matrix during thermal cure.

Table 4.1: Properties of the Montmorillonite clays considered in this study

Trade name	Organic Modifier	Chem. Structure	% Weight Loss	Density (gr/cm^3)	CEC (meq/100g)
C10A	2MBHT	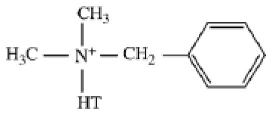	39.0	1.90	125
C20A	2M2HT	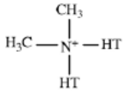 $H_3C-N^+(CH_3)(HT)-HT$	38.0	1.77	95
C93A	M2HT	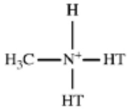 $H_3C-N^+(H)(HT)-HT$	39.5	1.88	95
C30B	MT2EtOH	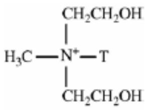 $H_3C-N^+(CH_2CH_2OH)_2-T$	30.0	1.98	90

Southern Clay Products®

The abbreviations of the ammonium ions are:

2MBHT:	dimethyl, benzyl, hydrogenated tallow, quaternary ammonium
MT2EtOH:	methyl, tallow, bis-2-hydroxyethyl, quaternary ammonium
M2HT:	methyl, dehydrogenated tallow ammonium
2M2HT:	dimethyl, dehydrogenated tallow, quaternary ammonium

Note: HT means hydrogenated tallow which is a chain distribution with the following composition: 65% C_{18}, 30% C_{16} and 5% C_{14}.

Table 4.2: Solvent Polarity Chart, for solvents used in this study

Relat. Polarity	Comp. Formula	Group	Representative Solvent Compound
Non Polar	Ar - H	Arene	Xylene
↓	R - CO - R	Aldehydes, Ketones	Acetone
↓	R - OH	Alcohols	Ethyl Alcohol
Polar	H - OH	Water	Water

Table 4.3: Chemical structure and density of solvents

Solvent	Density at 20° C (g/cm^3)	Chemical structure
Acetone	0.790	CH_3COOCH_3
Ethyl Alcohol	0.789	CH_3CH_2OH
o-Xylene	0.880	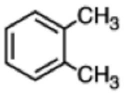
Water	0.9982	H_2O

4.3 Characterisation Techniques

4.3.1 Thermal analysis

The monitoring of how a substance changes when its temperature is increased is often used as a characterisation method. This is called Thermal Analysis (TA). The changes that are monitored are chemical or physical in nature.

Two specific methods of thermal analysis were employed in the present work. Differential Scanning Calorimetry (DSC) measures the heat capacity of the sample as a function of temperature; Thermogravimetric Analysis (TGA) measures the mass loss of a sample during heating.

Differential Scanning Calorimetry (DSC)

DSC measures the heat flow and the temperature associated with physical transitions and chemical reactions. The difference in heat flow between a sample and a reference material is measured under precisely controlled conditions. The method measures heat flow into or out of a sample as exothermic or endothermic changes in energy.

The DSC measurements were performed with a PL-DSC instrument, Thorn Scientific Services Ltd. Each sample was placed in an aluminium encapsulating crucible, a specific type of container able to withstand very high temperatures. The samples were first heated to a temperature of 75° C and maintained at this temperature for 1 min. Then, they were heated from 75° C to 200° C at a heating rate of 10° C/min. The temperature was maintained at 200° C for 2 minutes and the samples were cooled down from 200° C to 75° C with the same rate of 10° C/min. The same cycle was performed once again for each sample. The particular measurements were mainly conducted to determine the glass transition temperature, T_g, of each sample.

Thermogravimetric Analysis (TGA)

TGA measures the change in mass as a function of temperature and time in different controlled atmospheres. The procedure is used for applications where a change in mass is expected. Since only information concerning the changes in mass is collected, nothing is revealed about the nature of the transitions that cause these changes. The energy involved, or whether it is absorbed or released, is not detected directly but can be estimated by the rate of change of the sample temperature compared to the programmed rate, if monitored, albeit with reduced accuracy in comparison to DSC.

TGA measurements are usually conducted in the temperature range of ambient to 1200 °C. In this study, they were performed to determine and verify the exact clay fractions of the samples. A Perkin-Elmer Instruments, Diamond TG/DTA instrument was used at temperatures between 100 to 950 °C with a heating rate of 50 °C/min and sampling rate of 0.5 points/s.

The initial sample weight was determined with a precision balance, Kern ALT 220-4M. The data were analysed with Muse Standard Analysis software to plot, export and analyse features such as peaks, glass transition temperature, purity, etc.

4.3.2 X-ray Diffraction Analysis (XRD)

XRD measures the distances between crystalline planes in solids. In our case it is also a useful tool for the investigation of the interactions between the clay inorganic particles and the polymer organic matrix. It is a non-destructive analytical technique, able to reveal information about the crystal structure, chemical composition, and physical properties of materials and thin films.

In this method a monochromatic X-ray beam is sent at an angle θ onto the sample and the reflection is measured. The angle is changed, the reflection is monitored and the resonance peaks are noticed and related to the distances between the reflecting objects (crystalline planes). The XRD pattern analysis is based on Bragg's equation which has the form of:

$$n\lambda = 2d_{001} \sin\theta \;\Rightarrow\; d_{001} = \frac{\lambda}{2} \sin\theta \;, \tag{4.2}$$

where: λ is the wavelength of the X-ray used, d_{001} is the inter-layer spacing of the nano-platelets and θ is half of the diffraction angle, since the diffraction peak is at 2θ and n is the reflection order, usually equal to 1 (for the first reflection).

Bragg's equation is used, in general, to calculate the parameters of a crystal lattice. In the case of layered silicates it enables one to detect the layer expansion of the clay in nanocomposites as it measures the distance between the layers. When the clay becomes exfoliated, then the periodic stacking of the platelets ceases and the corresponding peak disappears.

The XRD measurements in this study were performed using a D8 Advance, Bruker AXS, diffractometer with radiation of a Cu anode. The diffraction patterns were collected between 2° and 15°, with the use of a position sensitive detector (PSD), Lynx-Eye. The scanning rate was 0.02°, the time step was 0.2 s and the X-ray wavelength was $\lambda = 1.5405$ Å.

4.3.3 Positron Annihilation Lifetime Spectroscopy (PALS)

Since the gas diffusion is determined by the mobility of the gas molecules through a membrane, the diffusion coefficient is partly determined by the free volume size in the material [Pethrick, 1997]. It is, therefore, of significant importance to investigate, e.g. through Positron Annihilation Lifetime Spectroscopy experiments, PALS, the free volume variation in the tested samples and determine the correlation between the free volume as measured by positron annihilation and the diffusion coefficient.

Positron annihilation lifetime spectroscopy is a non-destructive technique, which is applied to the study of both solid state matter, to measure voids and defects, as well as of soft matter to estimate the free volume in polymers. In this technique positrons are injected into the matter and their lifetimes are measured.

The positron energy decreases in the matter by non-elastic interactions. The mean positron penetration depth of this so-called thermalisation process is of the order of 100 µm. The thermalisation time is usually around a few ps which compared to the positron lifetime can be neglected. On reaching thermal energies, the positron diffuses in the periodic lattice potential before it gets trapped in a lattice defect. The diffusion

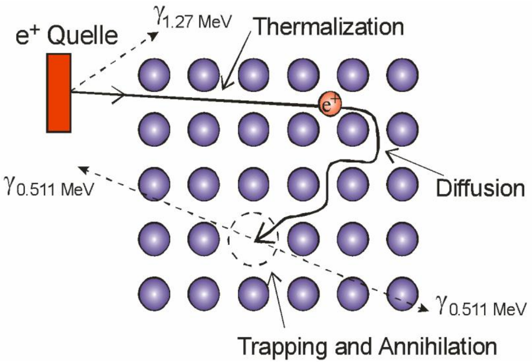

Figure 4.3: Positron trapping in crystal lattice defects. [Krausse-Rehberg, 2012]

length is in the order of 100 nm. This distance determines the number of atoms to be probed for positron traps during the positron lifetime. Hence, the diffusion length strongly determines the sensitivity of the positron methods to detect defects. The trapping process of the positron is provided in figure 4.3

The positrons can either be obtained by a pair production or from the β^+ decay of unstable radioactive isotopes, such as ^{22}Na, according to the decay reaction:

$$^{22}Na \rightarrow\ ^{22}Ne + \beta^+(0 - 540KeV) + \nu_e + \gamma(1.28MeV)$$

Except ^{22}Na, other isotopes can also be used (for instance ^{64}Cu, ^{58}Co), but are less common.

According to the reaction above, a proton of ^{22}Na emits a positron, β^+, with an energy that extends up to 540 keV, and an electron neutrino, ν_e, and becomes a neutron. The ^{22}Na is transformed, thus, to the excited state of ^{22}Ne, which, due to its instability, emits a γ-quantum photon with energy of 1.28 MeV. This photon emission takes place only 3 ps after the positron emission. These two emissions can be regarded as simultaneous actions, since the positron lifetime in matter is longer than 100 ps. This photon is the start signal of the lifetime measurement. When the emitted positron finds an electron somewhere and they annihilate, two photons are emitted, with energy of 511 keV each. These photons designate the stop signal for the lifetime measurement.

During the PALS measurements, a positron from the source meets an electron from the tested sample and there are two possibilities for the annihilation process: Either the direct annihilation of the positron with an electron, with an average lifetime of τ_2 = 0.4 ns or the formation of a temporary bound state of an electron and a positron. This state is called positronium, Ps, and is only formed in low electron density regions.

There are two kinds of Ps atoms. The para-positronium (p-Ps), in which the spins of the positron and electron are anti-parallel, has the shortest lifetime of τ_1 = 0.125 ns by self-annihilation in vacuum. The ortho-positronium (o-Ps), in which the spins of the positron and electron are parallel, has the longest lifetime of τ_3 = 142 ns in vacuum. However, in polymers the o-Ps lifetime is shortened to a few ns (1-5 ns) by the pick-off

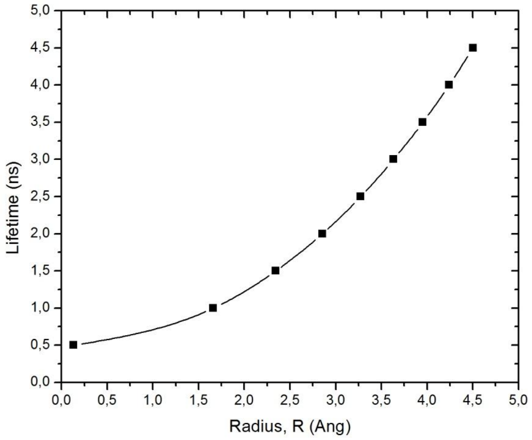

Figure 4.4: Plot of the τ_{o-Ps} lifetime (τ_3) as a function of the radius, R, of the free volume holes.

annihilation mode with an electron from the surrounding molecules.

The positron's lifetime depends on the electron density (rich or poor) of the surrounding region. A poor electron density region stands for scarce or even absent electrons and corresponds to high positron lifetimes. When the o-Ps falls in a free volume hole, the possibility for this pick-off mechanism to occur depends on the size of the hole. The larger the hole the longer it survives before annihilation. The relationship between the o-Ps lifetime, τ_3, and the radius of the free volume hole, R, has been established by an empirical equation proposed by Tao and Eldrup [Pethrick, 1997]:

$$\tau_3 = \frac{1}{2}\left[1 - \frac{R}{R+\Delta R} + \frac{1}{2\pi}\,\text{sin}\,\frac{2\pi R}{R+\Delta R}\right]^{-1}, \tag{4.3}$$

where ΔR is the fitted empirical electron layer thickness on the wall of the hole, with a value usually equal to around 1.66 Å.

The o-Ps lifetime, τ_3, as a function of the hole radius R is illustrated in figure 4.4. The values for the radius correspond to results of the Tao – Eldrup calculator (eq. 4.3).

The fractional free volume V_f (%) corresponds to the total amount of free space in the polymer per unit of total volume. V_f is related to I_3 by an empirical equation (eq. 4.4).

$$V_f = CV_hI_3 \tag{4.4}$$

Where I_3 is the o-Ps intensity (%), C is a constant, empirically determined to be around 0.0018 for most polymeric systems, and V_h is the volume of the average spherical hole: $V_h = (4/3)\pi R^3$.

The positron sources are usually prepared by evaporating a solution of a ^{22}Na salt on a thin metal or polymer foil. In this study, a thick Kapton foil was used to seal the radioactive source of $^{22}NaCO_3$, because Kapton has approximately the same lifetime as

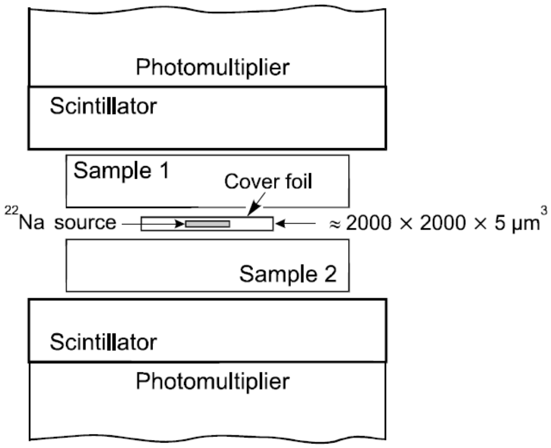

Figure 4.5: Measurement setup – “sandwich arrangement”. [Krausse-Rehberg, 2012]

the source. The time resolution of the apparatus and the source components were estimated through the measurement of a reference sample. It should be noted that the activity of the source must be sufficiently low in order to ensure that on average only one positron is in the sample at any time; this avoids the intermixing of start and stop quanta originating from different annihilation events. The ‘sandwich’ arrangement of foil source is to ensure that all positrons emitted from the source are penetrating the specimen volume. The schematic representation of the setup is provided in figure 4.5.

The PALS experimental arrangement is depicted in figure 4.6. The lifetime is measured as the time difference between the appearance of the start and end γ-quanta. PM responds to the photomultiplier and Single-Channel Analyzer (SCA). The amplitude of the time-to-amplitude converter (TAC) analog output pulse is proportional to this time difference. The whole lifetime spectrum $N(t)$ is stored in a multi-channel analyser (MCA).

The positron lifetime spectrum, $N(t)$, is given by:

$$N(t) = \sum_{i=1}^{k+1} \frac{I_i}{\tau_i} \text{exp} \left(-\frac{t}{\tau_i} \right) \quad , \tag{4.5}$$

where τ_i denotes the mean (characteristic) lifetime of the positron state i, and I_i is the relative intensity of the corresponding lifetime component. After the data analysis, one can obtain information about the kind of defects present in the sample from the values of τ_i, whereas the values of I_i are related to the defect concentration as explained above.

The radioactive source used in this study had radiation strength of 10 µCi ≈ 0.37 MBq. The scintillators were made of either plastic or BaF_2. The experimental spectra were decomposed into three discrete lifetime components using the software ”Lifetime” (LT). A contamination monitor, Berthold LB 124 SCINT, evaluating the radiation

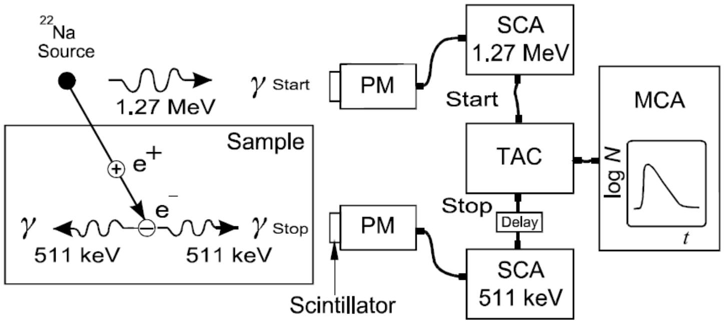

Figure 4.6: Scheme of the PALS experimental arrangement, called 'fast - fast coincidence' setup. [Krausse-Rehberg, 2012]

in Bq/cm^2, was used in the laboratory for personal radiation protection. To obtain a reliable and complete lifetime spectrum, more than 10^6 annihilation events were recorded.

Since the radioactive source is covered by thin foils, one should correct the measured spectrum by subtracting the fraction of positrons which annihilate in the source [Staab and Somieski et al, 1996]. The source correction is determined using a defect-free reference sample of known lifetime. There are three different source contributions, due to:

1. The positron annihilation in the reference sample, with lifetime of 219 ps
2. The radioactive salt, ^{22}Na, with corresponding lifetime values that vary between 380-450 ps (0.4 ns approximately)
3. The fraction of the positrons that annihilate in the Kapton foil (glue), with lifetime of approximately 3.70 ns.

Various results and analysis patterns can be found in the literature regarding PALS measurements conducted in polymer/clay nanocomposites. This indicates that each nanocomposite system should be treated differently. For instance, PALS experiments on a binary mixture of epoxy and polyurethane resin [Jia et al, 2007] confirmed that the addition of organophilic MMT decreased the fractional free volume of the samples. As the results denote, the lowest o-Ps lifetime was obtained for organophilic MMT content of 1 %. As for 3 and 5 wt% addition, the lifetime was increased, yet remained below the pure resin. Moreover, studies in epoxy-rectorite nanocomposites [Wang et al, 2007] show that for low filler content (0 – 2 %) the free volume hole size remains nearly the same, whereas the intensity and, thus, the concentration of free volume holes decreases with increasing filler content. The value of I_3 drops from 23% to 21.7% with increasing rectorite content from zero to 2 %. This is attributed to the decrease in the probability of Ps formation.

4.3.4 Gas permeation through the coating

When a gas permeates through a membrane, several consecutive steps are involved: The gas is sorbed at the entering face; it dissolves there, with equilibrium rapidly being established between the two phases; the dissolved penetrant molecules diffuse through the membrane via a random-walk mechanism; and they desorb at the exit face of the membrane.

The driving force behind the transport process, which involves the sorption, the diffusion and the permeation of the gas molecules, is the difference in the concentration between the two faces of the membrane. The transport process slowly tries to equalise this concentration difference. The process can be described in terms of Fick's first law of diffusion, according to which the mass flux J along the direction x, is proportional to the concentration gradient ($\partial c/\partial x$):

$$J = -D\frac{\partial c}{\partial x} , \tag{4.6}$$

where the proportionality constant, D is the diffusion coefficient.

Equation 4.6 applies only when the concentration does not change with time and the diffusion is in the steady state. Making a mass balance around a volume element we get Fick's second law, which describes the non-steady state for the mass transport process, and gives the rate of change of the penetrant concentration ($\partial c/\partial t$),

$$\frac{\partial c}{\partial t} = \frac{\partial J}{\partial x} . \tag{4.7}$$

For constant D this becomes:

$$\frac{\partial c}{\partial t} = D\frac{\partial^2 c}{\partial x^2} . \tag{4.8}$$

The rate at which the gas molecules transport through a membrane can be expressed in terms of the permeability coefficient, K (mol Pa^{-1} m^{-1} s^{-1}). Since the whole process involves sorption, diffusion and dissorption of the gas molecules at the membrane, this coefficient is given as the product of the diffusion coefficient, D (m^2/s), and the sorption coefficient or solubility, S (mol m^{-3} Pa^{-1}):

$$K = D \times S . \tag{4.9}$$

If we plot the time evolution of the gas concentration, we observe that the curve which describes the amount of gas per unit time, becomes linear after a certain time. Extending the linear part of the curve (constant flow) to meet the time axis, one obtains the time-lag, t_0 (Fig. 4.7).

$$t_0 = \frac{d^2}{6D} . \tag{4.10}$$

The time-lag for the permeation, t_0, is a measure of the time required to obtain a constant and steady flow through a membrane of thickness d. Hence, the diffusion coefficient can be calculated from the experimentally determined time-lag and the known thickness of the sample membrane. A typical graph of such experimental data is provided in figure 4.7. The dotted line indicates the extrapolation to find t_0.

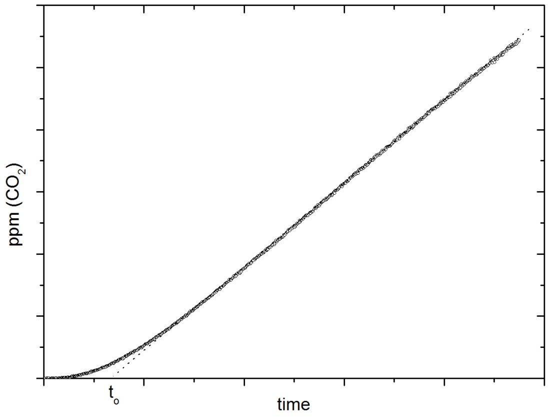

Figure 4.7: Experimental data plot indicating the time-lag value, t_0.

Further, the permeability of the samples, K, can be estimated directly from the the steady state flux, J, i.e. the slope of the permeation curve at steady state, the pressure, P, and the membrane thickness, d:

$$K = J\frac{d}{P} \ . \tag{4.11}$$

4.3.5 Gas permeability in nano-composites

In the present work the barrier properties of polymers filled with inorganic fillers are investigated. Our attention is specifically directed to the nanoclay and matrix interactions, and their effects on the barrier properties of the nanocomposites.

The addition of filler particles contributes to the permeation properties of polymer/clay nanocomposites; the presence of the particles lengthens the travel path of the gas penetrants, prolongs the required time to travel through the film, and, thus, reduces the diffusion coefficient. It is possible, though, that inadequate interaction between the clay filler, the dispersion medium and the organic matrix might result in extra free volume at the interfaces. This will augment the gas permeability properties and increase the diffusion coefficient instead of reducing it. Further, as the clay content is increased, the filler particles might create aggregations in order to minimise the interfacial regions between them and the rest of components involved in the system.

The nano-fillers are considered physical, impermeable barriers against the flow of the gas penetrants. They decrease the diffusion coefficient of the nanocomposite because they force the penetrant molecules to follow a longer tortuous travel path around them in the polymer matrix [Nielsen, 1967]. A longer path means slower diffusion.

The ratio of the permeability coefficient of the nanocomposite K_{nanoc} to one of the polymer matrix K_{resin} is given by:

$$\frac{K_{nanoc}}{K_{resin}} = \frac{1-\phi}{\tau} \, , \tag{4.12}$$

where ϕ is the volume fraction of the clay filler and τ is the tortuosity factor. This factor represents a ratio of distances and can be expressed as below:

$$\tau = \frac{d'}{d} \, , \tag{4.13}$$

where d' describes the distance that the molecules have to travel due to the filler addition and d is the distance that they would have to travel without the filler barriers (membrane thickness). The tortuosity factor can be expressed in terms of the clay volume fraction and the aspect ratio of the particles:

$$\tau = 1 + \frac{L}{2W}\phi \, , \tag{4.14}$$

where L and W represent the length and the thickness of the clay platelets respectively; and ϕ is the filler volume fraction. The diffusion coefficient, D, is strongly affected by the tortuosity factor:

$$D_{nanoc} = \frac{D_{resin}}{\tau} \, . \tag{4.15}$$

Since d, the membrane thickness, remains constant, τ only increases with an increase in the distance d'. Therefore, as the diffusion path becomes more tortuous, the diffusion coefficient of the sample decreases and D_{nanoc} is reduced compared to D_{resin}. This is the main goal of the present work.

In this study, the diffusion coefficient was determined directly by conducting measurements in a permeation cell. The measurement set-up is shown in figure 4.8. The permeation cell was separated by a membrane of thickness d in two chambers. The penetrating gas was carbon dioxide, CO_2, and was introduced under constant pressure P_o in the volume V_o of the left chamber (Fig. 4.8). The right hand side compartment was used to monitor the evolving concentration of the gas that permeated through the membrane. Prior to every permeation measurement, helium gas, He, was used to remove any residue of CO_2 in the chamber. Details on the design of the cell and its function can be found at the PhD dissertation of Choudalakis [under preparation, 2012].

All permeation measurements were conducted in ambient conditions at temperatures varying from 20 to 23° C. The actual average thickness of the membrane was calculated as:

$$d = \frac{m_s - m_f}{\rho_{nanoc} A} \, , \tag{4.16}$$

where m_s is the mass of the sample, including the substrate filter, and m_f is the mass of the substrate. For the substrate used for XRD this is 0.06 g, while for the filter used

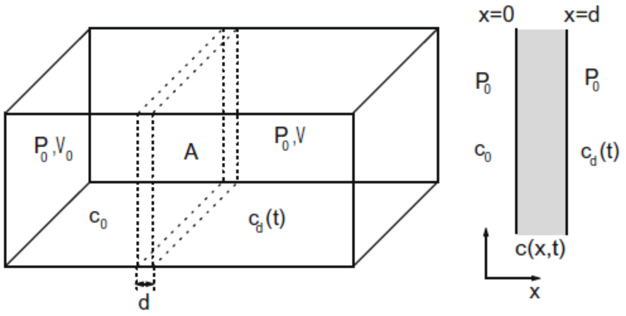

Choudalakis and Gotsis [2009]

Figure 4.8: Measurement set-up for the permeation measurements.

for the permeation measurements this was 0.32 g. The area, A, of the sample is $A = \pi R^2 = 23.76$ cm^2, since 2R = 55 mm for the fibre filters. The nanocomposite density can be evaluated as:

$$\rho_{nanoc} = \frac{\rho_{clay}\rho_{resin}}{w\rho_{resin} + (1-w)\rho_{clay}} \ , \tag{4.17}$$

where w is the particle mass fraction and ρ is the density (g/cm^3). The volume fraction, ϕ, of the particles is:

$$\phi = \frac{\rho_{nanoc}}{\rho_{clay}} w \ . \tag{4.18}$$

The gas permeability is a crucial property of the polymer/clay nanocomposites studied in the present work. It is, thus, important to appraise the parameters that affect the gas barrier properties of nanocomposite systems. Regarding the addition of the inorganic clay, three factors have a strong impact on gas permeability [Sapalidis et al., 1995]:

- the aspect ratio of the platelets,
- their volume fraction, and
- their orientation in relation to the diffusion direction.

Effect of nano-platelet orientation

The orientation of the particles in the polymer matrix has a significant effect on the gas barrier properties of nanocomposites. Most of the models are based on the assumption that the nano-platelets are perfectly oriented normal to the diffusion direction. However, it is experimentally difficult to control the orientation of the particles and, in most of the actual samples, the orientation is far from perfect. Fig. 4.9 demonstrates the nano-platelets possible spatial and orientational distributions in the polymer matrix [Mittal, 2010].

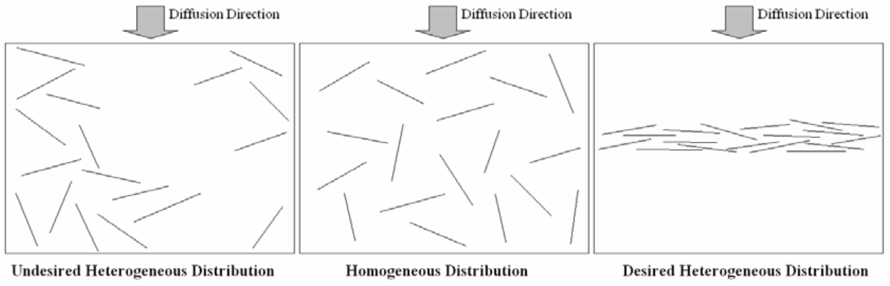

Figure 4.9: Illustration of possible distributions of nano-platelets in the polymer host regarding the permeation properties. [Mittal, 2010]

Effect of aspect ratio

The incorporation of impermeable filler particles into a polymer matrix improves the barrier properties of the nano-film; it is the geometry and, thus, the aspect ratio of the clay particles that affects the strongest the gas barrier properties of the coating.

Three common types of filler particles are used for the fabrication of polymer/clay nanocomposites as shown in fig. 4.10. These can be isometric particles e.g. sphere, cylindrical particles (needles) or flakes. The particles are arranged in periodic lattices and can be oriented parallel to the membrane surface or perpendicular to the diffusion direction. The various types of nano-filler will have a different effect upon the permeation path of the gas molecules penetrants. This effect is reflected on the permeability of the composite.

In films with dispersed spheres, the permeability, K_{nanoc}, is related to the permeability of the pure resin, K_{resin}, as follows:

$$\frac{K_{resin}}{K_{nanoc}} = \frac{1+\dfrac{\phi}{2}}{1-\phi} \; . \tag{4.19}$$

Similar results are obtained for dispersed cylinders:

$$\frac{K_{resin}}{K_{nanoc}} = \frac{1+\phi}{1-\phi} \; . \tag{4.20}$$

In both these cases the permeability is only dependent on the volume fraction of the dispersed phase, ϕ.

Unlike spheres or cylinders the aspect ratio of nano-platelets contributes to the barrier properties of the nanocomposite, as eq. 4.12 and 4.14 suggest. As a consequence, successful nanocomposites for gas permeation properties, typically, do not include fillers that are spherical or cylindrical, but rather platelets. Studies regarding the effect of nanofiller type can be found in literature; for instance, [Ogasawara et al, 2006] revealed that the dispersion of nanoclay platelets in a polymer matrix is more

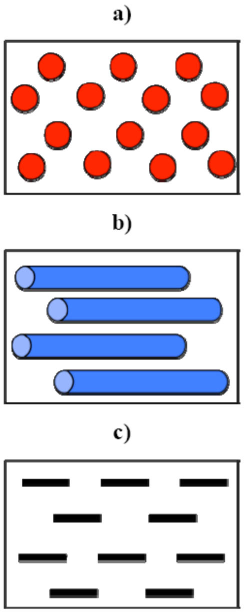

Figure 4.10: Composites formed with regularly-arrayed a) spheres, b) cylinders, and c) flakes. [Mittal, 2010]

effective in improving the gas barrier properties compared to cylindrical or spherical clay fillers.

Chapter 5

RESULTS

5.1 Differential Scanning Calorimetry (DSC)

DSC measurements were conducted on samples of water-borne polyurethane (PU), acrylic water-borne resin (AR), polyurethane solvent-based resin (2C) and a sample of 5.0 wt% MMT added in the acrylic resin (ARBE50). Figure 5.1 depicts the value of the heat flow measured as a function of the (variable) temperature for all tested samples.

The glass transition temperature can be determined by plotting the DSC data, e.g. from the traces of $\Delta H(T)$ (Fig. 5.1) during the cooling or heating stages. Linear fits around the point where the slope changes and extrapolation can provide an approximate value for the T_g. This value is not always the "equilibrium" T_g, as this quantity may depend on the heating/cooling rate. Figure 5.2 plots the DSC results for the cooling process. The dotted lines represent the linear fits and the extrapolation.

The patterns in this figure indicate that the solvent-borne resin exhibits a T_g in the region of 130 – 140 °C. The water-borne resins exhibit a lower T_g in the region of 120 – 130 °C. The sample ARBE50, which consists of 5 wt% clay in the AR resin, shows a T_g approximately at 125 °C. The addition of the filler does not seem to have a noticeable effect on the glass transition temperature of the resin.

5.2 Thermogravimetric Analysis (TGA)

The exact amount of clay loading was confirmed by conducting TGA measurements for the various samples. The three resins returned values of zero residues as no clay was involved in the tested samples and were used to calibrate the instrument. For the samples with 1 wt% and 5 wt% clay content the residue (ash) found at 950 °C was in agreement with the theoretically calculated values used for their preparation.

The TGA graphs for the three resin types and two nanocomposite samples are shown in figures 5.3 and 5.4 respectively.

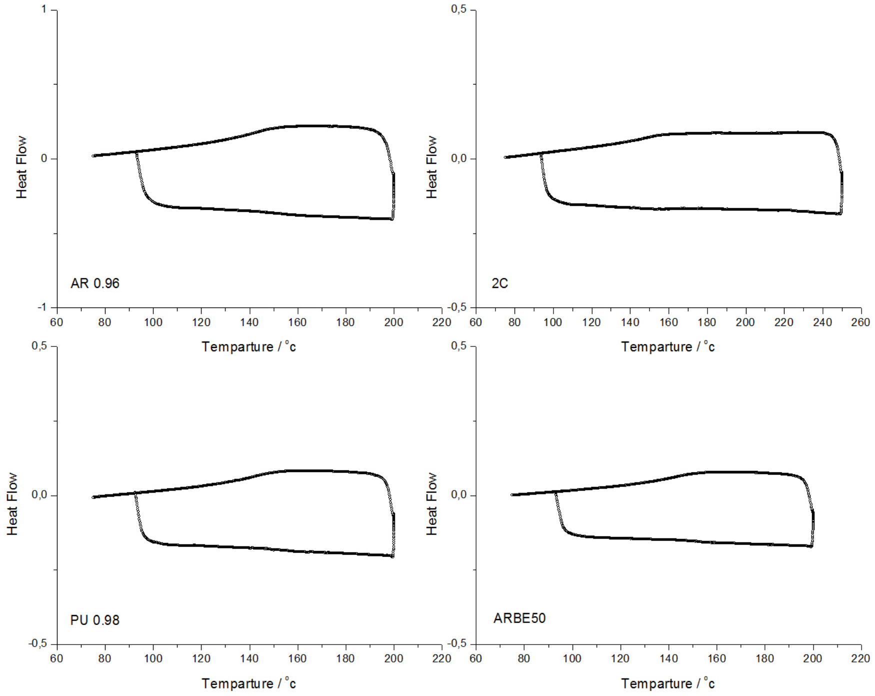

Figure 5.1: DSC curves of samples throughout the entire measurement

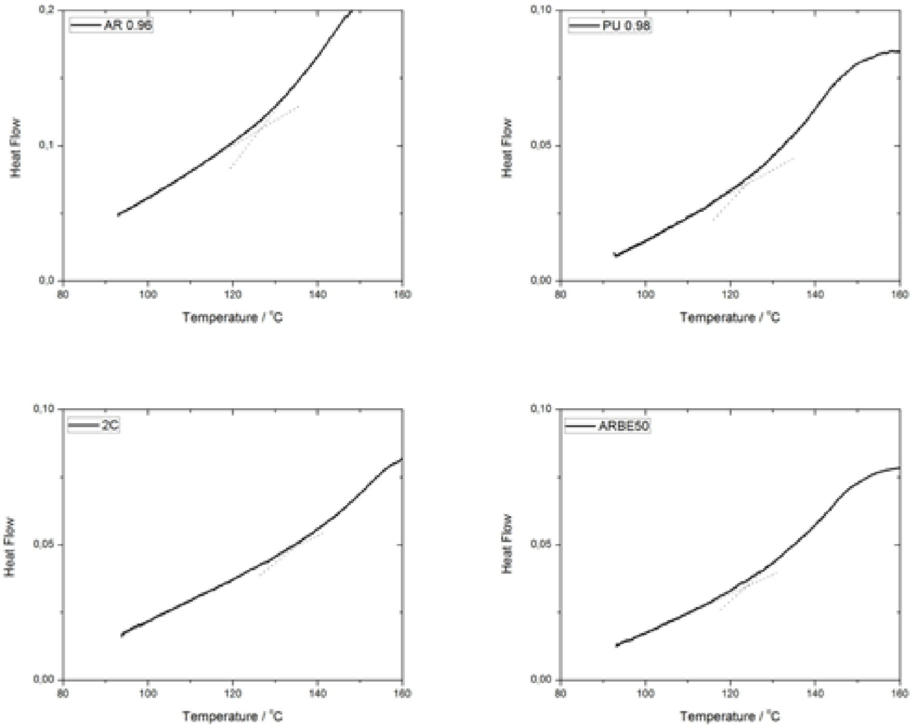

Figure 5.2: DSC curves of tested samples upon cooling

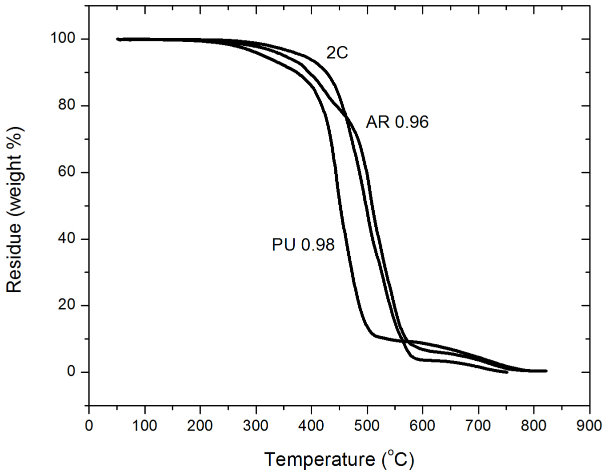

Figure 5.3: TGA graph for all three resins (zero clay loading)

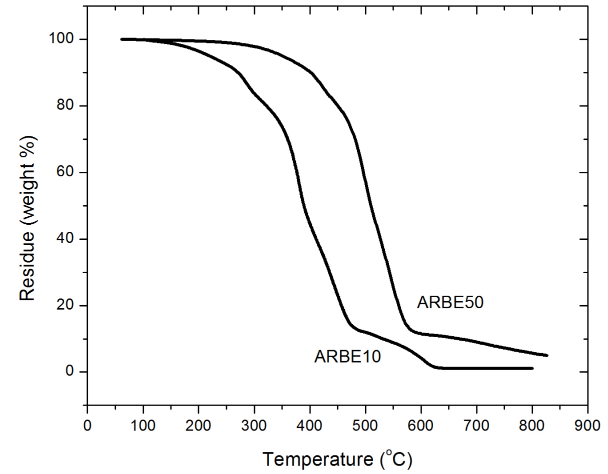

Figure 5.4: TGA graph for samples ARBE10 and ARBE50 (clay loading of 1.0 wt% and 5.0 wt%, respectively).

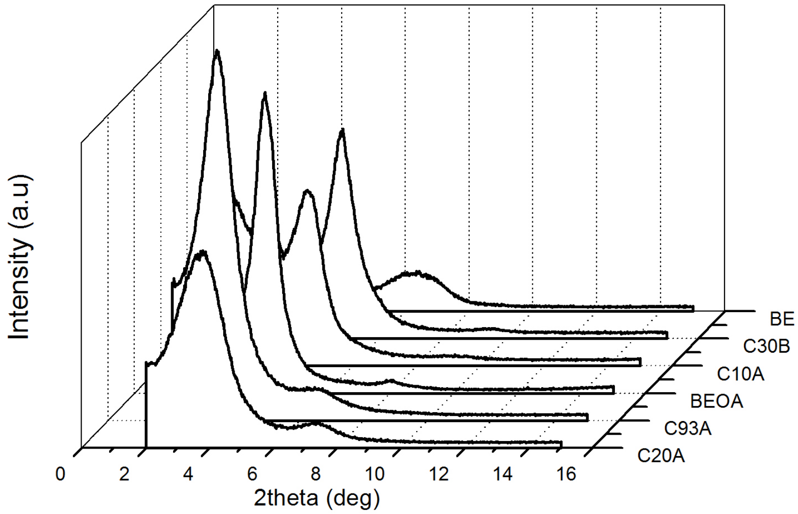

Figure 5.5: XRD patterns for all clay types used in this study.

5.3 X-ray Diffraction Analysis (XRD)

5.3.1 Organoclays

Due to the organophilic modification of MMT (from its pristine state to the chemically modified Cloisite® clay), the inter-gallery d-spacing is increased significantly, depending on the type and conformation of the alkyl chains of the ammonium ion. The pristine clay has its diffraction peak at a 2θ value which corresponds to $d \approx 14$ nm, whereas for the organically modified clay the inter-gallery expansion can reach the value of 24 nm (in the case of C20A). The corresponding X-ray graphs and data are provided in figure 5.5 and table 5.1, respectively.

The increase in the distance between the layers will strongly affect and stimulate the entry of the solvent molecules into the inter-gallery regions, leading to more efficient swelling of the nanoclay.

As claimed by the supplier, Cloisite® Nanoclays are surface-treated to be compatible with a whole host of systems. Their relative hydrophobicity are shown in Table A.5, as obtained from the supplier. Apparently, as the d-spacing decreases (in the order of: C20A, C93A, C10A, C30B) the surface hydrophobicity of the clay decreases. For instance, C15A, stated as the most hydrophobic clay, displays the highest value of

Table 5.1: Inter-gallery spacing of organically modified clays and diffraction peak values from X-ray data graphs.

Name	Diffr. Peak, 2θ (°)	d_{001} spacing (Å)	hydrophobicity
Cloisite C30B	4.77	18.5	↓
Cloisite C10A	4.59	19.2	↓
Cloisite C93A	3.74	23.6	↓
Cloisite C20A	3.65	24.2	↓
BE	6.36	13.9	
BEOA	4.10	21.5	

inter-gallery spacing, d = 31.5 Å. In addition, C30B, which is the most polar type of nanoclay (due to its two ethanol groups), has the lowest d-spacing and is more hydrophilic. This trend is rather expected since the surface modification is done in order to make hydrophilic clays more hydrophobic.

5.3.2 Water-borne resins

Nanocomposites with various contents of organophilic or untreated montmorillonite have been prepared by adding the clay filler to the water-borne or solvent-borne resins. The graphs in the following pages show the X-ray patterns for each combination with the dotted lines indicating the location of the peak reflection. The intensity is in arbitrary units (a.u.); the values are only presented to indicate the intensity of each reflection peak.

Fig. 5.6 shows the XRD spectra for the nanocomposites of untreated MMT in PU 0.98. The patterns indicate that there is an exfoliated structure only for clay addition in the order of 0.50 wt% or less. For clay load just a little above 0.50%, the diffraction peak appears approximately at 6°. This is reminiscent of the peak that indicates the distance between the crystalline clay in the pure (aggregated) clay. The intensity of this peak tends to increase as the MMT content is increased.

In the case of untreated MMT in the acrylic resin, AR 0.96, the nanocomposites are exfoliated for clay load 0.5 wt% and 1.0 wt%. For values equal to 2.0 wt% clay loading (and above) the diffraction peak appears again at 6°. Similar to Fig. 5.6 the intensity of this peak increases with the MMT content.

The graphs in Fig. 5.8 depict the behaviour of nanocomposites for various clay loads of C10A, initially dispersed in acetone or ethyl alcohol and then incorporated in the polyurethane resin PU.98. Similar graphs are shown for the C93A and C30B clays in Fig. 5.9 and Fig. 5.10, respectively.

When acetone is used as a dispersion medium, the clay is completely exfoliated for concentrations of 0.6, 1.2, and 1.8 wt/wt%. On the other hand, when ethyl alcohol

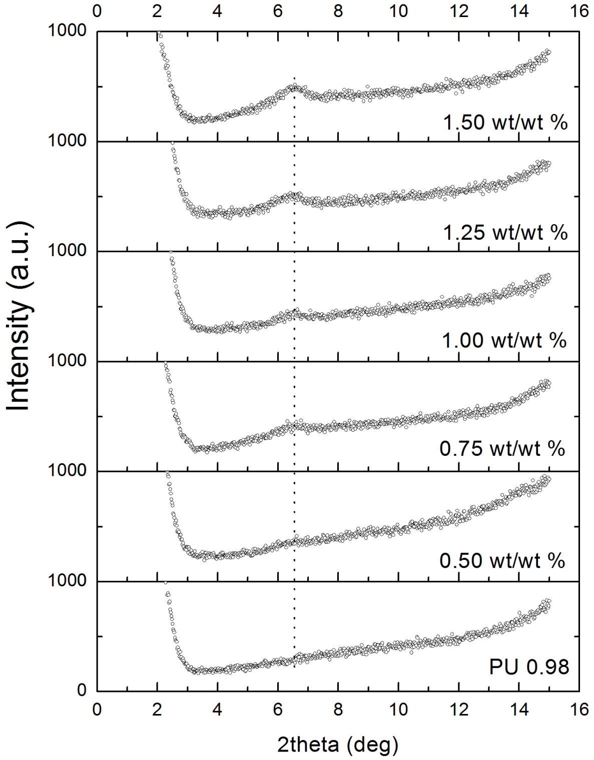

Figure 5.6: XRD curves of PU 0.98 nanocomposites for different clay content of untreated MMT dispersed in water

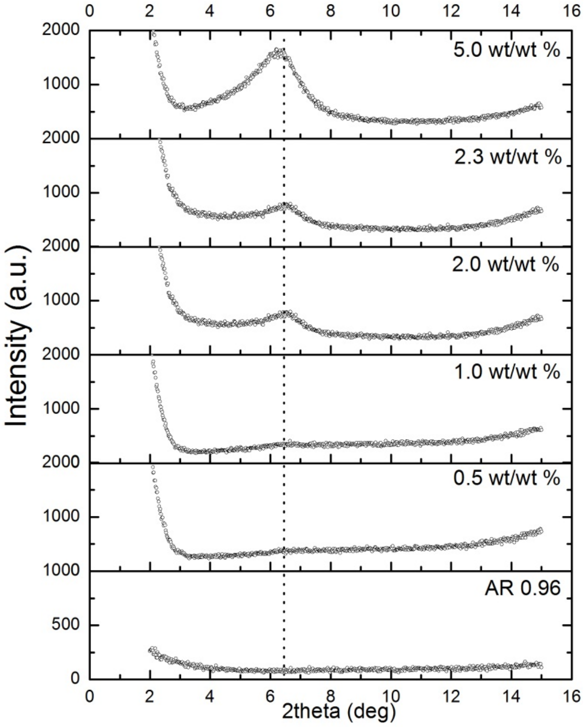

Figure 5.7: XRD curves of AR 0.96 nanocomposites for different clay content of untreated MMT dispersed in water

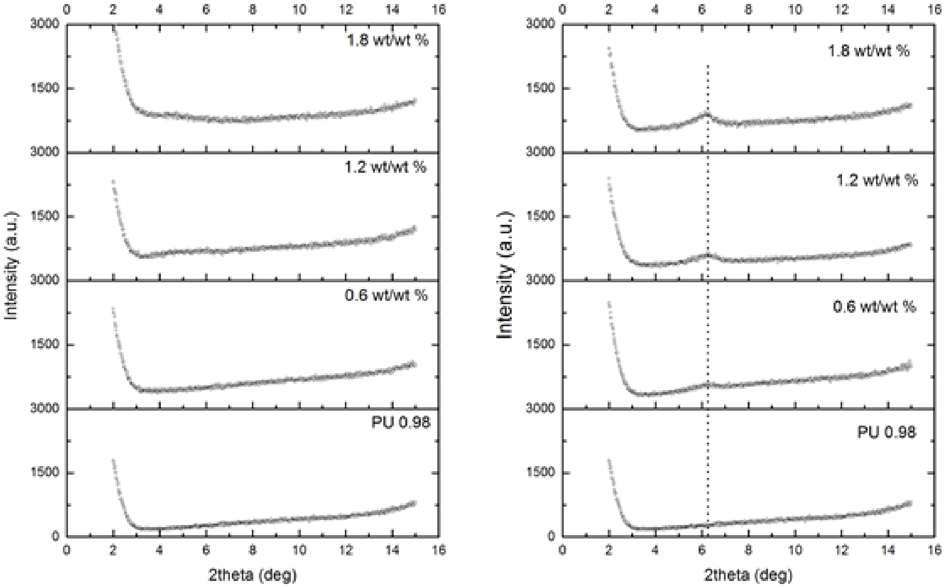

Figure 5.8: XRD patterns of PU 0.98 nanocomposites for different clay loads of C10A dispersed in acetone (left) and ethyl alcohol (right)

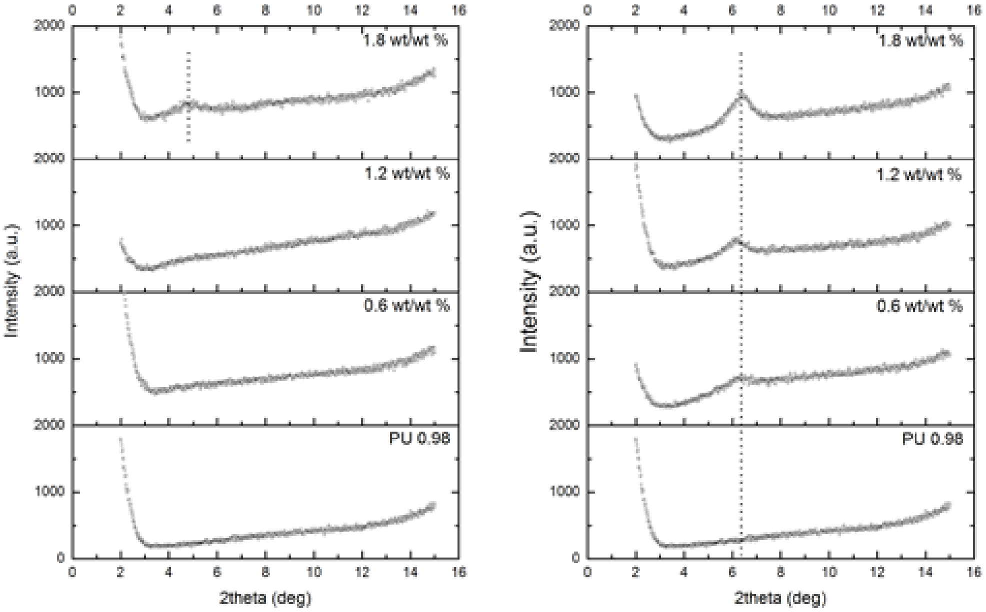

Figure 5.9: XRD patterns of PU 0.98 nanocomposites for different clay loads of C93A dispersed in acetone (left) and ethyl alcohol (right)

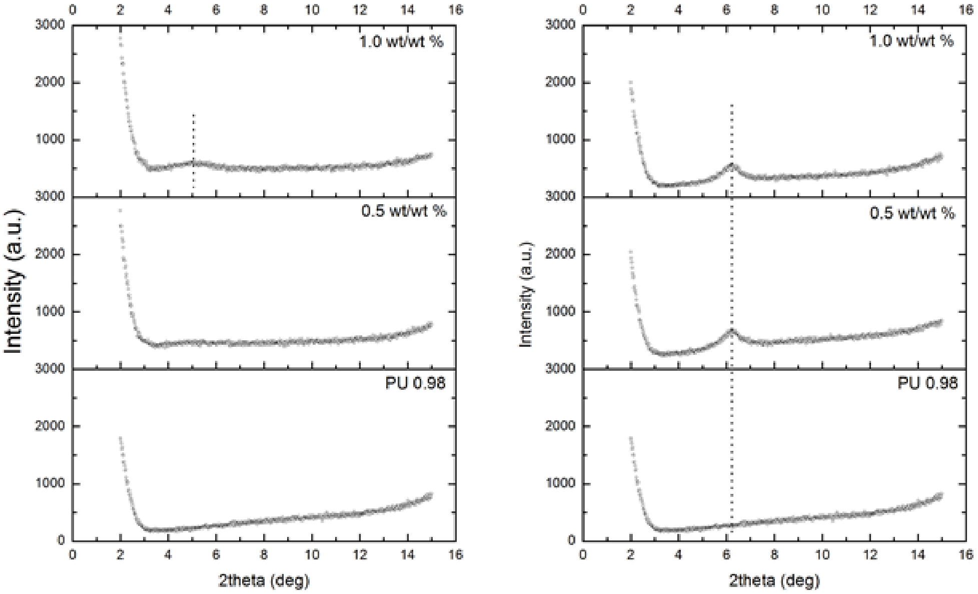

Figure 5.10: XRD patterns of PU 0.98 nanocomposites for different clay loads of C30B dispersed in acetone (left) and ethyl alcohol (right)

is used as the dispersion medium, the nanocomposites are not exfoliated, even for very low clay addition; a diffraction peak appears always at an angle around 6° when this solvent is used. Even though the peak of pure C10A clay is at around 4.6°, the peak in the nanocomposites is at 6°, which is exactly at the same angle as seen for the untreated MMT clay.

The XRD spectra of Fig. 5.9 are reminiscent of the ones obtained for the C10A clay (Fig. 5.8). When ethyl alcohol has been used as the solvent for the clay dispersion, the diffraction peak of the not-exfolliated particles is found at around 6°. When acetone has been used, then the structures are exfoliated for clay addition up to 1.2 wt%. Only for clay addition of 1.8 wt% there is a small peak at around 5° in this case. The diffraction peak of C93A clay powder is at 3.74°, thus the peak for the 1.8 wt% sample indicates a slightly intercalated nanocomposite.

Figure 5.10 shows the XRD patterns of the C30B nanocomposites with the water borne polyurethane as matrix and where the clay particles were first dispersed in acetone or ethanol. This figure shows that no exfoliated nanocomposite could be prepared in this matrix when ethyl alcohol was used as the dispersion medium for the clay. On the other hand, when acetone was the dispersion medium, the diffraction peak of the clay is not present, at least for clay addition up to 0.5 wt%. For 1 wt% the peak appears at approximately 5°. This peak can be attributed to the same reflection seen for the C30B powder clay, which shows a diffraction peak at 4.8°.

Nanocomposites were also prepared consisting of BEOA dispersed in PU 0.98 in

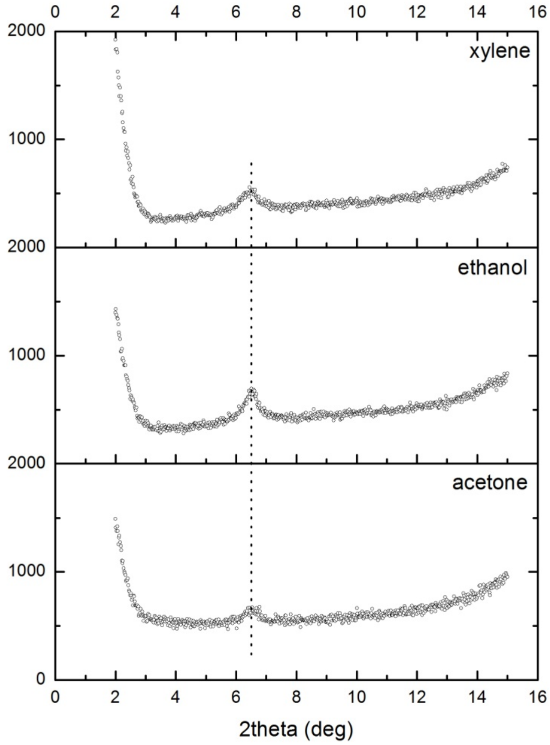

Figure 5.11: XRD patterns of PU 0.98 nanocomposites for BEOA clay addition

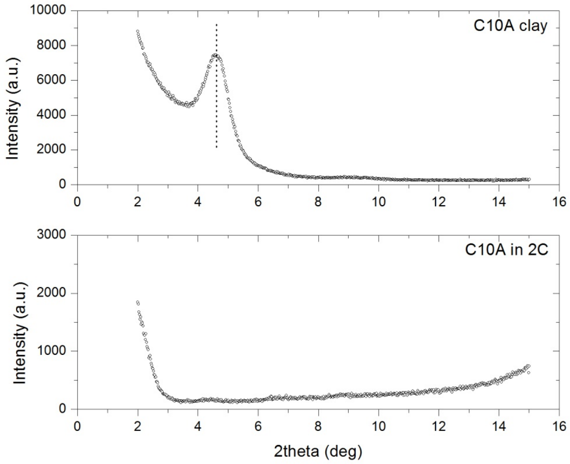

Figure 5.12: XRD patterns of 1 % C10A clay addition dispersed in the resin “2C”

concentrations of 1 wt%. A variety of organic solvents were used as the dispersion medium for the clay: xylene, acetone and ethyl alcohol. The X-ray patterns of these samples are shown in Figure 5.11. In all cases a diffraction peak was found at 6°, which is the reflection of untreated MMT.

The same reinforcement was also dispersed in resin AR 0.96 using ethyl alcohol and pentanol as clay dispersing media and a similar pattern was observed in the results. Although the diffraction peak of BEOA clay powder is 4.1°, the peak for all tested samples was the one of MMT. It seems that the trend applies to both water-borne resins.

5.3.3 Solvent-based resin

For the solvent-borne resin ‘2C’ a binary mixture of solvents was used as dispersion medium for the clays. This mixture consisted of 70 wt% xylene and 30 wt% ethyl alcohol. The fraction of the clay types C10A, C20A, C30B, and BEOA in the nanocomposite was 1 wt%. Figures 5.12 - 5.15 illustrate the XRD patterns of these nanocomposites for each clay type.

The addition of a small content of C10A clay in the resin results in a fully exfoliated nanocomposite. There is no diffraction peak. The probable reason is that the exchanged ions of C10A contain a phenyl group, similar to the one of xylene and their solubility parameters are very close, as it will be discussed later (section 6.3.1).

In the case of C30B, the nanocomposite structure is intercalated for 1 wt% clay (figure 5.13). The peak faintly shifts to lower 2θ values. The calculation of the interlayer distance gives a d-spacing of 18.5 Å (2θ = 4.77°) for the C30B clay and a d-spacing of 20.7 Å (2θ = 4.27°) for the nanocomposite containing the clay. The difference in the d-spacing of 2.2 Å results in an interlayer spacing increase of 12 %.

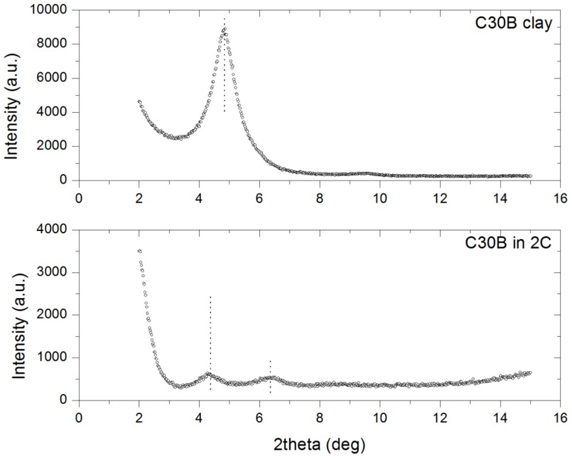

Figure 5.13: XRD patterns of 1 % C30B clay addition dispersed in the resin "2C"

A second peak is also observed for both the powder clay (2θ = 9.6°) and the nanocomposite that contains the C30B clay (2θ = 6.4°). The latter peak is close to the diffraction peak of the untreated clay powder, i.e., the peak of the BE clay and not the (used) C30B. This behaviour indicates that, even though the nanocomposite is exfoliated to some degree, the bulk of the clay is aggregated but it has lost its organic modification, its interlayer distance having been reduced to that of the untreated clay. The modifier MT2EtOH seems to have been partially extracted from the surface of the clay particles by the solvent and cannot fulfill its role any more.

Figure 5.14 shows the case of C20A dispersed in this way in the 2-component resin. The diffraction peak now is slightly shifted towards higher 2θ values, resulting in a decrease in the interlayer d-spacing. The 2θ peak for the powder is at 3.65° giving a d-spacing of 24.2 Å, while the peak for the nanocomposite is at 4.7° giving a d-spacing of 18.8 Å. The inter-layer spacing has decreased by around 5 Å. This shift to higher 2θ values can also be found in literature [Filippi et al, 2011]. The nanofiller undergoes a 'd-spacing collapse'. This behaviour can be attributed to a probable reorganisation of the alkyl chains inside the galleries of the clay modifier. A second peak is observed for both the powder clay and the nanocomposite. In that case, the peak is also faintly shifted to lower values.

Figure 5.15 shows that an intercalated structure is developed in the nanocomposite prepared with BEOA dispersed in the mixture of the solvents and then mixed with the 2C resin. The d-spacing of the BEOA clay powder is 21.5 Å (2θ = 4.10°) and the d-spacing in the nanocomposite is 34.5 Å (2θ = 2.56°). The difference for the d-spacing is approximately 13 Å which results in an increase of the interlayer spacing in the order of 60 %. The BEOA powder clay exhibits a second diffraction peak at 8°, which shifts to values of around 5° in the nanocomposite.

BEOA was also dispersed in the binary mixture of solvents (xylene to ethanol =

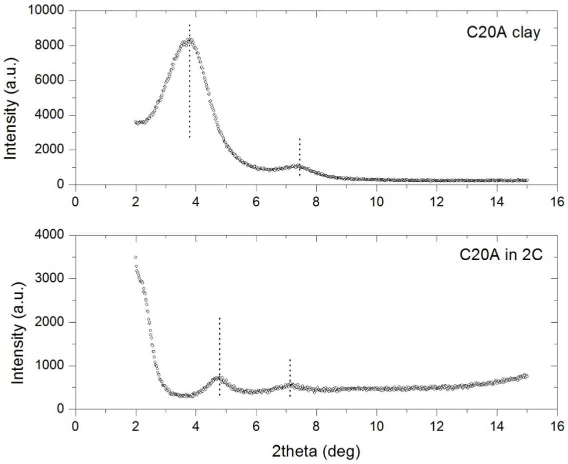

Figure 5.14: XRD patterns of 1.0 % C20A clay addition dispersed in the resin "2C". Note the shift of the first peak in the nanocomposite from 3.65° to 4.7°, which indicates a d-spacing collapse

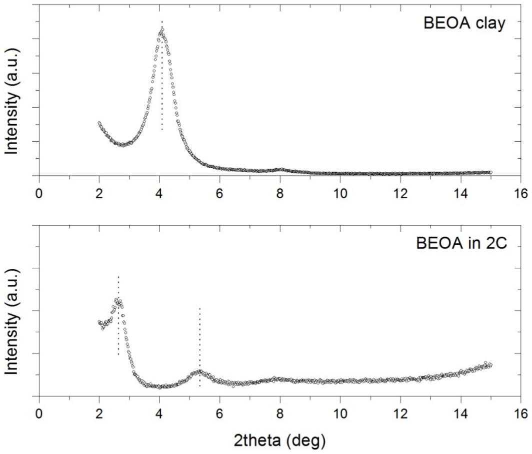

Figure 5.15: XRD patterns 1.0 % BEOA clay addition dispersed in the resin "2C"

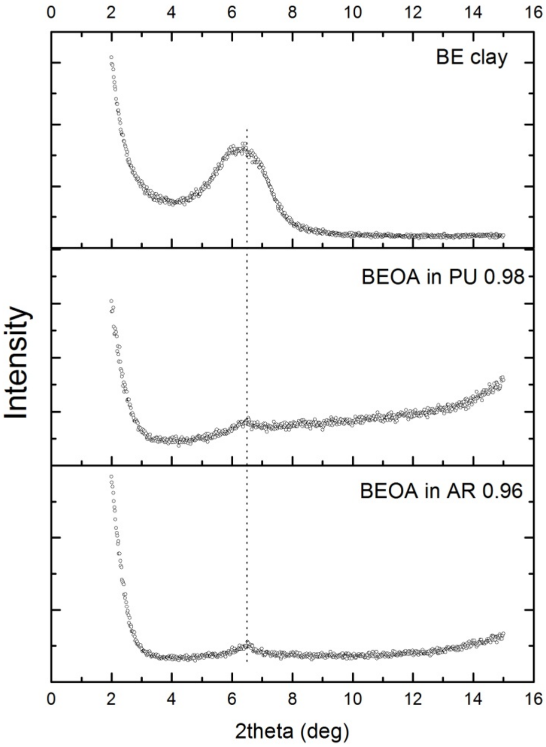

Figure 5.16: XRD patterns for 1.0 % BEOA clay addition dispersed in the resin “AR 0.96” and “PU 0.98”

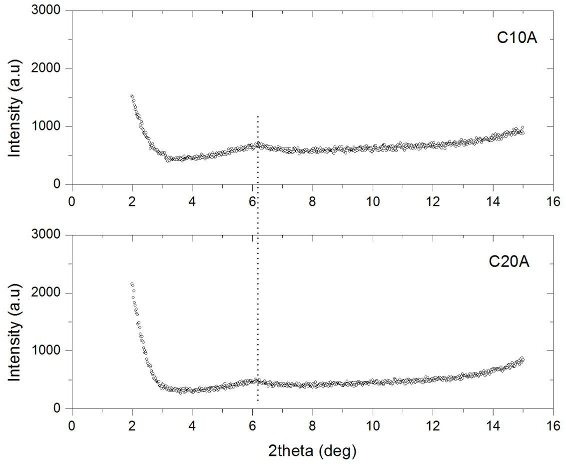

Figure 5.17: XRD patterns for 1 % C10A (top) and C20A (bottom) clay dispersed in the resin “PU 0.98”. The dispersion medium was a binary mixture of 70/30 wt/wt% xylene/ethanol.

70/30 wt/wt%) and was introduced in the water-based resins to prepare a 1 wt% composite. Even though, there was no indication of sedimentation in the final suspension, a peak appears in the nanocomposite at 6°, the same angle as for the untreated MMT.

If we compare the behaviour of the BEOA nanocomposites in the different types of organic matrix we can see that (i) in the case of the water-borne resins (PU and AR) the diffraction peak is approximately at 6°, whereas (ii) for the solvent-borne resin (2C) there are two peaks, at around 2° and 5°. For the water-based resins the peak is reminiscent of the one of the untreated clay, where the interlayer distance is smaller than that of the BEOA clay, whereas for the solvent-based resin there is a shift at lower 2θ angles. That is, when not fully exfoliated, the BEOA clay nanocomposites contain stacks of clay platelets which are intercalated when solvent based resin is used and not intercalated when water borne resin is used.

5.4 Positron Annihilation Lifetime Spectroscopy (PALS)

The PALS experiments are conducted in order to investigate the polymeric matrix of the nanocomposites. The o-Ps lifetime obtained from PALS is not ascribed to annihilation occurring in the inorganic clay but derives from the annihilation in holes in the polymer matrix, as well as, possibly at the interface between the clay and matrix [Yu et al, 2006].

The values of o-Ps lifetime and o-Ps intensity were obtained directly from the PALS measurements. The radius, R, of each free volume hole was evaluated using the Tao-Eldrup relation assuming spherical free volume cavities of equal radius.

Measurements were conducted at room temperature and above room tempera-

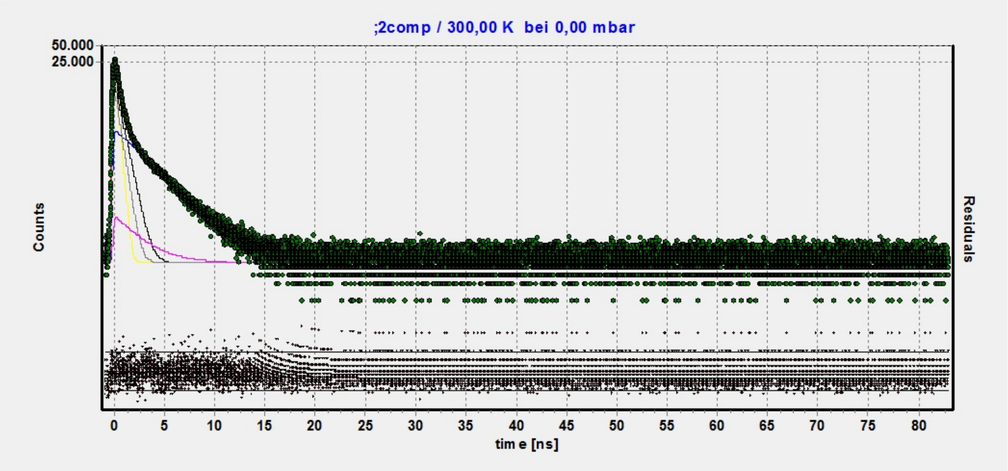

Figure 5.18: Typical PAL spectrum (screen-shot from the LT program, measurement for the 2C resin).

ture. It should be noted that a different set-up geometry and radioactive source was used for these two groups of experiments. A typical PAL spectrum is provided in figure 5.18.

- Measurements at room temperature

  The source contribution was determined to be in the order of 19%. The time resolution was found to be a sum of two Gaussians with FWHM$_1$ = 0.278 ns (70 %) and FWHM$_2$ = 0.205 ns (30 %). (FWHM = full width at half maximum). All measurements were conducted at a temperature of 300 K.

- Measurements above room temperature

  In this case the source contribution was determined to be in the order of 15%. The time resolution was again a sum of two Gaussians with FWHM$_1$ = 0.2138 ns (27 %) and FWHM$_2$ = 0.276 ns (73 %). The positron lifetime spectra were measured as a function of temperature, from 300 to 473 K, for two samples: AR 0.96 (pure resin), and ARBE10 (the same resin with 1 wt% clay addition). The upper temperature is limited by the thermal stability of the glue that was used between the Kapton foil and the source, which starts to disintegrate at temperatures above 200 °C.

5.4.1 Measurements at room temperature

The o-Ps lifetime and o-Ps annihilation intensity as well as the radius of the holes (R) and fractional free volume (V_f) are provided in figures 5.19 to 5.23, for all tested samples. Detailed tables of the results of the PALS experiments are given in appendix A.

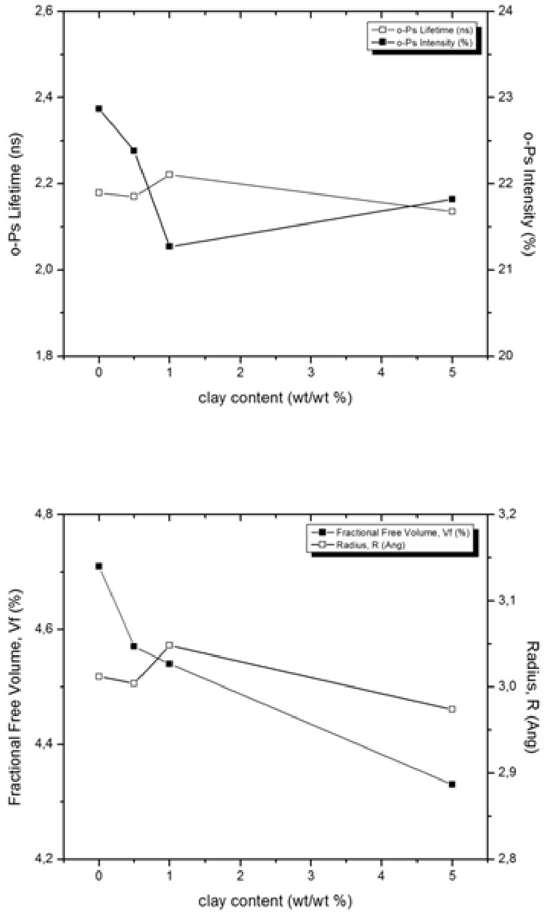

Figure 5.19: o-Ps lifetime and intensity (top), hole radius and fractional free volume (bottom) for samples of AR 0.96 with addition of untreated MMT clay

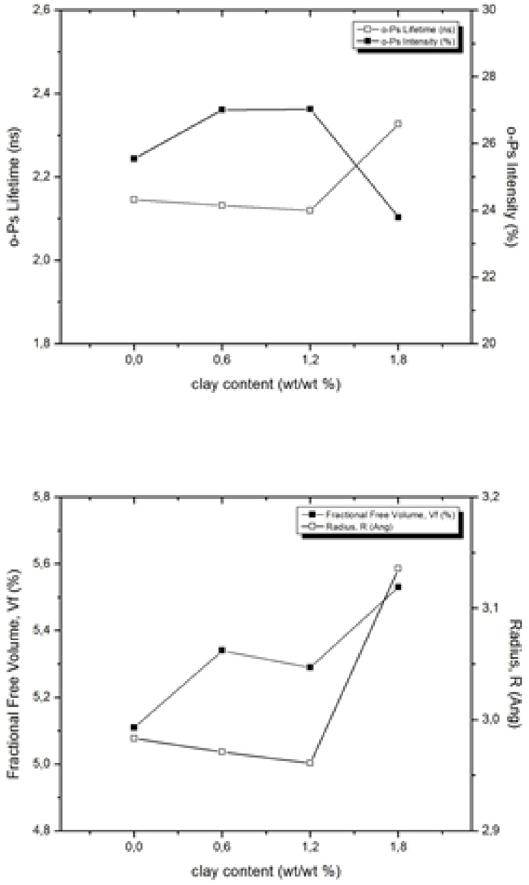

Figure 5.20: o-Ps lifetime and annihilation intensity (top), hole radius and fractional free volume (bottom) for samples of PU 0.98 with C93A clay addition

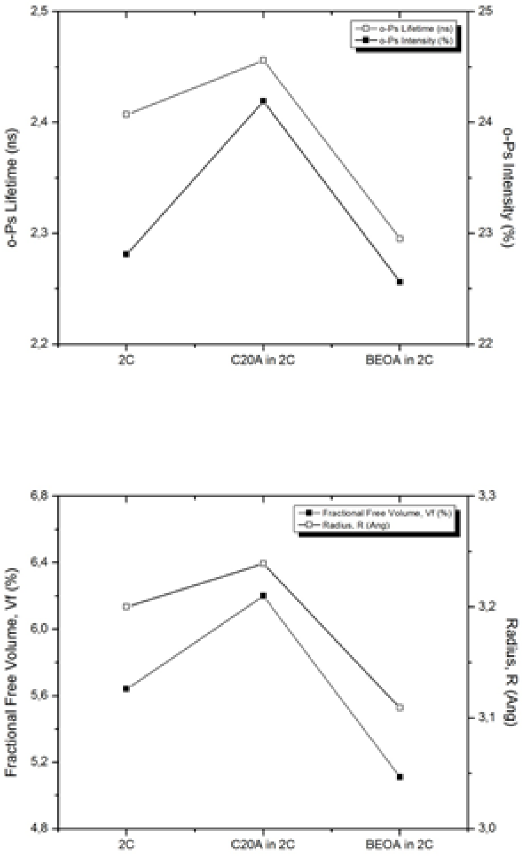

Figure 5.21: o-Ps lifetime and annihilation intensity (top), hole radius and fractional free volume (bottom) for samples of 2C with clay addition of 1 wt% BEOA or C20A

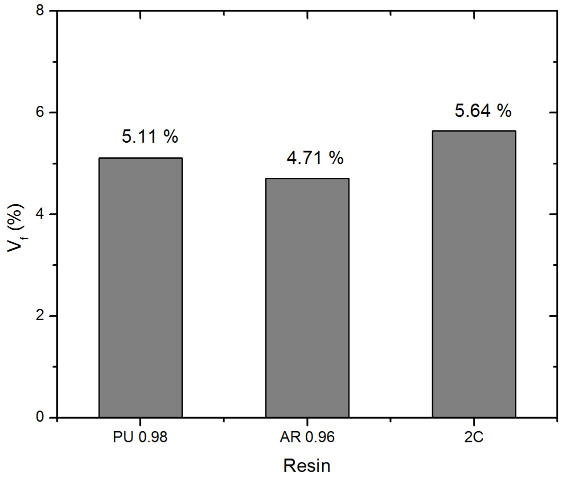

Figure 5.22: The fractional free volume, V_f (%), for the resins used in this study

The radius of the free volume holes and the total fractional free volume of the neat resins are important parameters and have to be taken into consideration. As the following graphs depict, the pure acrylic resin exhibits the lower value of V_f, in comparison to the two polyurethane resins, whereas the highest value of the hole radius is obtained for the solvent-based resin.

The neat acrylic resin exhibits a lifetime of 2.179 ns and intensity of 22.8%. These values correspond to free volume holes with radius of 3 Å and fractional free volume equal to 4.71%. The results reveal no significant changes either in the lifetime or in the radius of the free volume holes, for clay addition of 0.50 and 1.0 wt%.

The lifetime and intensity of PU 0.98 is 2.146 ns and 25.55%, respectively. These results correspond to free volume holes with radius of 3 Å and fractional free volume in the order of 5.11%. The nanocomposite sample of 0.5 wt% clay addition returned the same values for τ_3 as the pure resin. Therefore, the free volume holes also have a radius of approximately 3 Å. The intensity, I_3 of the nanocomposite, though, decreases slightly. This leads to a small decrease in the amount of fractional free volume of the sample: V_f = 5.11% for the resin and V_f = 4.92% for the nanocomposite.

The solvent-based resin exhibits a lifetime τ_3 of 2.407 ns, which corresponds to free volume hole radius of 3.2 Å. The intensity, I_3 leads to fractional free volume in the order of 5.6%. The samples of BEOA and C20A were also under study with the PALS technique. The results are in total agreement with the ones obtained from X-ray analysis. The incorporation of 1.0 wt% C20A leads to the increase in the fractional free volume; 5.6% for the untreated resin and 6.2% for the nanocomposite, whereas the incorporation of 1.0 wt. % BEOA leads to a slight decrease of the lifetime as well as

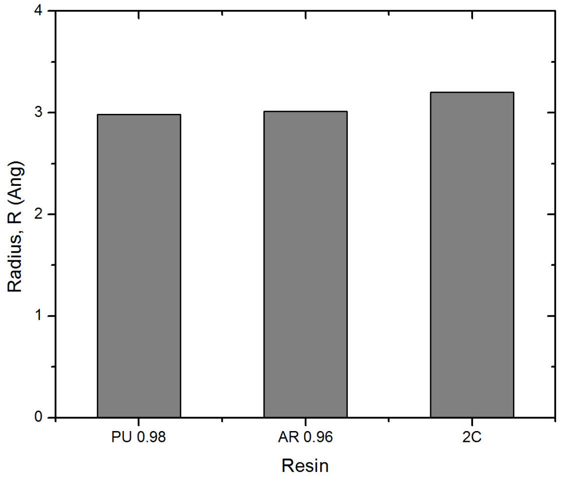

Figure 5.23: The average radius, R, of the free volume holes for the resins used in this study

radius of free volume holes.

5.4.2 Measurements above room temperature

The variations of o-Ps lifetime, τ_3 (ns), and o-Ps annihilation intensity, I_3 (%), that result from changing the temperature are depicted in figures 5.24 and 5.25, respectively. Complete details are included in tables in appendix A.

The o-Ps lifetime undergoes a dramatic change at the glass transition temperature; this transition can also be observed in terms of the free volume hole sizes, since τ_3 is directly related to the radius R of the free volume holes.

The glass transition temperature, T_g, can be estimated by defining the temperature at which the slope of the curve of figure 5.24 changes. As the temperature steps were taken to be approximately 10 degrees, the T_g is estimated to be between 373 K and 383 K. The linear fits of the curve approach seems viable since the values for the correlation coefficient R^2 were R^2 = 0.996 for the points below the change of the slope and R^2 = 0.994 for the points above it. Fig. 5.26 shows the fit for the sample ARBE10.

An important factor that indicates the accuracy of the PALS measurements is the variance of the fit for each tested sample, which should be as close to 1.0 as possible. In this study, three exponential components were required to obtain a good fit with a variance of close to 1.0. The dispersion of the fit variance for measurements at and above room temperature is illustrated in figures 5.27 and 5.28, respectively.

The intermediate lifetime, τ_2, and intensity, I_2 that correspond to the direct anni-

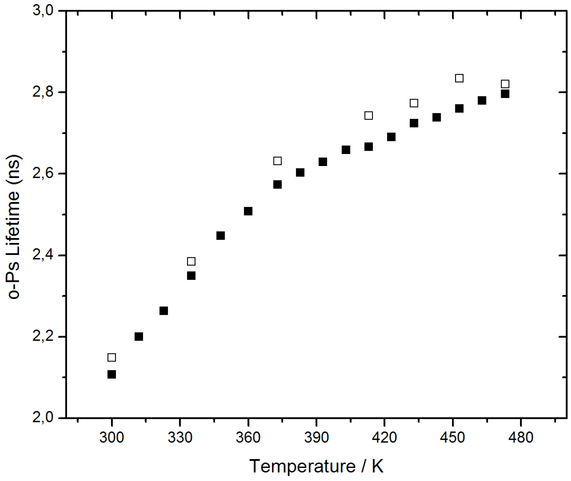

Figure 5.24: o-Ps lifetime for the samples "AR 0.96" (open symbols) and "ARBE10" (solid symbols), at increasing temperature values (300 to 473 K)

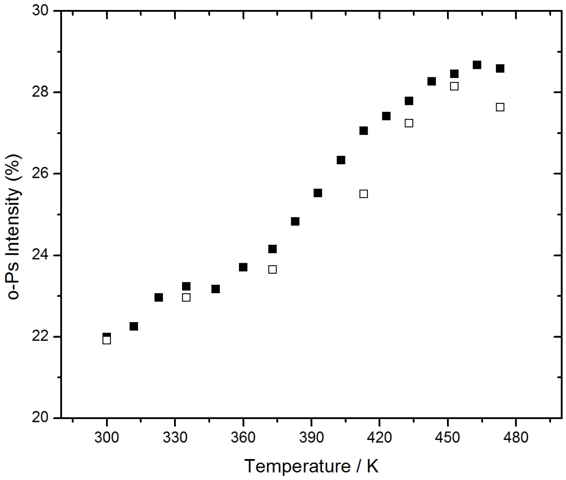

Figure 5.25: o-Ps intensity for the samples "AR 0.96" (open symbols) and "ARBE10" (solid symbols), at increasing temperature values (300 to 473 K).

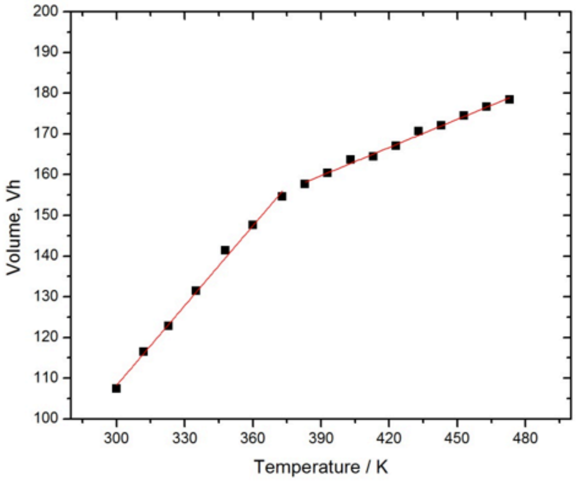

Figure 5.26: The volume, V_h, of an average free volume hole as a function of temperature for sample "ARBE10".

hilation of the positrons in the polymer are shown as functions of the temperature in figures 5.29 and 5.30 for the resin AR 0.96 and the composite ARBE10, respectively. It has been reported [Yu et al, 2006] that the intermediate component might contain information concerning the structure of the interfacial regime between the clay particles and the polymer matrix. However, no clear indication for a transition can be seen at any temperature in these graphs in our data. This mode of positron annihilation, therefore, does not seem to be able to probe the free volume in the polymer or the interfaces in our nanocomposites.

5.4.3 The glass transition temperature

It has already been mentioned that it is possible to obtain different values for he glass transition temperature when using different experimental techniques. Thus, the results of the DSC and PALS methods indicate that $T_{g,DSC}$ is higher than $T_{g,PALS}$, something that is usually seen in the literature.

The discrepancy between the two measurements is attributed to the sensitivity differences of the two methods [Kim et al, 2007]. Further, the measured value of T_g depends on the experimental rate of heating or cooling. The lower $T_{g,PALS}$ values are attributed to the fact that the glass transition temperature depends on the experimental rate and since the heating rate during the PALS measurements is slower than during the DSC scans, this T_g is shifted towards lower temperatures.

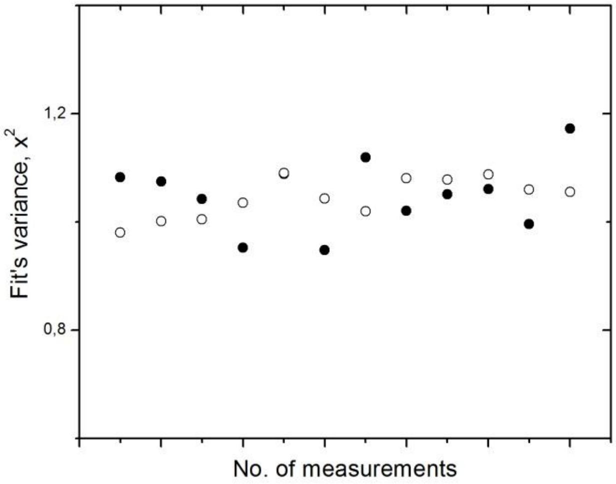

Figure 5.27: Fit variance for tested samples at room temperature. Open and solid symbols correspond to two sets of measurements of the same sample.

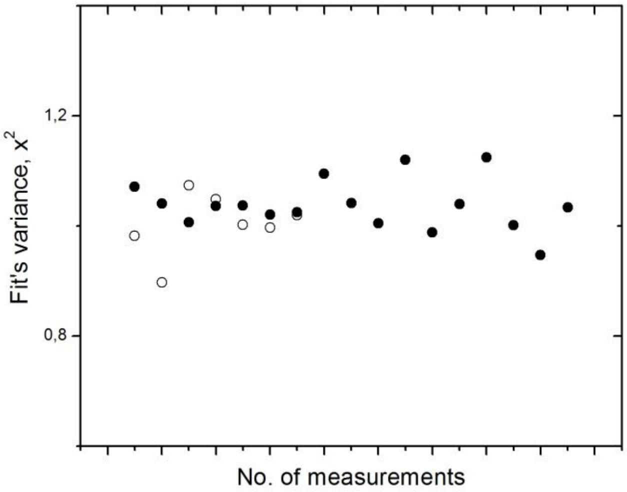

Figure 5.28: Fit variance for tested samples above room temperature (solid symbols correspond to “ARBE10”, open symbols to the pure resin “AR 0.96”).

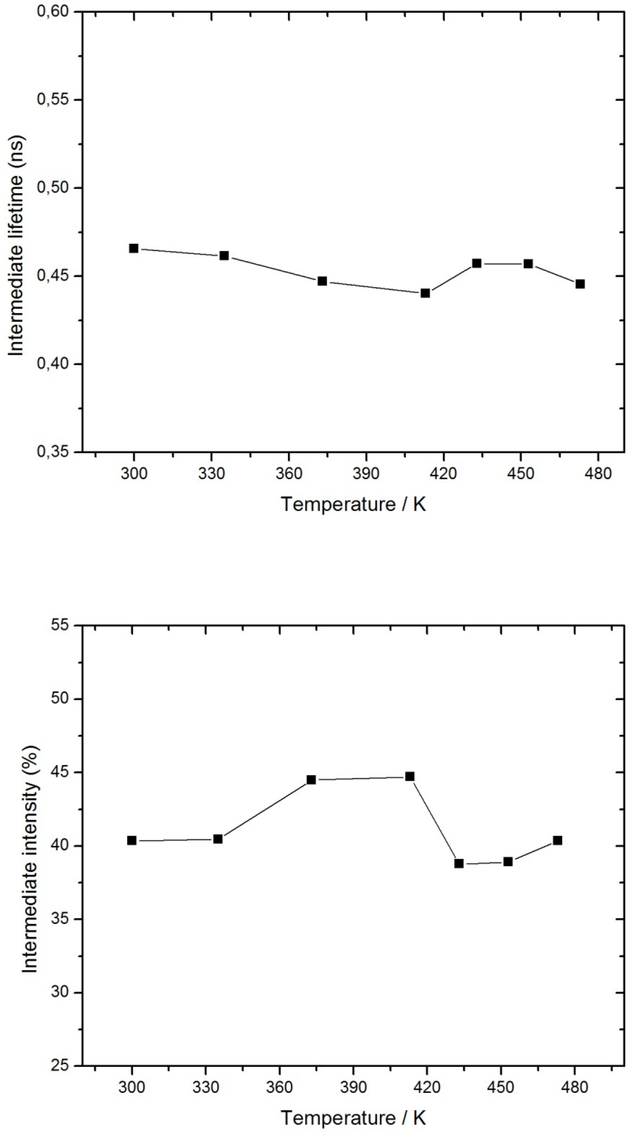

Figure 5.29: Intermediate lifetime τ_2 (top), and intermediate intensity I_2 (%) (bottom) as a function of temperature for sample "AR 0.96".

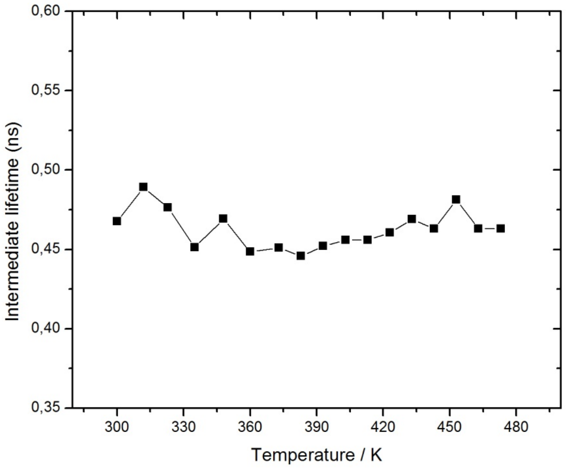

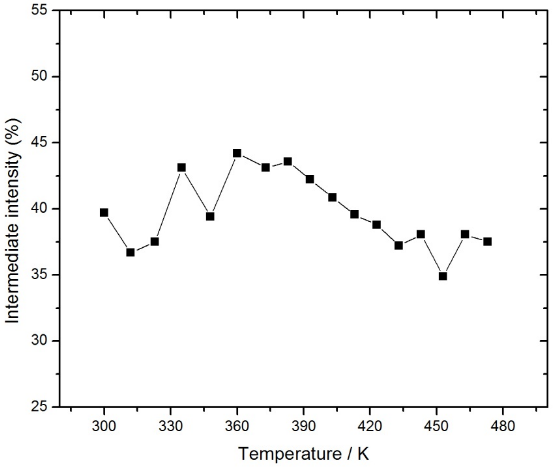

Figure 5.30: Intermediate lifetime τ_2 (top), and intermediate intensity I_2 (%) (bottom) as a function of temperature for sample “ARBE10”.

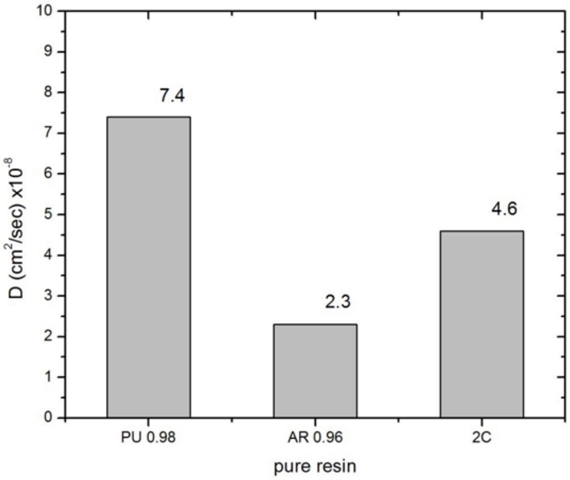

Figure 5.31: Values of the diffusion coefficient, D, for three resins (no clay addition)

5.5 Gas permeability

5.5.1 Diffusion coefficient

Measurements of gas permeability were conducted using various samples. The diffusion coefficient, D (cm^2/s), is an indicator of the gas barrier properties of each tested material. The results are provided in figures 5.31 - 5.35 and complete details are given in the appendix.

The rate of diffusion of gases in the neat resins is not the same for all. PU 0.98 has the highest value for the diffusion coefficient, equal to 7.4 $\times$ 10^{-8} cm^2/s, followed by the 2C (4.8 $\times$ 10^{-8} cm^2/s) and the AR 0.96 (2.3 $\times$ 10^{-8} cm^2/s). From figures 5.31 to 5.35 it can be seen that the incorporation of clay in the resins decreases their diffusivity, even at very low volume fractions.

The hydrophilic, untreated clay dispersed in demineralised water and mixed in the polyurethane resin resulted in a significant decrease of the diffusion coefficient, even though the clay filler was as low as 0.5 wt. %. The decrease in the diffusion coefficient was in the order of 72 %; the diffusion coefficient was from 7.4 10^{-8} cm^2/s for the neat polyurethane resin to 2.1 10^{-8} cm^2/s for the nanocomposite (fig. 5.32).

The untreated montmorillonite clay was also dispersed in the acrylic water-based resin. Completely exfoliated nanocomposites were obtained for clay addition of 0.5 and 1.0 wt. %. The diffusion coefficient decreased from 2.3 $\times$ 10^{-8} cm^2/s for the pure resin to 1.8 $\times$ 10^{-8} cm^2/s for the 0.5 wt% nanocomposite but increased for further addition of clay (fig. 5.33). The fact that the diffusion coefficient increased from 2.3 $\times$ 10^{-8} cm^2/s to 3.8 $\times$ 10^{-8} cm^2/s for the nanocomposite of 1% MMT clay addition can

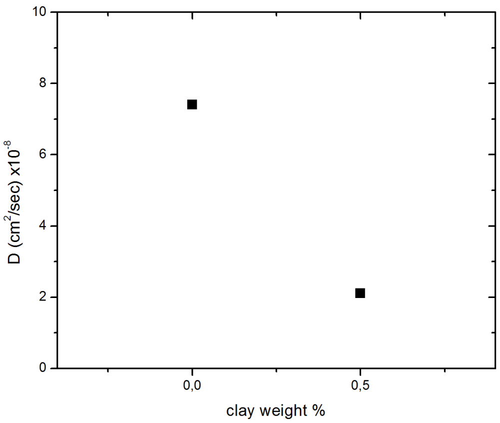

Figure 5.32: Values of the diffusion coefficient, D, for untreated MMT clay nanocomposites in resin PU 0.98. The clay content is zero (for the pure resin) and 0.5 wt%. The dispersion medium is demineralised water.

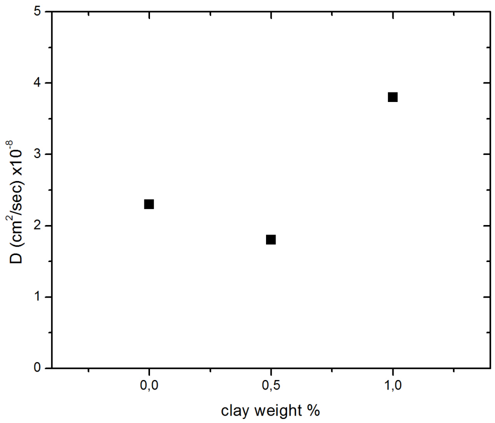

Figure 5.33: Values of the diffusion coefficient, D, for untreated MMT clay nanocomposites in resin AR 0.96. The clay content is zero (for the pure resin), 0.5 wt% and 1.0 wt%. The dispersion medium is demineralised water.

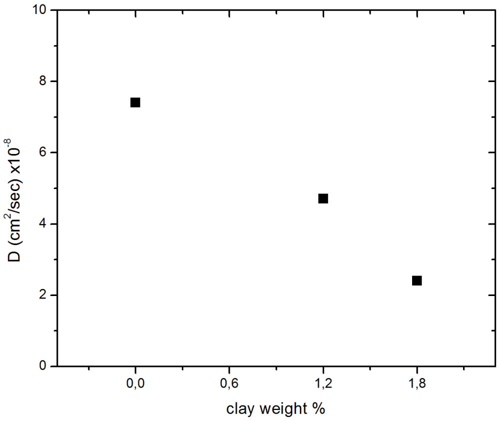

Figure 5.34: Values of the diffusion coefficient, D, for C10A clay nanocomposites in resin PU 0.98. The clay content is zero (for the pure resin), 1.2 wt% and 1.8 wt%. The dispersion medium is acetone.

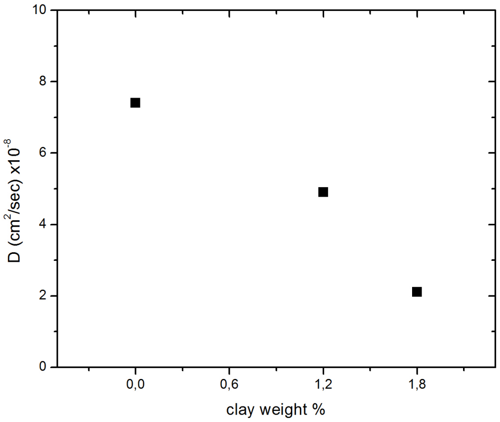

Figure 5.35: Values of the diffusion coefficient, D, for C93A clay nanocomposites in resin PU 0.98. The clay content is zero (for the pure resin), 1.2 wt% and 1.8 wt%. The dispersion medium is acetone.

Table 5.2: Coefficients of: diffusion, D, sorption, S and permeability, K, for the prepared membranes obtained from gas permeation measurements.

Sample	d [mm]	slope of st. state	D [m^2/s] x 10^{-12}	S [mol/(m^3 Pa)] x 10^{-6}	K [mol/(Pa m s)] x 10^{-16}
PU 0.98	0.96	0.03015	7.4	0.039	0.0289
PUBE05	0.57	0.01853	2.1	0.051	0.0106
C93A20A	0.60	0.07952	4.9	0.097	0.0477
C93A30A	0.62	0.03094	2.1	0.091	0.0192
C10A20A	0.62	0.06718	4.7	0.089	0.0417
C10A30A	0.59	0.05316	2.4	0.131	0.0314
AR 0.96	1.05	0.01370	2.3	0.063	0.0144
ARBE05	0.93	0.01236	1.8	0.064	0.0115
ARBE10	1.02	0.01869	3.8	0.050	0.0191
2C	0.83	0.03298	4.6	0.060	0.0274

by attributed to the solidification process since the XRD spectra suggest a completely exfoliated sample; the formation of the film was not successful, leading, thus, to an imperfection on the surface of the film.

The incorporation of 1.2 and 1.8 wt% of the organically modified clay C10A in PU 0.98 resulted in a decrease of the diffusion coefficient in the order of 37% and 68%, respectively. The neat polyurethane resin exhibits a diffusion coefficient of 7.4 $\times$ 10^{-8} cm^2/s whereas the nanocomposites with 1.2 and 1.8 wt% exhibit 4.7 $\times$ 10^{-8} cm^2/s and 2.4 $\times$ 10^{-8} cm^2/s, respectively (fig. 5.34). Similar reduction was achieved for the C93A nano-clay in the water borne polyurethane. The decrease was in the order of 34% and 72% for addition of 1.2 and 1.8 wt%, respectively. The diffusion coefficients were 4.9 $\times$ 10^{-8} cm^2/s and 2.1 $\times$ 10^{-8} cm^2/s, respectively (fig. 5.35).

5.5.2 Sorption and permeability coefficients

The permeability of the samples was determined directly from the slope of the permeation curve at steady state, the pressure in the chambers and the membrane thickness (eq. 4.11). The permeability coefficient for all tested resin membranes is depicted in fig. 5.36 - 5.39. The estimation of the sorption coefficient was based on the relation of $K = D \times S$. All data regarding the coefficients are provided in Table 5.2.

The data verify the need for proper resin selection (Fig. 5.36); the acrylic water-based resin exhibits the lowest diffusion coefficient, D (fig. 5.31), as well as perme-

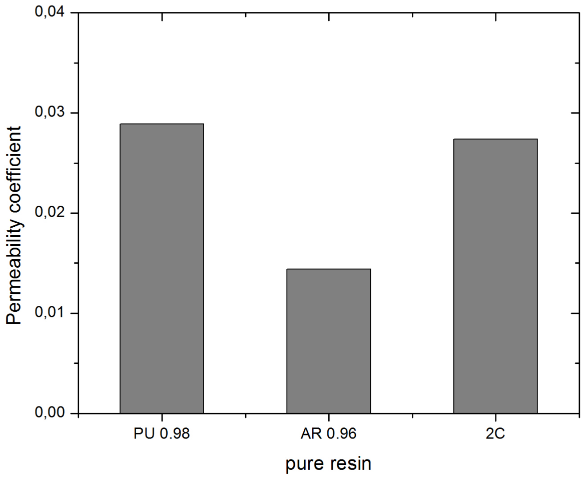

Figure 5.36: Values of the permeability coefficient, K ($\times 10^{-16}$ mol Pa^{-1} m^{-1} s^{-1}), for three resins (no clay addition).

ation coefficient, K, in comparison to the two polyurethane resins (water- and solvent-based). The nanocomposite films show a decrease in the diffusion coefficient, regardless of the type of montmorillonite clay (untreated or organically modified) that has been incorporated in the polymer matrix. On the other hand, the sorption and permeability coefficients, are influenced by the type of clay. The permeability decreases in cases where the untreated MMT clay has been dispersed in the matrix, as shown in fig. 5.37. In those cases, however, the sorption coefficient increases slightly. As for the films based on organically modified nano-particles (C10A and C93A), the permeability coefficient increases (fig. 5.38 and 5.39). While the diffusion coefficient is still lower for these samples, the increase of the permeability reflects the significant increase of the sorption coefficient, S. This particular behaviour, regarding the C10A and C93A films may be attributed to the lack of affinity between the penetrating gas molecules of CO_2 and the organic modifier of the nanoparticles, since the sorption coefficient is a parameter that depends on the strength of the interactions between the components involved in PCNs.

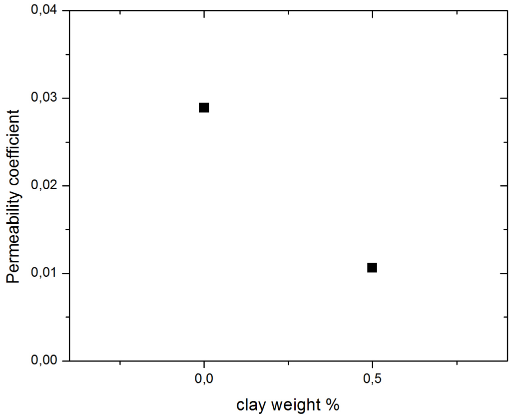

Figure 5.37: Values of the permeability coefficient, K ($\times 10^{-16}$ mol Pa^{-1} m^{-1} s^{-1}), for untreated MMT clay nanocomposites in resin PU 0.98. The clay content is zero (for the pure resin), 0.5 wt%. The dispersion medium is demineralized water.

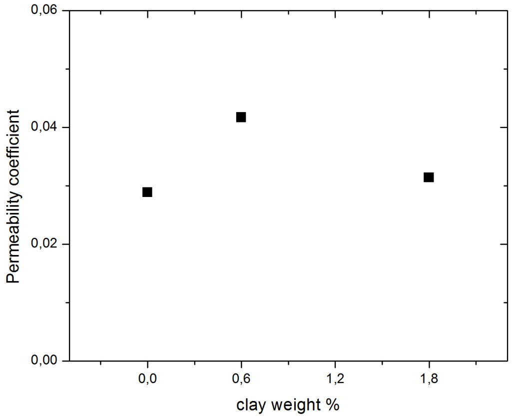

Figure 5.38: Values of the permeability coefficient, K ($\times 10^{-16}$ mol Pa^{-1} m^{-1} s^{-1}), for C10A clay nanocomposites in resin PU 0.98. The clay content is zero (for the pure resin), 1.2 wt% and 1.8 wt%. The dispersion medium is acetone.

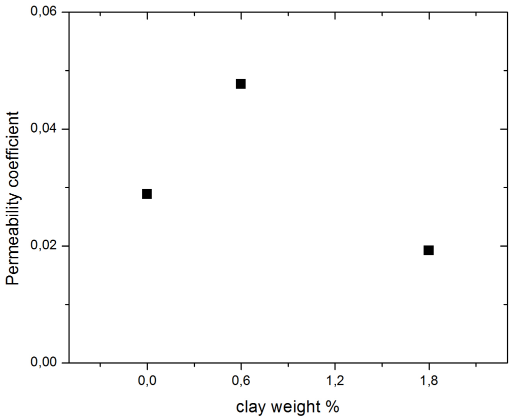

Figure 5.39: Values of the permeability coefficient, K ($\times 10^{-16}$ mol Pa^{-1} m^{-1} s^{-1}), for C93A clay nanocomposites in resin PU 0.98. The clay content is zero (for the pure resin), 1.2 wt% and 1.8 wt%. The dispersion medium is acetone.

Chapter 6

DISCUSSION

6.1 Water-borne resins

The thermal behaviour of the samples was investigated using two methods of thermal analysis in the present study. The experimental techniques of DSC and TGA reveal the heat capacity of the sample as a function of temperature and the mass loss of the sample during heating, respectively.

The DSC experiments were conducted to determine the glass transition temperature of each tested sample. The results confirmed the speculation that a low filler content of MMT does not have a strong impact on the value of T_g. The sample of 5 wt% clay addition, as well as the neat acrylic resin, exhibit a T_g in the regime of 120 -130 °C. The same results are obtained for the polyurethane resin, whereas the solvent-based resin exhibits a higher T_g in the regime of 130 - 140 °C. The obtained values of T_g for the tested polymer matrices are a useful indicator for probable application areas of the particular nanocomposite materials. It should noted that all these resins produce nanocomposite coatings that can be safely used well above room temperature, perhaps up to the normal boiling point of water.

TGA measurements were performed in order to verify the exact clay fractions of the tested samples. The results of the residue were in agreement with the theoretical calculated values used for the preparation of the nanocomposite samples. This indicates the absence of problems of precipitation of the clay in the samples and verifies the accuracy of the mass fraction data of the components of the final composite.

The X-ray diffraction analysis was utilised to reveal information regarding the structure of the prepared nanocomposite films. The obtained structures can be defined as intercalated or exfoliated according to the layer expansion of the clay in the nanocomposites. When the clay becomes exfoliated, the characteristic peak disappears, whereas in case of intercalated structures the corresponding peak is shifted towards lower 2θ values.

XRD measurements were performed for all pure nanoclay powders. The characteristic peak of each type of clay was translated to the interlayer spacing by making use of Bragg's equation. The data confirm that as the surface hydrophobicity increases, the interlayer spacing also increases. This should be expected, since a more hydrophobic modification of the clay surface is usually obtained by longer aliphatic chains, which, when they enter the inter-layer galleries, inhibit the ionic attractions of the clay platelets and can push them further apart.

The XRD spectra of the nanocomposites indicate that the dispersion of the untreated montmorillonite particles in demineralized water was successful for both water-based resins, but only in very low filler content. The maximum clay addition, for which fully exfoliated nanocomposites were obtained, was 0.5 wt% and 1.0 wt% for the polyurethane and acrylic resin, respectively. For clay loads higher than these values a diffraction peak is present at 6.4°, which is the characteristic peak of the aggregated unmodified montmorillonite clay. In this case there are remaining aggregated clay particles suspended in the matrix that are neither exfoliated nor intercalated. These particles are not expected to contribute significantly to the reduction of the permeability of the coating.

When organophilic (modified) montmorillonite have been added to the polyurethane water-based resin the dispersion media included two organic solvents, acetone and ethyl alcohol, used because of their miscibility with water. In the cases where acetone was used, and for low clay loadings, exfoliation was obtained. On the contrary, ethyl alcohol did not present the characteristics of an appropriate solvent. This pattern of interaction could be attributed to the fact that acetone combines both polar and apolar characters. This can be described in terms of thermodynamics, as it will be discussed further on.

6.2 Solvent based resin

Regarding the solvent-based resin, a binary mixture of solvents, constituted of 70 wt% xylene and 30 wt% ethyl alcohol, was used for the dispersion of the nano-particles. The particular solvents were not only chosen due to their miscibility at room temperature conditions but also because they combine high polarity (e.g., hydroxyl groups in ethyl alcohol) with a high organophilic character (o-xylene). The dispersion of 1 wt% BEOA, C20A and C30B resulted in intercalated, to some degree, structures. On the contrary, the dispersion of 1.0 wt% C10A was successful. The latter can be attributed to the interactions of xylene with the benzyl groups of the exchanged ions.

It is interesting to note that all organically modified clays dispersed in the binary mixture of ethyl alcohol and xylene resulted in initial dispersions that were gel-like and remained stable over several days. However, when these dispersions were introduced into the resin and composites were made, the XRD graphs showed mainly intercalated structures. This could be attributed to the presence of ethyl alcohol in the mixture. Even though the addition of ethanol was low, its presence in the final mixture could cause miscibility issues, since the resin included only xylene as solvent.

As far as the shift to higher 2θ values observed in the XRD graph of the 1.0 wt% C20A nanocomposite (Fig. 5.14) similar trends have been reported by Filippi et al [2011]. The nanofiller in this case undergoes a 'd-spacing collapse', which can be attributed to a probable reorganisation of the alkyl chains of the clay modifier inside the galleries or a partial removing of the modifier from the surfaces.

6.3 Interactions and Solubility parameters

The dispersion of nano-particles in various organic solvents is the key for acquiring an exfoliated nanocomposite, since the preparation method followed in the present work is solvent-based. At first glance, it seems that the non-polar part of the solvents could be compatible with the long carbon chains (hydrogenated tallow) included in the surfactant of each organoclay whereas the polar part of the solvents could favour, for instance, hydrogen bonds with the hydroxyl groups (-OH). During the preparation and characterisation processes of PCNs, though, the idea is not that simple.

The underlying mechanism for a successful preparation of gas-barrier nanocomposites can be found by examining the interactions between the components used in polymer/clay nanocomposites and particularly upon determination of the parameters that control the dispersion of the MMT nanoclay in various organic solvents used as the initial dispersion media. The interactions between the substances/components involved in the preparation of the polymer/clay nanocomposites have been studied extensively and many results and suggestions can be found in the literature. In the present work the preparation method that was followed forced the dispersion of the nano-layers in a solvent-suspension medium, prior to the dispersion into the polymer matrix. It is, thus, reasonable to claim that the process of the dispersion of the organoclay into the initial suspension medium controls and determines to some degree the final properties of the film. Thus, it is useful to evaluate and determine the physical parameters that dominate the clay dispersion process in the solvents used.

6.3.1 Solubility parameters and surface energy of solvents and surfactants

The organic modification of the MMT clays used in the present study was based on a surfactant that displays an organic character and insulates the inorganic nature of the pure, untreated clay. Consequently, the selection of a specific modified nanoclay for the polymer/clay composites should be based on the modifier's chemical structure and thermodynamic properties. The study of the surface chemistry of the constituents, therefore, is critical for the understanding of the complex technology of nanocomposites.

The organoclays used in the present work have very different surface properties which are due to the structure and the chemistry of the modifier/surfactant. For instance, the C20A and C93A are the most hydrophobic clays because of the densely organised aliphatic chains of the modifier (Table 4.1). The C30B is the most polar nanoclay because of the two ethanol groups of the modifier, and the C10A seems to display an intermediate behaviour, since its modifier contains a phenyl group.

A useful way of evaluating the interactions between the components of polymer/clay nanocomposites and the solvents used for their preparation, as well as obtaining a more quantitative picture, is to estimate the solubility parameters of the organo-modifiers and all other components, by summing the group contributions of the molecules [van Krevelen, 1990]. The correlation between the solubility parameters of the organophilic nanoclays and those of the solvents used as dispersion medium could lead to

Table 6.1: Group contributions to the cohesive energy and molar volume of functional groups used to estimate the solubility parameter for the organo-modifiers of MMT nanoclay

Group	E_{coh} (J/mol)	V_m (cm^3/mol)
$-CH_3$	4707	33.5
$-CH_2-$	4937	16.1
$-OH$	29790	10
Phenyl	31924	71.4
Nitrogen	4184	9

[Fedors, 1974]

the understanding of nanocomposites behaviour and, thus, to suggestions of probable combinations of miscible or compatible materials. In general, when the values of the solubility parameters of two substances are close to each other, then the substances are miscible or compatible to each other. Thus, the possibility of the solvent entering the galleries of the modified clay and resulting in exfoliation of the clay follicles increases with the better matching of the values of the solubility parameters of the solvent and the modifier.

The solubility parameter (δ) of each surfactant can be estimated at room temperature by adding the cohesive energy and molar volume contributions of each functional group and each fragment of the parent structure of the molecule. This method is called Fedors Group Contribution Method and is expressed as:

$$\delta = \sqrt{\frac{\sum_i E_{coh,i}}{\sum_i V_{m,i}}} \tag{6.1}$$

where δ is the solubility parameter of a molecule, $E_{coh,i}$ is the cohesive energy of the i functional group of the molecule, and $V_{m,i}$ is its molar volume. The data of cohesive energy and molar volume for the functional groups involved in the organo-modifiers are presented in table 6.1.

The interfacial tension γ_{int} is another indicator for the compatibility between the clay modifier and the solvent. When the two are miscible, γ_{int} should be zero. The closer γ_{int} is to zero, the more compatible these are. The interfacial tension can be estimated by the difference of the values of the surface tensions of the two phases. The surface tension, γ_s, of each surfactant can be deduced from its solubility parameter according to an empirical relationship proposed by van Krevelen [1990]:

$$\gamma_s = 0.75\delta^{4/3} \tag{6.2}$$

The calculated solubility parameters and the values of the surface tension of the modifiers are reported in table 6.2.

Table 6.2: Solubility parameter and surface tension of the organic modifiers

Surfactant	Solubility parameter, δ, at 20 °C, (MPa)$^{0.5}$	Surface tension, γ_s at 20 °C, (mN/m)
C10A	17.5	34.1
C20A	16.8	32.3
C93A	17.1	33.0
C30B	20.6	42.4

The solubility parameters are calculated according to eq. 6.1 and the surface tension according to eq. 6.2

Table 6.3: Hansen's solubility parameters (MPa)$^{1/2}$ and surface energy (dyn/cm) of solvents

Solvent	δ_0	δ_d (MPa)$^{1/2}$	δ_p	δ_H	H-bond	Surf. energy (dyn/cm)
acetone	20.1	15.5	10.4	7	moderate	23.32
ethyl alcohol	26.6	15.8	8.8	19.4	strong	22.32
o-xylene	18	17.8	1	3.1	weak	30.3
water	47.9	15.5	16	42.4	strong	72.8

The solubility parameter for the surfactant on the C30B clay platelet surface has been calculated using various methods by McLauchlin and Thomas [2009]. They obtained a value of 17.33 MPa$^{1/2}$ for δ following the Hoftijzer - Van Krevelen method, 19.67 MPa$^{1/2}$ following Hoy's method and 20.6 MPa$^{1/2}$ following Fedors. Our calculated solubility parameter of C30B (δ = 20.6 MPa$^{1/2}$) is in agreement with Fedors' results.

Regarding the values of Hansen solubility parameters for the organic solvents, they can be found in the literature [Brandrup et al., 1999]. The solubility parameters and surface energy of the solvents used in the present study are provided in table 6.3.

The solvents used for the initial dispersion, acetone and ethanol, were chosen also to be somewhat miscible/compatible to water, as the clay suspension should be mixed with the water-borne dispersions of the resins. For the solvent based systems, the solvents were chosen to be compatible with the solvent of the resin (o-xylene). Thus, the ultimate requirements for the solvent was to bridge the organically modified surface of the clay to that of the solvent/suspension medium of the resin. After the suspension medium evaporates, this would also lead to compatibility of the clay to the (modified) surface of the resin droplets at the beginning and during the process of the hardening of the resin and the formation of the film.

It can be seen in these tables that the solubility parameters of the organo-modifiers are closer to the total solubility parameters (δ_0) of acetone than those of ethyl alcohol. This indicates better compatibility with the former than the latter. This trend agrees with the XRD results of the nanocomposites made from C10A, C93A and C30B clays initially dispersed in acetone or in ethyl alcohol. According to the diffraction graphs, the use of acetone resulted in fully exfoliated or intercalated structures, whereas the use of ethyl alcohol resulted mostly in immiscible, phase-separated structures and the appearance of a diffraction peak located around 2θ = 6.4° (the same as the diffraction peak of pure MMT).

The value of δ_0 of o-xylene is also close to the one of the C10A clay. Indeed, this clay seems to be readily dispersed in this solvent. The successful dispersion of C10A in a binary mixture of solvents (xylene and ethyl alcohol) could be attributed to the fact that xylene was the solvent in excess (70 wt%), in comparison to the small proportion of ethyl alcohol (30 wt%), thus lowering the total solubility of the dual mixture.

The analysis according to group contribution theory suggests that for a successful nanocomposite the solubility parameters of the clay surfactant should be close in value to the ones of the solvents used as the initial dispersion medium. Equal values of the solubility parameters reflect the ability for interaction between the functional groups involved and, thus, indicate better miscibility between the components. The quantitative approach presented here is in agreement with the results obtained from XRD measurements.

On the other hand, the chemical structure of ethyl alcohol suggests that it could be a proper dispersion medium for clay C30B, due to the two ethanol groups present on the modifier ion. However, it might be misleading to rely solely on the simple observation of the chemical structure of the components involved. It is, thus, imperative that the solubility parameters of the solvents and the organoclays be matched to achieve a good dispersion of the clay in the composite.

6.3.2 Kinetics

Beyond the solubility parameters, the fact that the utilisation of acetone results in fully exfoliated nano-structures could be explained in terms of kinetics. A possible mechanism is due to the rapid evaporation of acetone, in comparison to ethyl alcohol, providing, thus, a random dispersion of the platelets in the matrix but without interfering with the components and causing miscibility problems.

6.4 Permeability

Polymer clay nanocomposites can exhibit highly enhanced barrier properties as it can be found in literature. It is reported that a reduction in gas permeability down to 50 - 500 times of that of the pure matrix can be attained by incorporating low silicate filler content, usually in the order of 5 wt% (or less) of dispersed nanoclay. For instance, [Wang et al, 2005] investigated a nanocomposite that involved a styrene-butadiene rubber as a matrix and rectorite as the clay filler. The rectorite/SBR permeability was only 31.2% of that of the pure SBR matrix. As it has been mentioned, this reduction in permeability can be attributed to the tortuous diffusional path due to the clay presence. Moreover, [Ogasawara et al, 2006] reported that increasing the montmorillonite loading in an epoxy matrix leads to a significant decrease of the gas diffusivity of Helium.

The diffusion of gases in polymers takes place by gas molecules jumping from free volume hole to free volume hole. The size and the number of these holes control the rate of diffusion, i.e., the diffusion coefficient. The presence of nanoplatelets prolongs the diffusion path, as it induces tortuosity, and helps to decrease this coefficient. The large surface area that the exfoliated particles have, however, and their incompatibility with the polymeric matrix may create extra free volume at the interfaces. This free volume will enhance the diffusion, if the holes created are large enough, and can cancel the effect of tortuosity.

PALS experiments were conducted in this work to estimate the availability of free volume in the polymer in the nanocomposites. The measurements that took place were performed at room temperature (300 K) as well as at various temperatures above room temperature (300 to 473 K). The values of τ_3 and I_3 of the PALS measurements, were translated to the radius of the free volume holes, R, and the fractional free volume V_f (%), assuming spherical free volume cavities.

The multiple temperature measurements were conducted only to study the glass transition of the polymeric matrix. The room temperature measurements were conducted to examine whether the filler particles created extra free volume in the composite.

The neat acrylic resin has free volume holes with radius of 3 Å and fractional free volume equal to 4.71%. The results reveal no significant changes, either in the lifetime or in the radius of the free volume holes, for clay addition of 0.50 and 1.0 wt%. The water-based polyurethane resin has free volume holes with radius of 3 Å and fractional free volume in the order of 5.11%. The nanocomposite sample of 0.5. wt% clay addition has free volume holes also with a radius of approximately 3 Å but slightly less fractional free volume V_f = 4.92%.

As for the solvent-based samples, the neat resin has free volume holes with average radius of 3.2 Å and fractional free volume in the order of 5.6 %. The samples of BEOA and C20A were also under study with the PALS technique. The results are in total agreement with the ones obtained from X-ray analysis. The incorporation of 1.0 wt% C20A to resin 2C leads to the increase in the fractional free volume to 6.2 %, whereas 1.0 wt% BEOA leads to a slight decrease of the radius of free volume holes.

From the above, it can be stated that no significant change in the free volume was found in the nanocomposites using PALS. This is probably due to the appropriate compatibilisation techniques that were applied. However, there is some uncertainty in the accuracy of these measurements in the case of untreated clays. In that case there may remain a strong charge on the surfaces of the clay that could repeal the positrons from that areas. This could underestimate the free volume there. If this was the case here, however, we would also have an increase in the permeability, which was not found.

To study the effects of the interactions between the components in the nano-films in terms of barrier properties we performed gas permeability experiments. The incorporation of the hydrophilic, untreated clay in demineralised water in the polyurethane resin resulted in a significant decrease of the diffusion coefficient,in the order of 72%, even though the clay filler was as low as 0.5 wt%. The untreated montmorillonite clay was also dispersed in the acrylic water-based resin. Completely exfoliated nanocomposites were obtained for clay addition of 0.5 and 1.0 wt%. and again the diffusion coefficient decreased, but to a lesser degree than for the polyurethane resin.

The permeation measurements were also conducted for nano-films that were based on the incorporation of organically modified nanoclay particles. The two types of organoclay which demonstrated exfoliated structures (C10A and C93A) were successfully dispersed in acetone and then introduced into the water-borne polyurethane resin. The gas permeation measurements, for both nanoclay types, showed enhanced barrier properties: a decrease in the diffusion coefficient in the order of 37% and 68% for 1.2 and 1.8 wt% of C10A clay in PU 0.98, respectively, and a decrease in the order of 34% and 72% for 1.2 and 1.8 wt% of C93A clay in PU 0.98, respectively.

As it has already been reported, the permeation of gas molecules through a membrane is a process that includes several consecutive steps. The gas is sorbed at the entering face of the film and it dissolves there; the dissolved penetrant molecules diffuse through the membrane via a random-walk mechanism; and they desorb at the exit face of the film. The sorption coefficient, S, is based on the first stages of the permeation process; the sorption of the gas molecules onto the film and the dissolution in it. It describes the affinity of the gas molecules with the matrix. On the contrary, the diffusion coefficient describes the kinetic process of the gas molecules into the polymer matrix. The mass flow and, thus, the permeability, K, of the coating depends on both the diffusion coefficient, D, and the sorption coefficient, S ($K = D \times S$).

The experimental results of all membranes, show a decrease in the diffusion coefficient, as a function of clay addition. This is expected and due to the more tortuous path for the diffusing gas penetrants. This reduction is indicative of the successful incorporation and, thus, dispersion of the nano-platelets into the organic matrix. It could be stated that the diffusion coefficient is not affected by the type of nano-clay used in the synthesis of PCNs. On the contrary, the results regarding the sorption and permeability coefficients suggest an influence of the modification applied on the clay involved. The trends regarding the permeation coefficient are only definitive when untreated MMT has been used, where a clear decrease has been observed upon addition of 0.5 wt%. When organically modified nano-particles, such as C10A and C93A, are used, the values of the sorption coefficient increase significantly compared to the ones of the resin. However, there is no definite trend for the sorption coefficent upon increasing the amount of filler. These results point towards the need of a better understanding of the interaction of the penetrating gas with the organic components in the PCN (mainly the organic matrix and the type of organic modifier of the clay nanoplatelets). The solubility paramenter of CO_2 is 14.56 (MPa)$^{1/2}$ [APIThailand, 2012], a value that shows a non-polar molecule. The presence of the organic modification on the MMT will enhance the affinity of the composite to the gas in comparison with the untreated (polar) clay. This could explain the differences in the value of the sorption coefficient between the nanocomposits made with treated and untreated clay in Table 5.2. The realisation of these differences, though, is useful. Polymer/clay nanocomposite films can be synthesised and tested for various types of gases; the results can, then, point out which types of gases will be better kept out of the particular nano-films.

Another point that should be mentioned here is regarding the size distribution of the free volume holes. As Choudalakis and Gotsis [2012] have indicated, for the same average size, a broad distribution with bias towards larger holes would induce faster diffusion, while the bias to smaller sizes would decrease the diffusion more dramatically. The size of the diffusing gas molecules sets a threshold size for the free volume holes. Holes with smaller size than this threshold do not contribute essentially to the diffusion. Some deviations from the trend of reducing the permeability with increasing loading of exfoliated clay, while the free volume remains unaffected, may be explained by such changes in the size distribution.

A conclusion can also be drawn regarding the suitability of the neat resins used in the present study for materials with barrier properties. The derived data from PALS point out that the water-based acrylic resin could be the most suitable, in comparison to the water and solvent-borne polyurethane resins, since it exhibits the lowest fractional free volume, V_f. Moreover, the gas permeability experimental results also point towards the same direction of resin selection, since the acrylic resin has the lowest diffusion coefficient, D, in addition to the lowest permeation coefficient, K.

The selection of the resin, though, is a complicated problem. The drawback of water-based resins can be expressed in terms of miscibility; they set a restriction in choosing a solvent as the dispersion medium, since water is involved in the mixture. On the other hand, the solvent-borne resins display the drawback of possible solvent residue in the cured composite. The solvent-borne resin used in the present work included xylene which has very low vapour pressure at room temperature and, thus, evaporates slowly. Moreover, the fact that, in some cases, a binary mixture of solvents yields a better degree of exfoliation might become an obstacle to the evaporation rates and finally lead to permeable films, due to different evaporation rates and probable residue of one of the solvents present in the mixture.

Summarising this chapter we can conclude that the best combination of solvent, clay, and resin that we attempted, aiming at the barrier properties of a cured nano-film, involves a water-based resin, as the polymer matrix, acetone as the initial clay dispersion medium and organically modified types of montmorillonite clay. The selection of water-borne resins, instead of solvent-based, relies mostly in examining miscibility factors. Various water miscible solvents can be utilised for such systems.

The particular interest over water-based systems can also be interpreted in terms of the increasing attention towards the environmental impact; the hazardous vapour emission reduction is due to the use of water instead of solvents, since water presents no toxic hazard. Moreover, with the use of water one does not need the expensive recycling of the solvents, resulting, thus, in reduced cost. In addition, in solvent-based systems, there is also the chance that a long time after the films have been formed, there may still be residual solvent left in them. The retention of solvents in films can be a major problem in systems designed to cure rapidly.

The selection of the initial clay dispersion medium (acetone in the present study) is based on the values of the solubility parameters; when the solubility parameters of two substances have matching values, then the substances are prone to be miscible or compatible to each other. According to the results derived from group contribution theory calculations, the matching of the values of the solubility parameters of the solvent and the organic modifier of the MMT clay enables the insertion of the solvent into the galleries of the modified clay, resulting, thus, in exfoliated nano-structures.

Finally, regarding the selection of the clay particles, the modified types of montmorillonite, rather than the untreated clay, favour the penetration of the solvent between the galleries; the organic modification of the clay surface leads to an increase of the gap between the layers, which could stimulate the entry of the solvent molecules into the inter-gallery regions, leading to more efficient swelling of the nanoclay. Additionally, the particular surface modification renders the particles more compatible with a whole host of polymeric matrices and systems. Of course the solubility parameter of the modifier should match the one of the initial dispersion medium (solvent). It seems that for our water-borne, heavily compatibilised resin systems the close matching of the solubility parameter of the resin itself to that of the modifier is initially of secondary importance, but it may be significant to avoid the collapse of the clay when the water and the solvents have evaporated. This is an area where additional study could be informative.

Chapter 7

CONCLUSIONS AND IMPLICATIONS

During their manufacturing stage, polymer/clay nanocomposites are essentially ternary systems; they are composed of clay nano-particles, with inorganic or organically modified surfaces, solvents or suspension media (could be water or organic) and a polymer matrix. The crucial stage (even before the manufacturing process) is the selection of the three components involved, which will also determine their future interactions.

The synthesis of PCNs has become a field of intensive research interest over the last years, yet alternative approaches have to be developed in order to circumvent the challenges during mixing and dispersion processes. The preparation techniques ought to be carefully designed in order to accomplish a uniform dispersion and complete exfoliation of the clay in the manner of fine particles or even single layers into the matrix and avoid the nanoparticles agglomeration.

The compatibility between all components should not be neglected and all interactions need to be taken into consideration. It is, thus, essential for the clay particles to be uniformly dispersed in the polymer host in order to create the highest possible amount of interfacial zone that will lead to improved properties with respect to pure polymers or conventional composite materials.

From both a theoretical and experimental point of view, montmorillonite, MMT, stands as a promising nanofiller, for various polymeric matrices. The high aspect ratio leads to enhanced barrier properties and decreased diffusivity of gas molecules, such as CO_2. The nano-films prepared during the present study reveal enhanced barrier properties in the order of 72 % decrease of the diffusion coefficient for MMT load as low as 0.5 wt%.

The experimental results of the present thesis suggest that the selection of the materials involved in polymer / clay nanocomposites is the most critical phase of the synthesis and much effort should be devoted to the choice of the components to ensure optimal properties of the material for the intended application. The deriving and proposed combination of resin, solvent and clay consists of a water-borne resin as the polymer matrix (mainly due to miscibility factors, in addition to a more environmentally-friendly and economically perspective), acetone as the dispersion media (due to matching of the solubility parameters of the particular solvent and the organic modifier of the clay) and organically modified clay particles (due to their increased distance between the layers and their compatibility with a whole host of polymeric matrices and systems).

Future work

The present research has left a number of open questions and possibilities that merit further investigation:

- Future work should be carried regarding the diffusion of other gas molecules in order to synthesise nano-structured barrier films applicable to many different areas.
- The effect of the kinetics of water/solvent evaporation is another area of needed research. It should be compared to the reaction kinetics of the thermosetting resin.
- The retention of solvent molecules in the film, their slow diffusion through the clay particles and the possible resulting free volume in the matrix is an area that has to be studied, as it influences the time stability of the properties of the coating.
- In the present study only the interaction between the solvents during the dispersion stage and the modification was examined. The interactions between the organic resin, the clay modifier and the penetrating gas constitute also an interesting subject of investigation, as they may influence the soprtion/disorption of the gas in the membrane.
- The orientation of the nano-platelets is a rather challenging issue, since it has a strong impact on the permeation properties of PCNs, in addition to their volume fraction and aspect ratio. Possible mechanisms that control the orientation of the platelets, relative to the diffusion direction, of the nano-platelets could vastly contribute to their gas barrier properties.

Bibliography

D. R. Paul and L.M. Robeson. Polymer nanotechnology: Nanocomposites. *Polymer*, 49:3187 – 3204, 2008.

Fengge Gao. Clay/polymer composites: the story. *materialstoday.*, 7:50 – 55, 2004.

Camargo et al. Nanocomposites: Synthesis, structure, properties and new application opportunities. *Materials Research*, 12:1 – 39, 2009.

Masami Okamoto. Polymer/layered silicate nanocomposites. *Rapra Review Reports (Toyota Technological Institute)*, 14(7), 2003.

K. Yano, A. Usuki, A. Okada, T. Kurauchi, and O Kamigaito. Synthesis and properties of polyimide-clay hybrid. *J. Polym. Sci. Polym. Chem.*, 31:2493 – 2498, 1993.

T. Lan, P.D. Kaviratna, and T Pinnavaia. On the nature of polyimide-clay hybrid composites. *J. Chem Mater.*, 6:573 – 575, 1994.

P.B. Messersmith and E.P Giannelis. Synthesis and barrier properties of poly(Œµ-caprolactone)-layered silicate nanocomposites. *J. Polym. Sci. Polym. Chem.*, 33:1047 – 1057, 1995.

K.E. Strawhecker and E Manias. Structure and properties of poly(vinyl alcohol)/Na$^+$ montmorillonite nanocomposites. *Chem. Mater.*, 12:2943 – 2949, 2000.

O. Gain, E. Espuche, E. Pollet, M. Alexandre, and PH. Dubois. Gas barrier properties of poly(Œµ-caprolactone)/clay nanocomposites: Influence of the morphology and polymer/clay interactions. *J. Polym. Sci. Polym. Phys.*, 43:205 – 214, 2005.

Z.F. Wang et al. Influence of fillers on free volume and gas barrier properties in styrene-butadiene rubber studied by positrons. *Polymer*, 46:719 – 724, 2005.

T. Ogasawara et al. Helium gas permeability of montmorillonite/epoxy nanocomposites. *Composites: Part A*, 37:2236 – 2240, 2006.

S. Sinha Ray and M. Okamoto. Polymer/layered silicate nanocomposites: a review from preparation to processing. *Prog. Polym. Sci.*, 28:1539 – 1641, 2003.

Vikas Mittal. Barrier properties of polymer clay nanocomposites. In *Nanotechnology Science and Technology Series*. 2010.

Jean-Pierre Pascault and Roberto J. J. Williams. *Epoxy Polymers, New Materials and Innovations*. Wiley, 2010.

Y.C. Ke and P. Stroeve. *Polymer-Layered Silicate and Silica Nanocomposites, 1st ed.* Elsevier, 2005.

Ali Olad. Polymer/clay nanocomposites. Advances in Diverse Industrial Applications of Nanocomposites. 2000.

M. Alexandre and P. Dubois. Polymer-layered silicate nanocomposites: preparation, properties and uses of a new class of materials. *Materials Science and Engineering*, 28:1 – 63, 2000.

Zeno W. Wicks, Frank N. Jones, S. Peter Pappas, and Douglas A. Wicks. *Organic Coatings, Science and Technology, 3rd Edition*. Wiley, 2007.

A. R. Marrion. *The Chemistry and Physics of Coatings, 2nd Edition*. 2004.

M. L. Nobel, E. Mendes, and S. J. Picken. Enhanced properties of innovative laponite-filled waterborne acrylic resin dispersions. *Journal of Applied Polymer Science*, 103: 687 – 697, 2007a.

P.A. Steward et al. An overview of polymer latex film formation and properties. *Advances in Colloid and Interface Science*, 86:195 – 267, 2000.

Patel et al. Modeling film formation of polymer-clay nanocomposite particles. *Langmuir*, 26:3962 – 3971, 2010.

T. Wang and J. L. Keddie. Design and fabrication of colloidal polymer nanocomposites. *Advances in Colloid and Interface Science*, 147-148:319 – 332, 2009.

G. Sewell. Importance and measurement of minimum film-forming temperature. *Pigment & Resin Technology*, 27:173 – 174, 1998.

D.L. Ho and C. J. Glinka. Effects of solvent solubility parameters on organoclay dispersions. *Chem. Mater.*, 15:1309 – 1312, 2003.

D. Burgentzle et al. Solvent-based nanocomposite coatings i. dispersion of organophilic montmorillonite in organic solvents. *Journal of Colloid and Interface Science*, 278: 26 – 39, 2004.

N.H. Tran et al. Dispersion of organically modified clays within n-alcohols. *Journal of Colloid and Interface Science*, 297:541 – 545, 2006.

John W. Jordan. Organophilic bentonites i. swelling in organic liquids. *J.Phys.Chem*, 53(2):294 – 306, 1949.

Emmanuel Stefanis and Costas Panayiotou. Prediction of hansen solubility parameters with a new group-contribution method. *Int. J. Thermophys.*, 29:568 – 585, 2008.

Richard A. Pethrick. Positron annihilation - a probe for nanoscale voids and free volume. *Prog. Polym. Sci.*, 22:1 – 47, 1997.

Reinhard Krausse-Rehberg. Positron annihilation at Martin Luther University, Halle, 2012. URL `http://positron.physik.uni-halle.de/`.

T.E.M. Staab and B. Somieski et al. The data treatment influence on the spectra decomposition in positron lifetime spectroscopy, part 2: The effect of source corrections. *Nuclear Instruments and Methods in Physics Research A*, 381:141 – 151, 1996.

Q.M. Jia et al. Effects of organophilic montmorillonite on hydrogen bonding, free volume and glass transition temperature of epoxy resin/polyurethane interpenetrating polymer networks. *European Polymer Journal*, 43:35 – 42, 2007.

S.J. Wang et al. Microstructure of polymer/clay nanocomposites studied by positrons. *Radiation Physics and Chemistry*, 76:106 – 111, 2007.

L.E. Nielsen. Models for the permeability of filled polymer systems. *J. Macromol. Sci. (Chem.)*, A1(5):929 – 942, 1967.

Giorgos Choudalakis. *Polymer/clay nanocomposite coatings with reduced gas permeability*. PhD thesis, Technical University of Crete, under preparation, 2012.

G. Choudalakis and A. D. Gotsis. Permeability of polymer/clay nanocomposites: A review. *European Polymer Journal*, 45:967 – 984, 2009.

Andreas A. Sapalidis, Fotios K. Katsaros, and Nick K. Kanellopoulos. PVA/montmorillonite nanocomposites: Development and properties. *Polymer Degradation and Stability*, 47:369 – 313, 1995.

S. Filippi et al. On the interlayer spacing collapse of Cloisite 30B organoclay. *Polymer Degradation and Stability*, 96:823 – 832, 2011.

Yu et al. Investigation of free volume, interfacial, and toughening behavior for cyanate ester/bentonite nanocomposites by positron annihilation. *J. Appl. Polym. Sci.*, 102: 1509 – 1515, 2006.

S.H. Kim et al. Determination of the glass transition temperature of polymer/layered silicate nanocomposites from positron annihilation lifetime measurements. *Polymer*, 48:4271 – 4277, 2007.

DWV van Krevelen. *Properties of polymers, 3rd edition*. Elsevier, 1990.

Robert F. Fedors. A method for estimating both the solubility parameters and molar volumes of liquids. *Polymer Engineering and Science*, 14:147 – 154, 1974.

A.R. McLauchlin and N.L. Thomas. Preparation and thermal characterisation of poly(lactic acid) nanocomposites prepared from organoclays based on an amphoteric surfactant. *Polymer Degradation and Stability*, 94:868 – 872, 2009.

J. Brandrup, E. H. Immergut, and E. A. Grulke. *Polymer Handbook, 4th Edition*. Wiley, New York, 1999.

APIThailand. CO_2 physical data, 2012. URL `http://www.apithailand.com/carbon.html`.

G. Choudalakis and A.D. Gotsis. Free volume and mass transport in polymer nanocomposites. *Current Opinion in Colloid and Interface Science*, 17:132 – 140, 2012.

A. Okada and A. Usuki. Twenty years of polymer-clay nanocomposites. *Macromol. Mater. Eng.*, 291:1449 – 1476, 2006.

G. Consolati et al. Positron annihilation study of free volume in cross-linked amorphous polyurethanes through the glass transition temperature. *Polymer*, 39:3491 – 3498, 1998.

G. Dlubek et al. Characterisation of free volume in amorphous materials by PALS in relation to relaxation phenomena. *url = http://positron.physik.uni-halle.de/*, 2003.

A. Sorrentino, M. Tortora, and V. Vittoria. Diffusion behavior in polymer-clay nanocomposites. *J. Polym. Sci. Part B: Polym. Phys.*, 44:265 – 274, 2006.

Perez-Santano et al. Effect of the intercalation conditions of a montmorillonite with octadecylamine. *Journal of Colloid and Interface Science*, 284:239 – 244, 2005.

X. Cao et al. Polyurethane/clay nanocomposites foams: processing, structure and properties. *Polymer*, 46:775 – 783, 2005.

G. Choudalakis, J.S Picken, H. Schut, and A.D. Gotsis. The free volume in acrylic resin/laponite nanocomposite coatings. *European Polymer Journal*, 47:264 – 272, 2011.

K. Yoon et al. Modification of montmorillonite with oligomeric amine derivatives for polymer nanocomposite preparation. *Applied Clay Science*, 38:1 – 8, 2007.

C.D. Han et al. Effect of organophilic montmorillonite on polyurethane/montmorillonite nanocomposites. *Journal of Applied Polymer Science*, 91:2536 – 2542, 2004.

Andrei A. Gusev and Hans Rudolf Lusti. Rational design of nanocomposites for barrier applications. *Adv. Mater.*, 13:1641 – 1643, 2001.

J. W. Jordan, B. J. Hook, and C. M. Finlayson. Organophilic bentonites ii. Organic liquid gels. *J.Phys.Chem*, 54(8):1196 – 1208, 1950.

J.W. Jordan and W. Williams. Organophilic bentonites. iii. Inherent properties. *Coll.Polym.Sci*, 137(1):40 – 48, 1954.

S. J. Tao. Positronium annihilation in molecular substances. *The Journal Of Chemical Physics*, 56:5499 – 5510, 1972.

Wei-I Hung and et al. *Advanced Anticorrosive Coatings Prepared from Polymer-Clay Nanocomposite Materials*. R. O. C., Taiwan.

Alan S. Michaels and Harris J. Bixler. Flow of gases through polyethylene. *J.Polym.Sci.*, pages 413 – 439, 1961.

Quang T. Nguyen and Donald G. Baird. Preparation of polymer-clay nanocomposites and their properties. *Advances in Polymer Technology*, 25:270 – 285, 2006.

E. E. Ahdel-Hady and A. M. A. El-Sayed. Free volume hole distributions of polymers via the positron lifetime technique. *Polymer Degradation and Stability*, 47:369 – 373, 1995.

M.L. Nobel, S.J. Picken, and E. Mendes. Waterborne nanocomposite resins for automotive coating applications. *Progress in Organic Coatings*, 58:96 – 104, 2007b.

P.C. LeBaron et al. Polymer-layered silicate nanocomposites: an overview. *Applied Clay Science*, 15:11 – 29, 1999.

Yang Yu. Positron annihilation lifetime spectroscopy studies of amorphous and crystalline molecular materials. *PhD Thesis*, Martin Luther University, Halle-Wittenberg, 2011.

P. Winberg et al. Free volume sizes in intercalated polyamide 6/clay nanocomposites. *Polymer*, 46:8239 – 8249, 2005.

M. Zanetti, S. Lomakin, and G. Camino. Polymer layered silicate nanocomposites. *Macromol. Mater. Eng*, 279:1 – 9, 2000.

Jia Qingming, Zheng Maosheng, Shen Renjie, and Chen Hongxiang. The glass transition temperature and microstructure of polyurethane/epoxy resin interpenetrating polymer networks nanocomposites. *Chinese Science Bulletin*, 51:293 – 298, 2006.

Jang et al. Relationship between the solubility parameter of polymers and the clay dispersion in polymer/clay nanocomposites and the role of the surfactant. *Macromolecules*, 38:6533 – 6543, 2005.

B. Somieski, R. Krause-Rehberg, H. Salz, and N. Meyendorf. Application of the positron lifetime spectroscopy as method of non-destructive testing. *Journal De Physique*, 5: C1 127 – C1 134, 1995.

H. T. Lee, J. J. Hwang, and H. J. Liu. Effects of ionic interactions between clay and waterborne polyurethanes on the structure and physical properties of their nanocomposite dispersions. *J. Polym. Sci. Part A: Polym. Chem.*, 44:5801 – 5807, 2006.

S. M. Aharoni. On free volume of polymers above the glass transition. *Journal of Applied Polymer Science*, 23:223 – 228, 1979.

L. Nobel, E. Mendes, and S.J. Picken. Acrylic-based nanocomposite resins for coating applications. *Journal of Applied Polymer Science*, 104(4):2146 – 2156, 2007c.

B. Somieski et al. The data treatment influence on the spectra decomposition in positron lifetime spectroscopy, part 1: On the interpretation of multi-component analysis studied by monte carlo simulated model spectra. *Nuclear Instruments and Methods in Physics Research A*, 381:128 – 140, 1996.

J. Soulestin et al. Morphology and mechanical properties of PET/PE blends compatibilized by nanoclays: Effect of thermal stability of nanofiller organic modifier. *J.Appl.Polym.Sci.*, in print:doi: 10.1002/app.38450, 2012a.

J. Soulestin et al. Compatibilization of immiscible polymer blends by organoclay: Effect of nanofiller or organo-modifier? *Macromol. Mater. Eng.*, in print:doi: 10.1002/app.38450, 2012b.

D. Satas and Arthur A. Tracton. *Coatings Technology Handbook, 2nd ed.* 2001.

Christian Reinchardt. *Solvents and Solvent Effects in Organic Chemistry, 3rd Edition*. Wiley, NY, 2003.

Burdick and Jackson. Miscibility of solvents, 2012. URL `http://macro.lsu.edu/HowTo/solvents/Miscibility.htm`.

Appendix A

Data Tables

Data tables from the results of the several experiments etc. are listed in this appendix.

Table A.1: Some sample codes used in this study

Sample	Description
AR 0.96	Water borne acrylic resin without filler
ARBE05	Nanocomposite with 0.5 wt% hydrophilic bentonite in waterborne acrylic resin AR 0.96
ARBE10	Nanocomposite with 1 wt% hydrophilic bentonite in waterborne acrylic resin AR 0.96
ARBE50	Nanocomposite with 5 wt% hydrophilic bentonite in waterborne acrylic resin AR 0.96
PU 0.98	Water borne polyurethane resin without filler
PUBE05	Nanocomposite with 0.5 wt% hydrophilic bentonite in waterborne polyurethane PU 0.98
C93A20A	Nanocomposite with 1.2 wt% modified clay (C93A) in waterborne polyurethane resin PU 0.98
C93A30A	Nanocomposite with 1.8 wt% modified clay (C93A) in waterborne polyurethane resin PU 0.98
2C	Solvent based two component polyurethane resin without filler
2C-BEOA	Nanocomposite with 1 wt% modified clay (BEOA) in the solvent based polyurethane resin
2C-C20A	Nanocomposite with 1 wt% modified clay (C20A) in the solvent based polyurethane resin

Table A.2: Particle mass, volume fractions and nanocomposite density

sample	ρ_{nanoc} (gr/cm^3)	wt/wt %	v/v %
PU 0.98	1.0	0	0
PUBE05	1.003	0.5	0.19
PU 0.98	1.0	0	0
C30B05A	1.002	0.5	0.25
C30B10A	1.005	1.0	0.51
PU 0.98	1.0	0	0
C93A10A	1.003	0.6	0.32
C93A20A	1.006	1.2	0.64
C93A30A	1.008	1.8	0.97
PU 0.98	1.0	0	0
C10A10A	1.003	0.6	0.32
C10A20A	1.006	1.2	0.64
C10A30A	1.009	1.8	0.96
AR 0.96	1.1	0	0
ARBE05	1.103	0.5	0.20
ARBE10	1.107	1.0	0.41
ARBE50	1.134	5.0	2.1
2C	0.9	0	0

Table A.3: Typical properties of solvents used in this study, regarding their evaporation rates

Organic Solvent	Boiling point (°C)	Vapour Pres., 20 °C (hPa)
Acetone	56.2	240
Ethyl Alcohol	78.5	59
o-Xylene	144.4	6.0
Water	100.0	17.5

[Reinchardt, 2003]

Table A.4: Solvents' miscibility

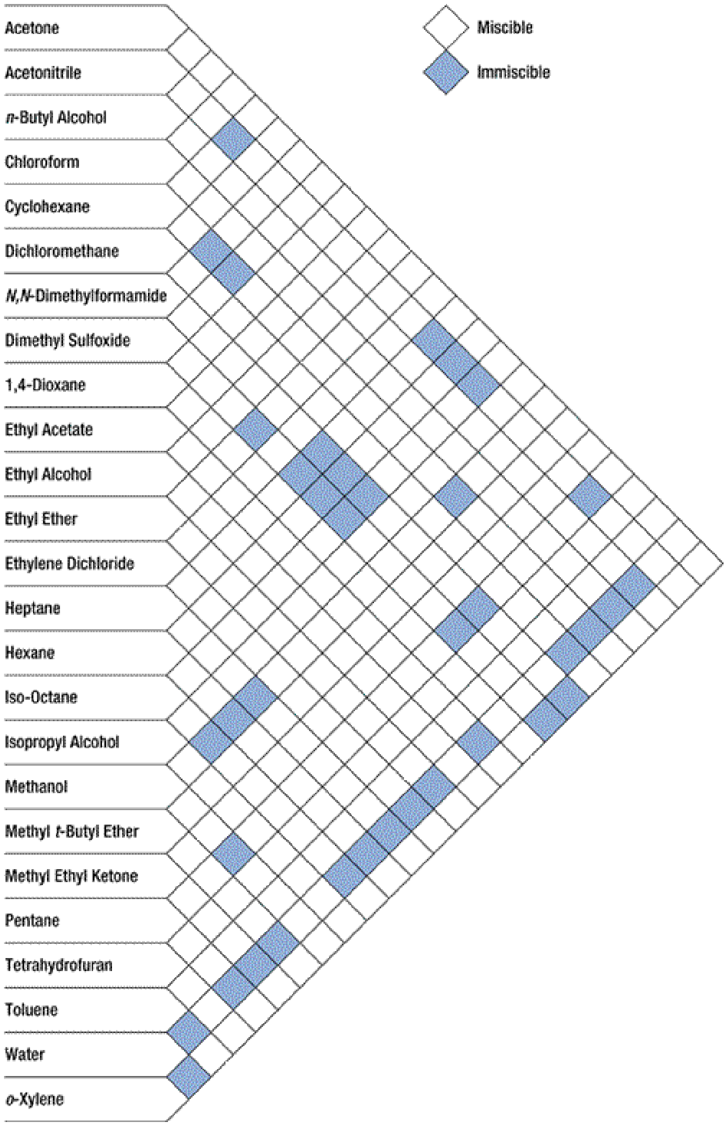

◇ Miscible

◆ Immiscible

	Acetone	Acetonitrile	*n*-Butyl Alcohol	Chloroform	Cyclohexane	Dichloromethane	*N,N*-Dimethylformamide	Dimethyl Sulfoxide	1,4-Dioxane	Ethyl Acetate	Ethyl Alcohol	Ethyl Ether	Ethylene Dichloride	Heptane	Hexane	Iso-Octane	Isopropyl Alcohol	Methanol	Methyl *t*-Butyl Ether	Methyl Ethyl Ketone	Pentane	Tetrahydrofuran	Toluene	Water
Acetonitrile	◇																							
n-Butyl Alcohol	◇	◇																						
Chloroform	◇	◇	◇																					
Cyclohexane	◇	◆	◇	◇																				
Dichloromethane	◇	◇	◇	◇	◇																			
N,N-Dimethylformamide	◇	◇	◇	◇	◆	◇																		
Dimethyl Sulfoxide	◇	◇	◇	◇	◆	◇	◇																	
1,4-Dioxane	◇	◇	◇	◇	◇	◇	◇	◇																
Ethyl Acetate	◇	◇	◇	◇	◇	◇	◇	◇	◇															
Ethyl Alcohol	◇	◇	◇	◇	◇	◇	◇	◇	◇	◇														
Ethyl Ether	◇	◇	◇	◇	◇	◇	◇	◆	◇	◇	◇													
Ethylene Dichloride	◇	◇	◇	◇	◇	◇	◇	◇	◇	◇	◇	◇												
Heptane	◇	◆	◇	◇	◇	◇	◆	◆	◇	◇	◇	◇	◇											
Hexane	◇	◆	◇	◇	◇	◇	◆	◆	◇	◇	◇	◇	◇	◇										
Iso-Octane	◇	◆	◇	◇	◇	◇	◆	◆	◇	◇	◇	◇	◇	◇	◇									
Isopropyl Alcohol	◇	◇	◇	◇	◇	◇	◇	◇	◇	◇	◇	◇	◇	◇	◇	◇								
Methanol	◇	◇	◇	◇	◆	◇	◇	◇	◇	◇	◇	◇	◇	◆	◆	◆	◇							
Methyl *t*-Butyl Ether	◇	◇	◇	◇	◇	◇	◇	◇	◇	◇	◇	◇	◇	◇	◇	◇	◇	◇						
Methyl Ethyl Ketone	◇	◇	◇	◇	◇	◇	◇	◇	◇	◇	◇	◇	◇	◇	◇	◇	◇	◇	◇					
Pentane	◇	◆	◇	◇	◇	◇	◆	◆	◇	◇	◇	◇	◇	◇	◇	◇	◇	◆	◇	◇				
Tetrahydrofuran	◇	◇	◇	◇	◇	◇	◇	◇	◇	◇	◇	◇	◇	◇	◇	◇	◇	◇	◇	◇	◇			
Toluene	◇	◇	◇	◇	◇	◇	◇	◇	◇	◇	◇	◇	◇	◇	◇	◇	◇	◇	◇	◇	◇	◇		
Water	◇	◇	◆	◆	◆	◆	◇	◇	◇	◆	◇	◆	◆	◆	◆	◆	◇	◇	◆	◆	◆	◇	◆	
o-Xylene	◇	◇	◇	◇	◇	◇	◆	◆	◇	◇	◇	◇	◇	◇	◇	◇	◇	◇	◇	◇	◇	◇	◇	◆

[Burdick and Jackson, 2012]

Table A.5: Cloisite Selection Chart indicating the clay's surface hydrophobicity

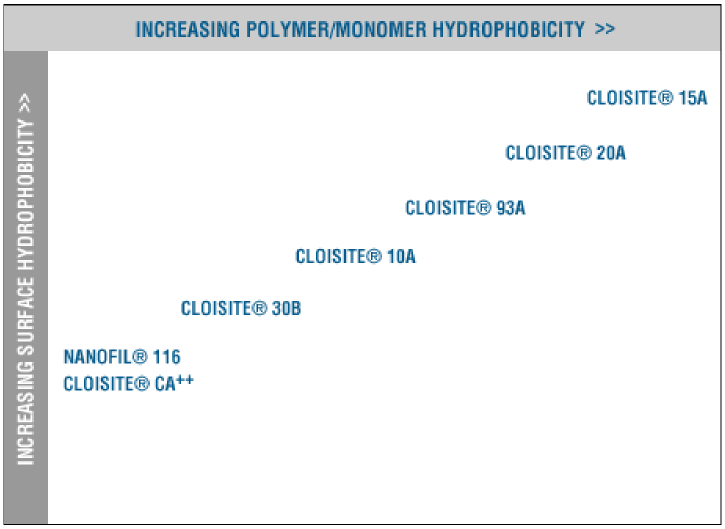

Southern Clay Products®, http://www.scprod.com/

Table A.6: Intermediate lifetime (ns) and relative intensity (%) data from PALS (1st and 2nd set of measurements) for different resin-based samples and varying percentage of clay addition

	Intermediate Lifetime τ_2 (ns)		Intermediate Intensity I_2 (%)	
Sample	1st set	2nd set	1st set	2nd set
AR 0.96	0.4775	0.4707	40.04	40.81
ARBE05	0.4646	0.4879	41.57	38.82
ARBE10	0.4566	0.4639	44.87	43.22
ARBE50	0.4762	0.4674	39.87	41.79
PU 0.98	0.4759	0.4681	38.61	40.16
PUBE05	0.4939	0.4730	37.84	39.97
C93A10A	0.4846	0.4900	36.79	36.41
C93A20A	0.4593	0.4825	40.64	36.94
C93A30A	0.4714	0.4808	40.71	39.93
2C	0.4914	0.4859	37.36	37.22
2C-BEOA	0.4879	0.4725	38.09	39.32
2C-C20A	0.5011	0.4970	34.47	35.76

Table A.7: o-Ps lifetime (ns) and relative intensity (%) data from PALS measurements for different resin-based samples and varying percentage of clay addition

1st set of measurements

Sample	τ_3 (ns)	I_3 (%)	Fit var. x^2
AR 0.96	2.1808	22.82	1.0822
ARBE05	2.1571	22.64	1.0745
ARBE10	2.2177	21.28	1.0420
ARBE50	2.1323	21.81	0.9521
PU 0.98	2.1508	25.52	1.0889
PUBE05	2.1613	24.23	0.9484
C93A10A	2.1311	26.99	1.1195
C93A20A	2.1151	27.13	1.0204
C93A30A	2.3191	23.90	1.0514
2C	2.4054	22.74	1.0603
2C -BEOA	2.3074	22.36	0.9964
2C - C20A	2.4491	24.22	1.1727

Table A.8: o-Ps lifetime (ns) and relative intensity (%) data from PALS measurements for different resin-based samples and varying percentage of clay addition

2nd set of measurements

Sample	τ_3 (ns)	I_3 (%)	Fit var. x^2
AR 0.96	2.1780	22.91	0.9806
ARBE05	2.1834	22.12	1.0011
ARBE10	2.2234	21.25	1.0050
ARBE50	2.1386	21.83	1.0354
PU 0.98	2.1419	25.59	1.0907
PUBE05	2.1402	24.64	1.0431
C93A10A	2.1334	27.02	1.0199
C93A20A	2.1247	26.93	1.0808
C93A30A	2.3356	23.67	1.0783
2C	2.4088	22.87	1.0876
2C -BEOA	2.2835	22.75	1.0595
2C - C20A	2.4629	24.16	1.0557

Table A.9: o-Ps lifetime (ns) and relative intensity (%) data from PALS measurements for different resin-based samples and varying percentage of clay addition

Average values of two sets of measurements.

Sample	o-Ps Lifetime, τ_3 (ns)	o-Ps Intensity, I_3 (%)
AR 0.96	2.179	22.87
ARBE05	2.170	22.38
ARBE10	2.221	21.27
ARBE50	2.135	21.82
PU 0.98	2.146	25.55
PUBE05	2.151	24.44
C93A10A	2.132	27.01
C93A20A	2.120	27.03
C93A30A	2.327	23.79
2C	2.407	22.81
2C - BEOA	2.295	22.56
2C – C20A	2.456	24.19

Table A.10: The radius, R (Å), of free volume hole, the volume, V (Å^3), of each hole, as well as the fractional free volume, V_f (%)

Sample	Radius R (Å)	Volume hole V (Å3)	Fract. free volume Vf (%)
AR 0.96	3.012	114.46	4.71
ARBE05	3.004	113.55	4.57
ARBE10	3.048	118.61	4.54
ARBE50	2.974	110.18	4.33
PU 0.98	2.983	111.19	5.11
PUBE05	2.988	111.75	4.92
C93A10A	2.971	109.85	5.34
C93A20A	2.961	108.74	5.29
C93A30A	3.1367	129.19	5.53
2C	3.200	137.26	5.64
2C - BEOA	3.109	125.88	5.11
2C – C20A	3.239	142.34	6.20

Table A.11: o-Ps lifetime, o-Ps intensity, and fit variance for tested sample “AR 0.96”, at increasing temperature values (300 to 473 K).

Temperature (K)	τ_3 (ns)	I_3 (%)	variance x^2
300	2.1487	21.91	0.9819
335	2.3840	22.96	0.8973
373	2.6313	23.65	1.0735
413	2.7426	25.50	1.0488
433	2.7735	27.24	1.0024
453	2.8343	28.15	0.9966
473	2.8200	27.63	1.0195

Table A.12: Intermediate lifetime, τ_2, and intermediate intensity, I_2, for tested sample “AR 0.96”, at increasing temperature values (300 to 473 K).

Temperature (K)	τ_2 (ns)	I_2 (%)
300	0.4656	40.36
335	0.4616	40.45
373	0.4471	44.50
413	0.4401	44.71
433	0.4572	38.77
453	0.4570	38.90
473	0.4455	40.35

Table A.13: Data obtained from PALS experiments, for tested sample “AR 0.96”, at increasing temperature values (300 to 473 K)

Temperature (K)	Radius R (Å)	Volume hole V (Å3)	Fract. free volume Vf (%)
300	2.986	111.50	4.40
335	3.182	134.93	5.58
373	3.373	160.69	6.84
413	3.454	172.63	7.92
433	3.476	175.98	8.63
453	3.519	182.62	9.25
473	3.509	181.05	9.00

Table A.14: o-Ps lifetime, o-Ps intensity, and fit's variance for tested sample "ARBE10", at increasing temperature values (300 to 473 K).

Temperature (K)	o-Ps Lifetime τ_3 (ns)	o-Ps Intensity I_3 (%)	Fit variance x2
300	2.1063	21.98	1.0709
312	2.2001	22.25	1.0409
323	2.2635	22.96	1.0065
335	2.3498	23.23	1.0366
348	2.4474	23.17	1.0374
360	2.5074	23.70	1.0203
373	2.5732	24.15	1.0252
383	2.6029	24.82	1.0947
393	2.6285	25.52	1.0412
403	2.6588	26.33	1.0044
413	2.6665	27.05	1.1203
423	2.6906	27.41	0.9879
433	2.7238	27.79	1.0395
443	2.7377	28.27	1.1242
453	2.7596	28.45	1.0016
463	2.7793	28.67	0.9469
473	2.7959	28.58	1.0338

Table A.15: Intermediate lifetime, τ_2, and intermediate intensity, I_2, for tested sample "ARBE10", at increasing temperature values (300 to 473 K).

Temperature (K)	τ_2 (ns)	I_2 (%)
300	0.4675	39.70
312	0.4891	36.69
323	0.4763	37.50
335	0.4513	43.10
348	0.4692	39.40
360	0.4484	44.20
373	0.4510	43.11
383	0.4457	43.57
393	0.4520	42.22
403	0.4560	40.86
413	0.4559	39.55
423	0.4604	38.78
433	0.4630	38.06
443	0.4630	38.06
453	0.4814	34.88
463	0.4629	38.07
473	0.4629	37.49

Table A.16: Data obtained from PALS experiments, for tested sample “ARBE10”, at increasing temperature values (300 to 473 K)

Temperature (K)	Radius, R (Å)	Volume hole, V (Å^3)	Fract. free volume, V$_f$ (%)
300	2.949	107.43	4.25
312	3.030	116.52	4.67
323	3.083	122.75	5.07
335	3.154	131.42	5.49
348	3.232	141.42	5.90
360	3.279	147.68	6.30
373	3.329	154.54	6.72
383	3.351	157.62	7.04
393	3.371	160.46	7.37
403	3.393	163.62	7.75
413	3.399	164.49	8.01
423	3.416	166.97	8.24
433	3.441	170.66	8.54
443	3.451	172.16	8.76
453	3.466	174.41	8.93
463	3.481	176.69	9.12
473	3.492	178.37	9.18

Table A.17: Diffusion coefficient,D, membrane thickness, d, linear fit, R^2, and ambient conditions during the measurements (RH % and temperature) from gas permeation experiments, for all tested samples.

Sample	d (mm)	%Clay w/w	D (cm^2/s x10^{-8})	Temp.(°C)	RH %	R^2
PU 0.98	0.96	0	7.4	21	38	0.99982
PUBE05	0.57	0.5	2.1	23	50	0.99949
C93A20A	0.60	1.2	4.9	22	44	0.99989
C93A30A	0.62	1.8	2.1	21	41	0.99962
C10A20A	0.62	1.2	4.7	20	51	0.99991
C10A30A	0.59	1.8	2.4	21	53	0.99972
AR 0.96	1.05	0	2.3	21	20	0.99976
ARBE05	0.93	0.5	1.8	22	60	0.99927
ARBE10	1.02	1.0	3.8	22	47	0.99982
2C	0.83	0	4.6	21	49	0.99988

Appendix B

Permeability graphs

The concentration vs. time graphs form the measurements in the permeation cell that were used to evaluate the diffusion coefficient, the sorption coefficient and the permeability of the nano-composites are included in this appendix.

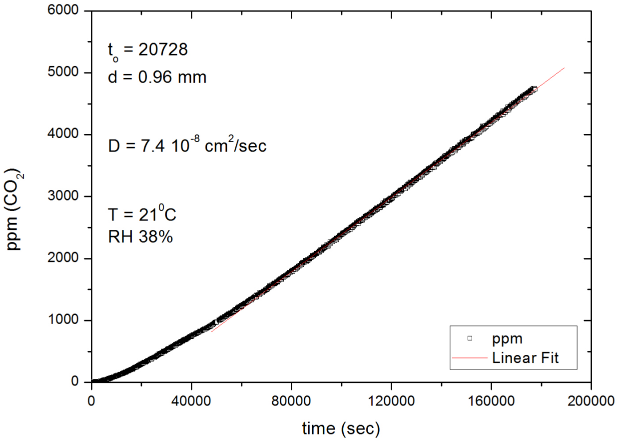

Figure B.1: Tested sample of the neat resin PU 0.98 in the form of a film

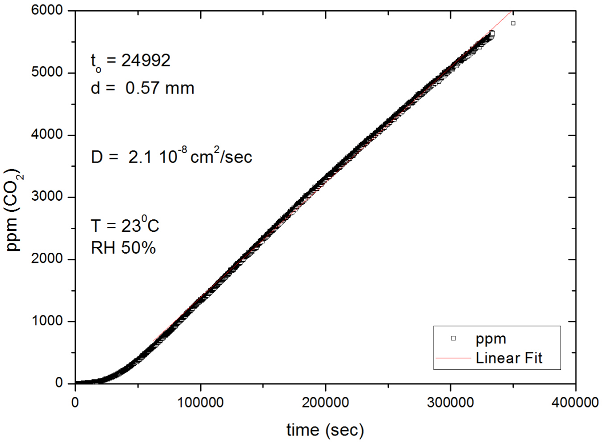

Figure B.2: Tested sample of PUBE05, 0.5 % clay, in the form of a film

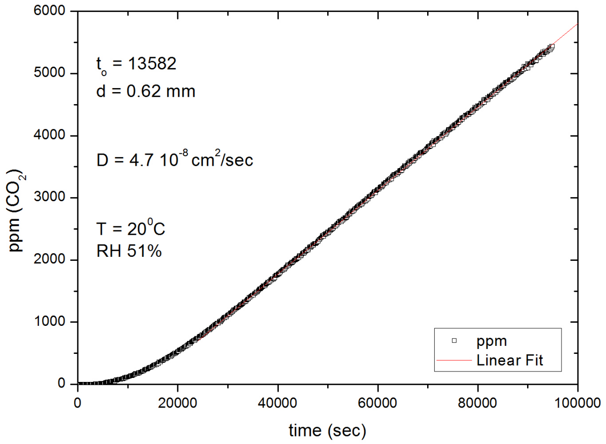

Figure B.3: Tested sample of C10A20A, 1.2 % clay, in the form of a film

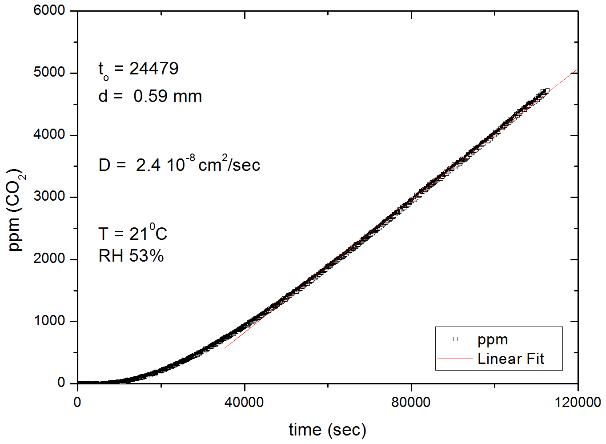

Figure B.4: Tested sample of C10A30A, 1.8 % clay, in the form of a film

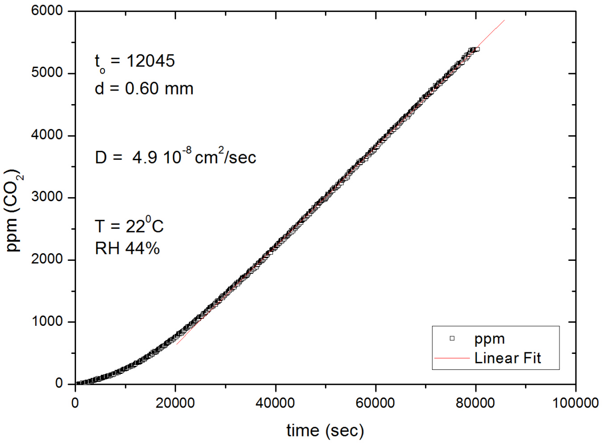

Figure B.5: Tested sample of C93A20A, 1.2 % clay, in the form of a film

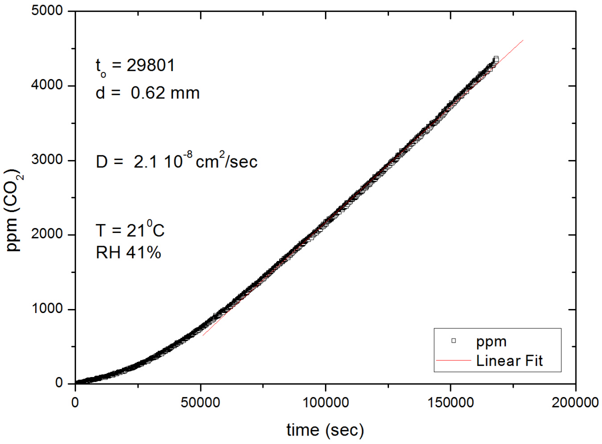

Figure B.6: Tested sample of C93A30A, 1.8 % clay, in the form of a film

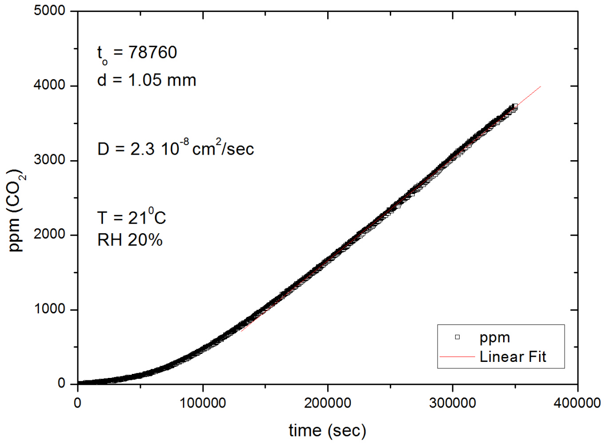

Figure B.7: Tested sample of the neat resin AR 0.96 in the form of a film

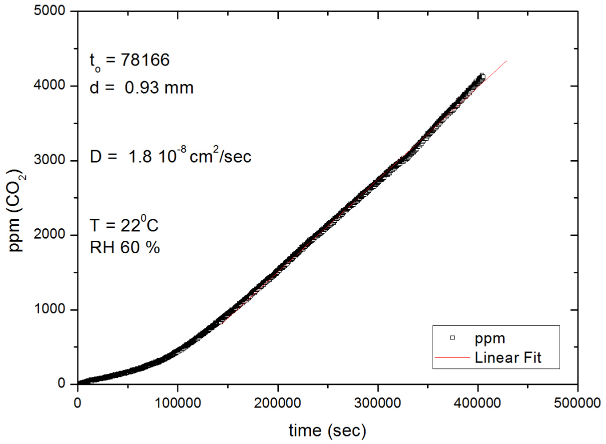

Figure B.8: Tested sample of ARBE05, 0.5 % clay, in the form of a film

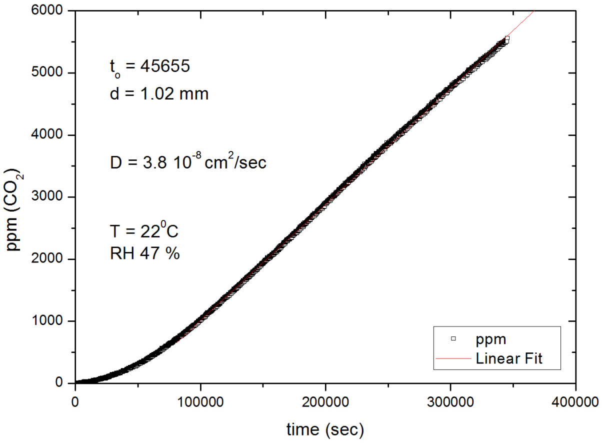

Figure B.9: Tested sample of ARBE10, 1.0 % clay, in the form of a film

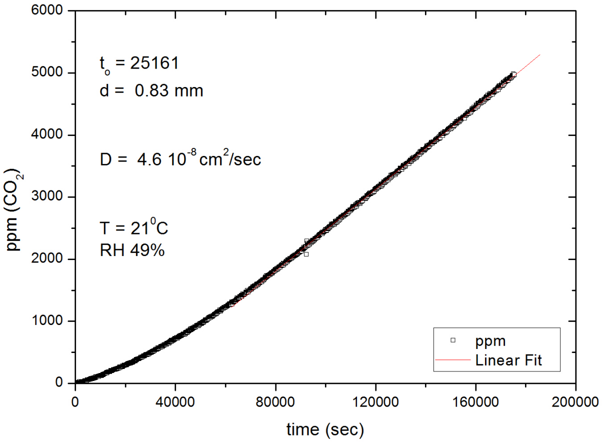

Figure B.10: Tested sample of the neat resin 2C in the form of a film

Appendix C

PALS raw data graphs

Some representative lifetime spectra measured using the positron annihilation technique are included in this appendix. The values of the free volume were calculated from these data.

Figures C.1, C.2, C.3 and C.4 illustrate the spectra of the tested sample ARBE10, at increasing temperature values of 300, 373, 423 and 473 K, respectively.

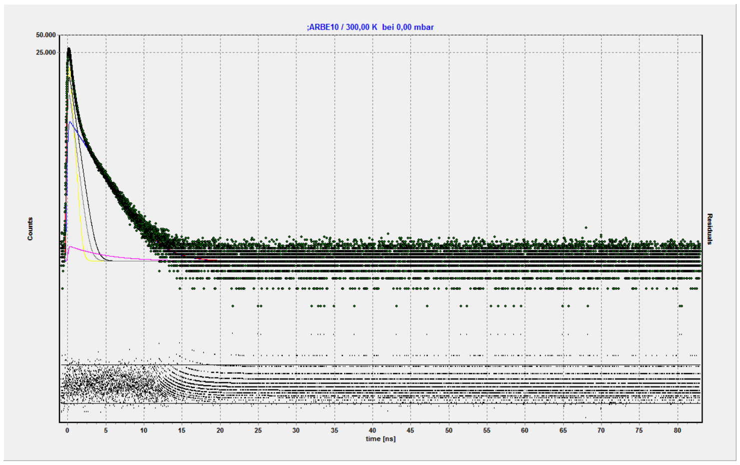

Figure C.1: PALS spectra of sample ARBE10, above RT, 300 K

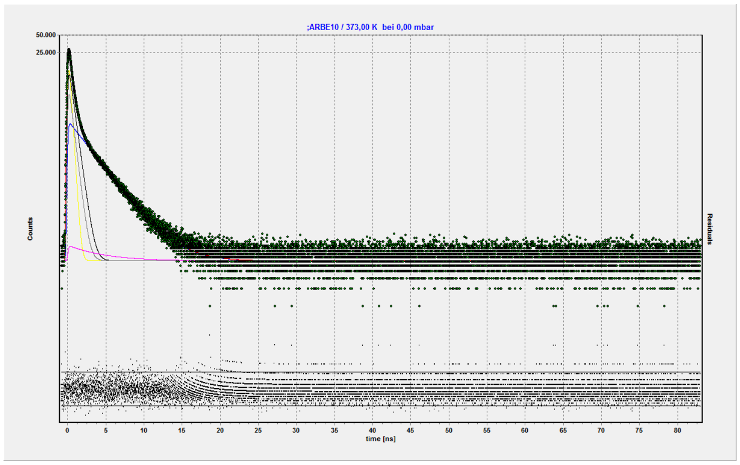

Figure C.2: PALS spectra of sample ARBE10, above RT, 373 K

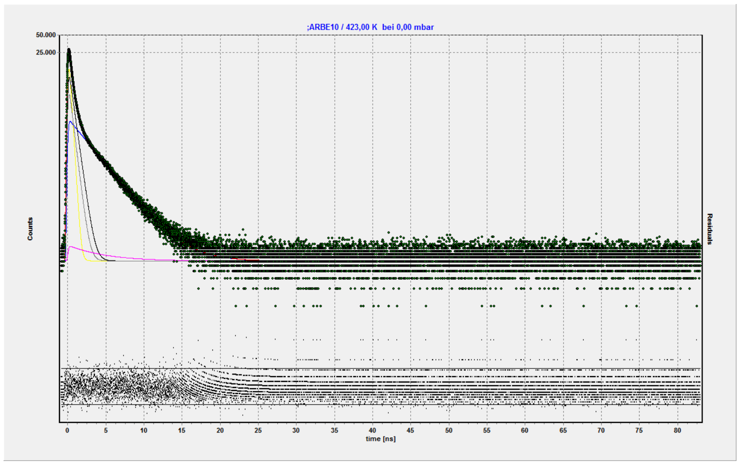

Figure C.3: PALS spectra of sample ARBE10, above RT, 423 K

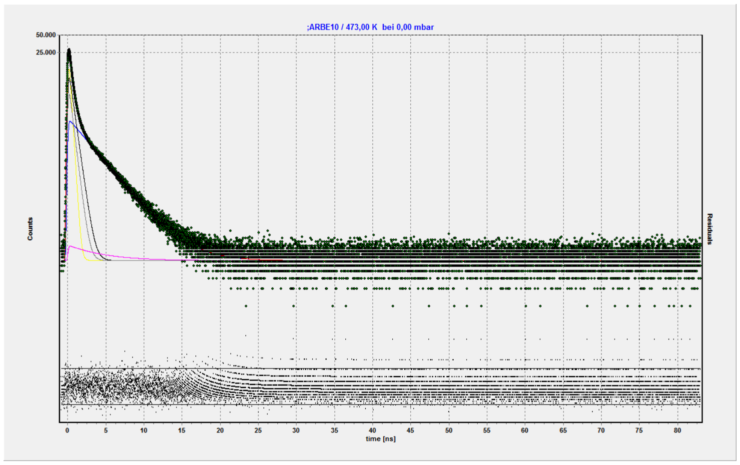

Figure C.4: PALS spectra of sample ARBE10, above RT, 473 K

List of Tables

List of Figures

Index

Curriculum Vitae

Maria S. Stratigaki
mstratigaki@isc.tuc.gr
Born on 26 February 1988 in Chania, Greece

- July 2012

  Experimental PALS measurements for the completion of the M. Sc. Thesis,
  under the supervision of Prof. Dr. Reinhard Krause - Rehberg.
  Positron Annihilation Laboratory
  Department of Physics in Martin - Luther University
  Halle an der Saale / Germany

- 2010 - 2012

  Master Thesis study
  Thesis on ”Nanocomposite coatings for enhanced barrier properties”,
  under the supervision of Prof. A. D. Gotsis.
  Technical University of Crete, Department of Applied Sciences

- 2010

  Summer project
  ”Dynamics and Rheology of Colloidal Star - Linear Polymer Mixtures”,
  under the supervision of Prof. D. Vlassopoulos.
  Institute of Electronic Structure and Laser, IESL
  Foundation for Research & Technology Hellas - FORTH, in Heraklion

- 2005 - 2010

  Diploma study
  University of Crete, School of Sciences and Engineering
  Department of Materials Science and Technology

- 2002 - 2005

  High school, Chania, Crete